Ca' Foscari
University
of Venice

Master's Degree programme

in

Sustainable Chemistry
and Tecnologies
"LM-54"

Final Thesis

Synthesis and characterization of manganese(II) and zinc(II) luminescent iminophosphorane complexes

Supervisor
Prof. Marco Bortoluzzi

Assistant supervisor
Dott. Valentina Ferraro

Graduand
Domenico Piccolo
Matriculation Number 848877

Academic Year
2022 / 2023

Index

Abstract

The thesis internship was focused on the preparation of iminophosphorane ligands to be coordinated to selected metal centres, with the aim of preparing new luminescent coordination compounds. The reaction with triphenylphosphine and aromatic or benzylic azides afforded the desired monodentate {N=P}-donors. The aromatic iminophosphorane revealed appreciable luminescence at the solid state. The reaction of the ligands with manganese(II) and zinc(II) halides in acetonitrile afforded neutral complexes. The use of protic solvents caused the decomposition of the ligands, and in selected cases the related phosphine oxide complexes were obtained. The luminescence of the zinc(II) complexes resulted to be ligand-based, enhanced by coordination and influenced by the spin-orbit coupling associated with the heavy halides. On the other hand, intense metal-centred luminescence was observed for manganese(II) complexes, in the green region for tetrahedral derivatives and in the reddish-orange for higher coordination numbers. The coordination geometry resulted dependent upon the N-bonded substituent. The results with monodentate ligands were confirmed using a bidentate iminophosphorane obtained from bis(diphenylphosphino)methane.

1. Introduction

1.1. General aspects of photoluminescence

Luminescence is the phenomenon that involves the emission of electromagnetic radiation after the absorption of energy by materials. When the energy absorbed comes from another electromagnetic radiation the process is called photoluminescence, and photons of appropriate energy are generally required to excite specific atoms and molecules in substances.

When electromagnetic radiation is absorbed the electrons in atoms or molecules gain energy, passing from a lower energy level to a higher energy one, *i.e.* from a ground to an excited state. The excited molecule soon loses the energy absorbed, and the electrons go back to the ground state. The loss of energy can occur either by non-radiative or radiative decay. The first mechanism is a vibrational decay, related to the vibrational structure of the compound. According to the Franck-Condon rules, non-radiative decay is favoured in the presence of high-energy oscillators and low-energy gaps. The second one is the photoluminescence phenomenon, which implies the emission of photons. If specific photoluminescence mechanisms such as up-conversion are neglected, the emitted photons are less energetic than the absorbed photons, and consequently the emission wavelength is longer than the excitation wavelength. The difference in excitation and emission wavelengths is called Stokes shift, as depicted in Figure 1 [1].

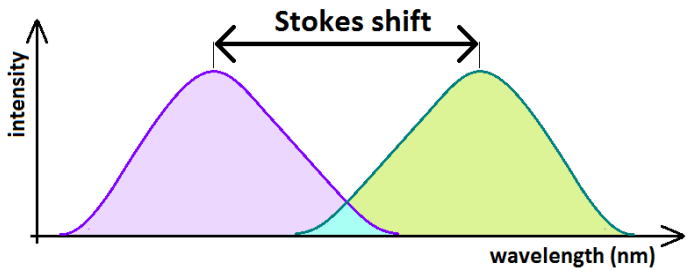

Figure 1. Stokes shift between absorption (violet) and emission (green).

The two best-known types of photoluminescence are fluorescence and phosphorescence, generally discriminated from an experimental point of view on the basis of the radiative decay time. Fluorescence takes place in a very short time interval, typically 10^{-9} s, and it is associated with the transition of an electron between two energy levels of the same multiplicity, e.g. from a singlet excited state to a singlet ground state, as depicted in Figure 2. The lack of spin change makes the transition fast. On the contrary, phosphorescence happens on a much longer time scale, typically ranging from 10^{-6} to 10^{-3} s, even if longer emission is possible, also indicated as afterglow. Phosphorescence implies the transition of an electron between energy states of different multiplicity, for instance from an excited triplet to a singlet ground state (Figure 2). Electrons can be promoted to a triplet excited state thanks to the occurrence of an intersystem crossing (ISC). The direct absorption leading to an excited state with different multiplicity with respect to the ground state is in fact a highly unlikely process because of the selection rules involved. After a spin-allowed excitation ($S_1 \leftarrow S_0$ in Figure 2), a non-radiative decay mechanism with associated spin change can occur, with population of a triplet excited state close in energy to the singlet excited state. Once the compound has reached the triplet state, it can go back to the singlet ground state by radiative decay. Since the phosphorescent transition happens between two energy levels with different multiplicity and it is thus forbidden by the selection rules, it takes longer time than fluorescence to occur.

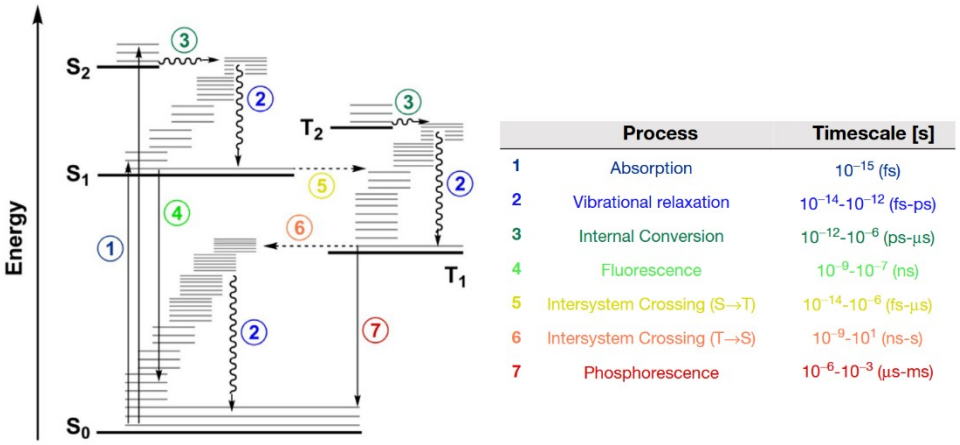

	Process	Timescale [s]
1	Absorption	10^{-15} (fs)
2	Vibrational relaxation	10^{-14}-10^{-12} (fs-ps)
3	Internal Conversion	10^{-12}-10^{-6} (ps-µs)
4	Fluorescence	10^{-9}-10^{-7} (ns)
5	Intersystem Crossing (S→T)	10^{-14}-10^{-6} (fs-µs)
6	Intersystem Crossing (T→S)	10^{-9}-10^{1} (ns-s)
7	Phosphorescence	10^{-6}-10^{-3} (µs-ms)

Figure 2. Jablonski energy diagrams comparing different radiative decay processes.

Intersystem crossing is promoted by strong spin-orbit coupling. Such an interaction between the magnetic moments associated with the spin and the orbits of the electrons has relativistic origin and depends upon the nuclear charge, and it alters the spectroscopic and magnetic properties of the compounds. The two *momenta* can interact aligning each other in the same direction or opposite direction, resulting in an alteration of both spectroscopic and magnetic properties. High nuclear charges magnify the effect, so the heavier the nucleus involved, the greater the interaction between *momenta*. The amount of interaction is generally represented by the coupling constant λ_{SO}, typically ranging from 0.02 − 0.07 eV, 0.1 − 0.2 eV and 0.3 − 0.5 eV respectively for 3d, 4d and 5d elements [2]. Spin-orbit coupling alters the electron energy levels, for example by reducing the energy gap between a singlet and a triplet excited state, thus relaxing the selection rules.

Another radiative decay formally in between fluorescence and phosphorescence is the thermally activated delayed fluorescence (TADF), represented in Figure 2 [3]. Such a phenomenon can occur when the lowest excited singlet and triplet states are very close in energy, a condition that is reached when the exchange energy between the unpaired electrons at the excited triplet state is low, for instance because the electrons are localized on different regions of the compound. As in phosphorescence, an intersystem crossing can happen after the excitation, with population of an excited triplet state. The opposite process, a back energy transfer from the excited triplet state to an excited singlet one, can however occur if the energy gap is low (reverse intersystem crossing, RISC). If the energy exchange between the two states is sufficiently fast their relative populations depend upon the temperature, according to the Boltzmann distribution. The different time scales of the radiative decay from the singlet and the triplet states can favour the emission from the singlet state, despite it is energetically higher than the triplet one. The whole process, composed by intersystem crossing, reverse intersystem crossing and emission, makes the TADF last longer than the common fluorescence.

The direct involvement of triplet states in phosphorescence and TADF is of current interest on considering other types of luminescence, such as electroluminescence. A modern electroluminescent device generates hole-electron pairs (excitons) that can be in singlet (25%) or triplet (75%) states. A pure fluorescent species can convert only the singlet excitons in photons, thus the ideal efficiency is 25%. On the other hand,

compounds able to give phosphorescence or TADF can instead convert all the excitons in light, with an ideal internal efficiency of 100% (Figure 3).

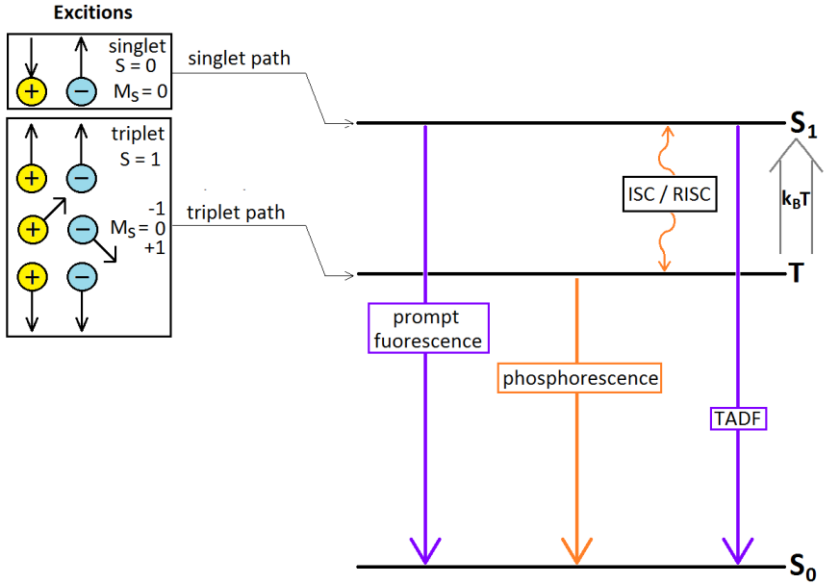

Figure 3. Conversion of excitons by fluorescence, phosphorescence and TADF.

1.2. Photoluminescence of d-block metal complexes

Many different types of molecules can give photoluminescence, including metal complexes of d-block elements. Most of the transition metal centres in their common oxidation states have a partially occupied d-shell. The transitions are influenced by the nature of the ligands and the geometry of the complexes because of the loss of degeneration of the d-shell, which can be described according to the crystal field or the molecular orbitals theories. The crystal field theory replaces the ligands with point charges surrounding the metal centre, and all the interactions are treated as electrostatic. The loss of degeneracy of the d-orbitals and their occupation determine a stabilizing contribution, the crystal field stabilization energy, that influences the geometry of the complex. On the other hand, the molecular orbitals theory describes the structure of coordination compounds on the basis of the superposition of metal-centred and ligand-centred orbitals, and the latter are usually grouped in symmetry-adapted linear combinations (SALCs). All the valence metal orbitals potentially participate in the covalent interactions with the ligands. The ligand-metal bonds are

dependent upon the symmetry and relative energies of the orbitals involved, and the molecular orbitals are commonly constructed as linear combinations of SALCs and metal orbitals. The molecular orbitals thus obtained can be bonding, non-bonding or antibonding and, depending upon their nature, their occupation can stabilize or destabilize the complex. The non-bonding orbitals remain localized on the starting atoms and do not participate in the formation of the bonds, but they can be however involved in electronic transitions [4].

The coefficients of the linear combinations determine whether the resulting molecular orbital is localized more on the metal centre or on the ligands. The description of a transition metal complex on the basis of the molecular orbital theory offers the possibility to postulate several different possible electronic transitions, whose nature depends on the molecular orbitals involved [5]. An example is reported in Figure 4. The picture refers to the possible absorptions in a regular octahedral complex.

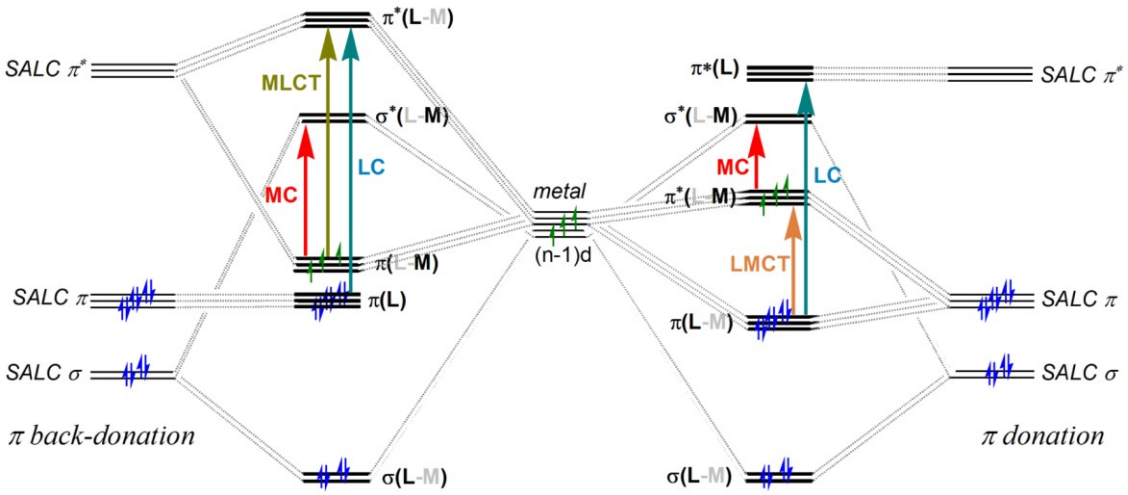

Figure 4. Molecular orbitals diagrams for a regular octahedral complex with σ and π metal-ligand interactions. Metal-centred (MC), ligand-centred (LC), metal-to-ligand charge transfer (MLCT) and ligand-to-metal charge transfer (LMCT) transitions are depicted.

When a transition occurs between orbitals localized on specific regions of the complex, it can be metal-centred (MC) or ligand-centred (LC). On the other hand, when the transitions occur between molecular orbitals localized on different parts of the molecule, they can have charge-transfer nature, either ligand-to-metal (LMCT) or metal-to-ligand (MLCT). In LMCT transitions the electron formally leaves a low-energy orbital mainly

localized on the ligand and occupies an orbital more localized on the metal centre. The reverse process occurs for MLCT transitions. The LMCT processes can be observed when metal centres are quite oxidant and the ligands are electron-rich, while the MLCT transitions are characteristic of metals in low oxidation state, surrounded by ligands with available empty orbitals of proper energy.

The processes depicted in Figure 4 do not account for all the possibilities offered by a transition metal complex. For instance, ligand-to-ligand charge transfer transitions (LLCT) are quite common, and also several cluster-centred transitions are known for polynuclear metal complexes. Moreover, the picture can be complicated by the population of states with different multiplicity due to the intersystem crossing. Depending upon the nature of the complex, an emitting state can thus have metal-centred, ligand-centred or charge-transfer nature, with multiplicity that can be the same or not with respect to the ground state.

1.3. Luminescent 3d metal complexes

The studies on luminescent transition metal compounds have been focused for a long time on derivatives of rare metals such as ruthenium, osmium, platinum, iridium and gold. Many complexes of these elements are of actual interest for advanced technology due to features such as good chemical stability, excellent luminescence quantum yield, large Stokes shifts and efficient harvest of singlet and triplet excitons. The high cost and the toxicity, together with geopolitical problems related to the supply of raw materials, have moved in recent years the interest towards more abundant and environmentally friendly elements, such as those belonging to the first transition series. Despite some doubts about the definition of transition element, zinc is generally included in the series [6-10]. The research on luminescent earth-abundant transition metal elements was less developed compared to the heavier congeners because of some limits, such as the generally lower chemical stability of the complexes. Moreover, according to the crystal field theory, the separation among d-type orbitals caused by the ligands is lower, thus non-radiative decay routes are favoured. Finally, the quite low atomic numbers make processes such as the intersystem crossing less probable, therefore radiative decays such as phosphorescence and TADF are less favoured. Nevertheless, promising results

were achieved with selected metal centres and properly designed coordinated ligands. For instance, chromium(III) complexes (d^3 configuration) with tailored heterocyclic N-donors are characterized by intense metal-centred emission [11], while heteroleptic copper(I) complexes (d^{10} configuration) with phosphines and polypyridines in the coordination sphere revealed easily tuneable luminescence, in most of the cases attributed to the population of singlet and triplet MLCT states [12]. Selected examples are shown in Figure 5. Other metal centres of recent interest for the development of efficient luminescent coordination compounds are manganese(II) and zinc(II), which will be discussed in detail in the next chapters.

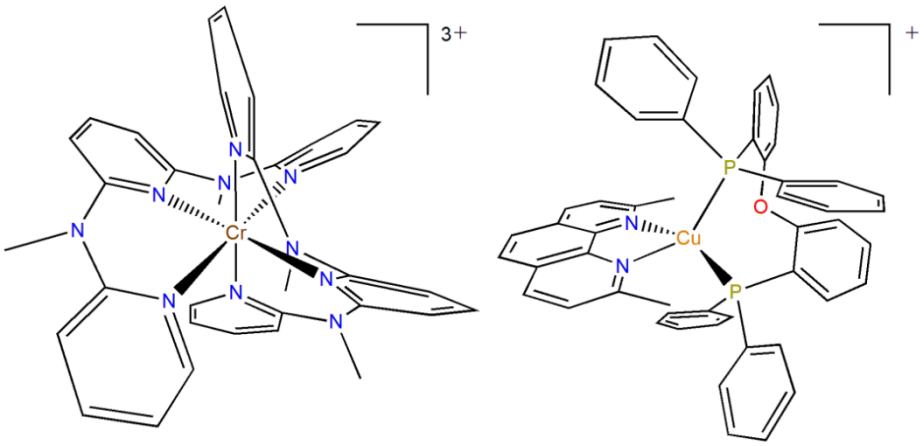

Figure 5. Examples of luminescent Cr(III) and Cu(I) complexes.

1.4. Manganese: oxidation states and luminescence

Manganese is a first-row transition metal that belongs to the seventh group along with technetium and rhenium. Manganese has atomic number 25 and electronic configuration [Ar]$4s^2 3d^5$, and it is one of the most abundant metals on Earth. In the form of oxide, the element can be found in minerals such as pyrolusite MnO_2, hausmannyte Mn_3O_4 and manganite $Mn_2O_3{\cdot}H_2O$. Manganese shows a wide range of oxidation states, formally going from Mn^{-III} (d^{10} configuration) to Mn^{VII} (d^0 configuration) [13]. Besides being an element characterized by ease of supply (please see the 2020 study on the EU's list of Critical Raw Materials available at https://ec.europa.eu/docsroom/documents/42883/attachments/1/translations/en/renditions/native), its toxicity is poor compared to many other transition elements.

Manganese is in fact involved in trace quantity in several biological processes, commonly related to the dioxygen metabolism [14].

In its highest oxidation state manganese behaves as a very strong oxidizing agent also towards water. A common reactant is the permanganate ion MnO_4^-, which forms a stable water solution only due to a very slow redox kinetic. The ion is purple-coloured because of a LMCT transition in the visible spectrum. The oxidation states Mn^{VI} (d^1) and Mn^{V} (d^2) are both quite unstable towards disproportion. The first one can be found in the manganate ion $[MnO_4]^{2-}$, stable only in basic solution. The solution chemistry of Mn^{V} is yet more limited, but the metal centre can be observed in some materials, such as synthetic apatites with partial replacement of tetrahedral phosphorus with manganese. Materials containing Mn^{V} are of potential interest because of the emission of this metal centre, usually in the near-infrared (NIR) range [15].

The oxidation states Mn^{IV} and Mn^{III} are also generally subjected to disproportion reactions, even if some coordination compounds can be stabilized with proper ligands [16,17]. Mn^{IV} is isoelectronic to Cr^{III} and it is another oxidation state of interest for the preparation of luminescent materials due to its emission, usually in the red range [18,19]. The oxidation states Mn^{IV} and Mn^{III} are also used instead of the permanganate ion in chemiluminescent reactants, owing to the formation of Mn^{II} derivatives with the metal centre in the excited state after reduction [20].

The most stable oxidation state is Mn^{II}, which hardly undergoes both oxidation and reduction process. Part of the stability is associated with the d^5 electronic configuration, that corresponds in the dominant high spin configuration to half of the d-shell filled with extra stabilization due to the exchange energy contribution. Most of the luminescent manganese compounds contain the metal centre in the divalent state, thus Mn^{II} luminescent compounds with be discussed in detail in the following chapter.

Lower oxidation states, ranging from Mn^{I} to Mn^{-III}, require π-acceptor ligands for their stabilization, such as carbonyl, isocyanides and nitrosyl. The related complexes generally obey to the 18-electrons rule. Recently, octahedral Mn^{I} complexes with tris-isocyanide ligands in the coordination sphere showed appreciable photoluminescence, and they are the first examples of $3d^6$ complexes with MLCT emission [21-23].

1.5. Manganese(II) coordination chemistry and luminescence

In the divalent oxidation state, the manganese centre exhibits typical coordination numbers from four to six, even if some examples of eptacoordinated Mn^{II} complexes were reported. Mn^{II} generally behaves as a hard Lewis acid, therefore according to Pearson's theory its chemistry is dominated by hard ligands such as oxygen and nitrogen donors, and by halide ions. The complexes commonly have high-spin configuration, while the low-spin one is limited to few compounds with very strong ligand fields [24].
The description of the spectroscopic properties for a high spin d^5 metal centre starts with the definition of the ground-state ^6S spectroscopic term, that represents the half-filled d shell as a spherical polyelectronic wavefunction (Figure 6). Given the S ground term, there is no possibility of loss of degeneration in the presence of a ligand field.

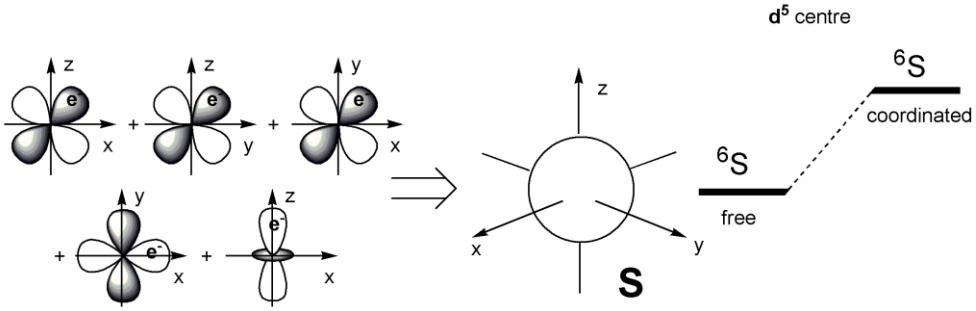

Figure 6. Graphical representation of a ^6S spectroscopic term for a d^5 metal centre.

The closest excited state implies a change of spin of almost one of the electrons, resulting in a change of multiplicity. According to the Tanabe-Subano diagram reported in Figure 7 [25], the excited state closest to the ground state for a high-spin octahedral or tetrahedral Mn^{II} complex is the $^4T_1(^4G)$ one. Other excited states with the same quartet multiplicity and accessible energy derive from the free ion ^4P and ^4D terms. The radiative decay from the $^4T_1(^4G)$ to the $^6A_1(^6S)$ state occurs with change of multiplicity and it is therefore assimilable to a phosphorescence, formally forbidden by the selection rules. Luminescence lifetimes are therefore long, from microseconds to milliseconds, making Mn^{II} derivatives of potential interest for the replacement of heavy transition elements and lanthanides in advanced technology. Moreover, the Tanabe-Sugano diagram reveals that the wavelength of the emission depends upon the ligand field

strength, since the increase of the Δ value causes a red-shift of the emission. Such a result can be understood by considering an octahedral complex as an example. The ^6S term implies the $t_{2g}^3e_g^2$ occupation of the d-shell, while in the ^4G term the occupation is $t_{2g}^4e_g^1$. The lower occupation of the e_g orbitals at the excited state reduces the repulsive effect exerted by the surrounding ligands compared to the ground state, therefore the excited state is less destabilized than the ground state on increasing the ligand field strength.

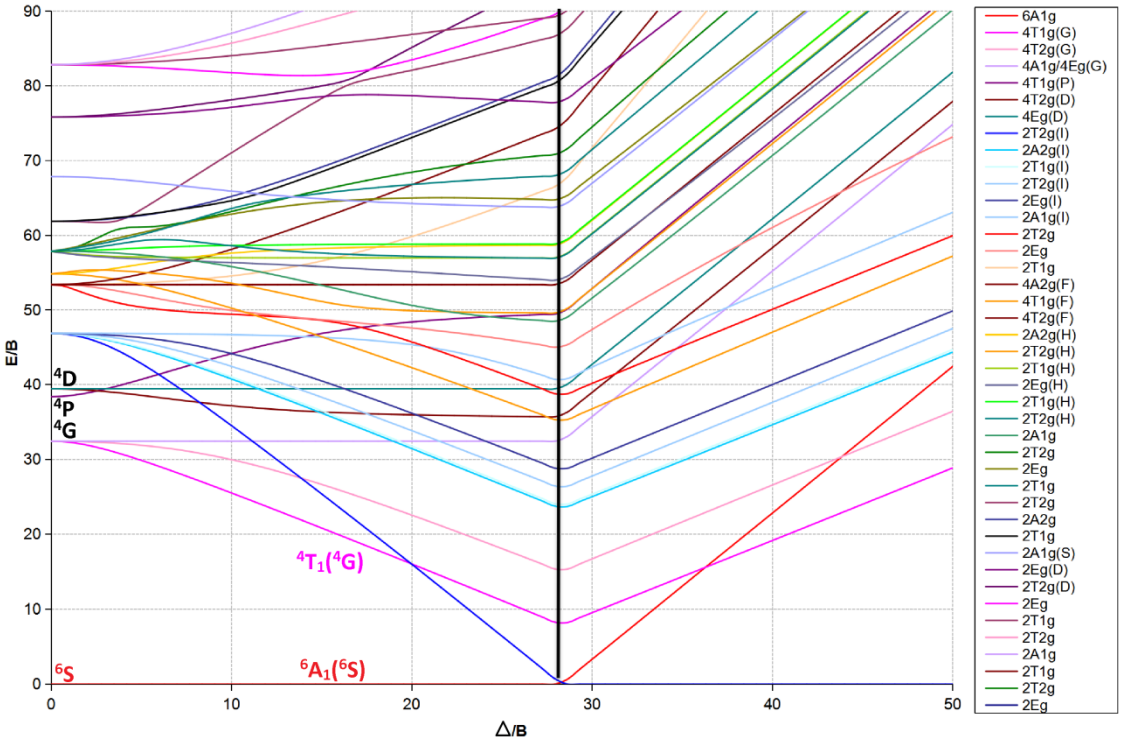

Figure 7. Tanabe-Sugano diagram for a d^5 metal centre. Plot generated thanks to the spreadsheets available at http://wwwchem.uwimona.edu.jm/courses/Tanabe-Sugano/TSspread.html. Δ represents the crystal field strength, while B is the Racah parameter related to the interelectronic repulsions in the d-shell.

The Δ value in Mn^{II} complexes is only in part determined by the nature of the coordinated ligands, given the affinity of the metal centre towards only a limited group of σ-donors. On the other hand, the coordination number plays a role of primary importance. For instance, tetrahedral complexes give emission in the green region, while octahedral derivatives commonly emit in the orange-red region. Such an outcome is in line with the higher energy gap between frontier orbitals in the case of octahedral

field (Δ_o) compared to the tetrahedral one (Δ_t). Figure 8 reports the molecular orbitals diagrams for the ideal octahedral and tetrahedral geometries in the case of σ-donor ligands. It is worth noting that for a high-spin d^5 complex the frontier orbitals are in the case of the octahedral geometry the non-bonding d_{xy}, d_{xz} and d_{yz} and the antibonding orbitals formed by the superposition of $d_{x^2-y^2}$ and d_{z^2} with the SALCs. The transitions have strong d→d character and thus are forbidden by the Laporte rule. In tetrahedral complexes with only σ interactions the frontier orbitals are instead all non-bonding and are pure d orbitals ($d_{x^2-y^2}$, d_{z^2}) and molecular orbitals derived from the superposition of the SALCs with d- and p-type orbitals of the metal centre. The Laporte rule is thus relaxed for tetrahedral complexes by the contribution of p-type orbitals and the lifetime of the radiative decay is expected to be shorter than for luminescent octahedral species.

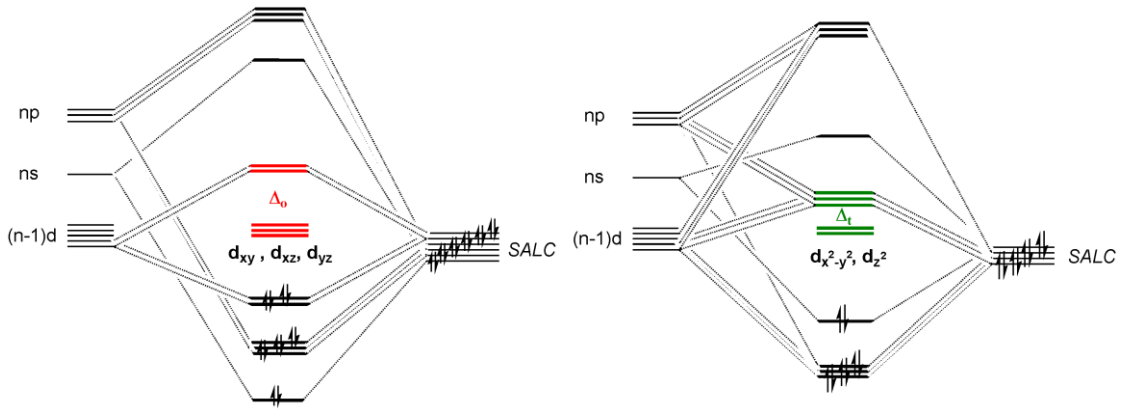

Figure 8. Molecular orbitals diagrams for ideal octahedral (left) and tetrahedral (right) metal complexes with σ interactions.

The Tanabe-Sugano diagram is not helpful to predict the luminescence of less symmetric Mn^{II} complexes, such as the five-coordinated ones. Experimentally, both trigonal bipyramidal and square pyramidal complexes were isolated, with emissions varying from yellow to red.

Considering selected examples of luminescent Mn^{II} derivatives, after Cotton's initial studies on tetrahalomanganate species [26], the metal-centred luminescence of $[MnX_4]^{2-}$ (tetrahedral, green emitter), $[MnX_5]^{3-}$ (trigonal bipyramidal, yellow emitter), $[Mn_3X_{12}]^{6-}$ (octahedral, red emitter) and $[MnX_3]_n^{n-}$ (octahedral, red emitter) anionic halide species have attracted recent interest for advanced technology applications, such as sensors, OLEDs, optical waveguides, X-ray scintillators and multifunctional devices

[27-44]. The general structures of the anions are shown in Figure 9. The luminescence performances of these compounds, sometimes defined as organic-inorganic hybrids, strongly depend upon the choice of the organic counter-cation.

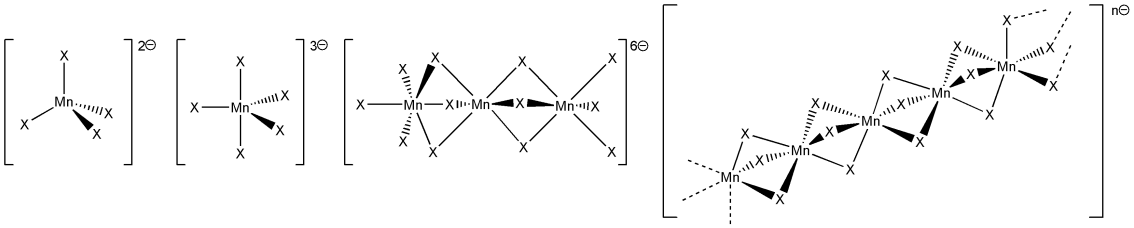

Figure 9. Structures of $[MnX_4]^{2-}$, $[MnX_5]^{3-}$, $[Mn_3X_{12}]^{6-}$ and $[MnX_3]_n^{n-}$ anions.

Noticeable luminescence was also observed by formally replacing some of the halides with suitable species in the Mn^{II} coordination sphere, and the most applied ligands in this field are polar oxygen donors containing the {O=P}-fragment as donor moiety [45,46]. Mono- and polydentate phosphines, phosphoramides, amidophosphates, phosphonates and *H*-phosphinates resulted suitable ligands for the preparation of luminescent Mn^{II} compounds [47-54]. Considering selected examples, the use of triphenylphosphine oxide allowed in the Sixties the isolation of the tetrahedral complex $[MnBr_2(O=PPh_3)_2]$ [55], a compound of current interest because of features such as ferroelectricity and triboluminescence [56-58]. Tetrahedral derivatives obtained by the introduction of selected substituents on one of the phenyl rings of triphenylphosphine oxide showed intense green luminescence applicable for luminescent printing [59].

Besides the energy transfer from the P-bonded organic fragments to the metal centre (antenna effect) and the possible competition between ligand- and metal-centred luminescence, the substituents on the phosphorus atom can influence the final geometry of the complexes and therefore their luminescence features. In particular, the coordination of polydentate phosphine oxides to Mn^{II} afforded in recent years mono-, di- and polynuclear complexes with coordination numbers from four to six, with emission maxima depending upon the coordination geometry [60-62]. Luminescent vapochromism and thermochromism, triboluminescence, polymorphic luminescence, dual emission and excitation-dependent luminescence are among the features to be cited [63-69]. Active materials for OLEDs [70] or for scintillators [71] were obtained by coordinating suitable bidentate phosphine oxides to Mn^{II} halides. Selected examples of

luminescent complexes with [O=P]-donors and different coordination geometries are shown in Figure 10.

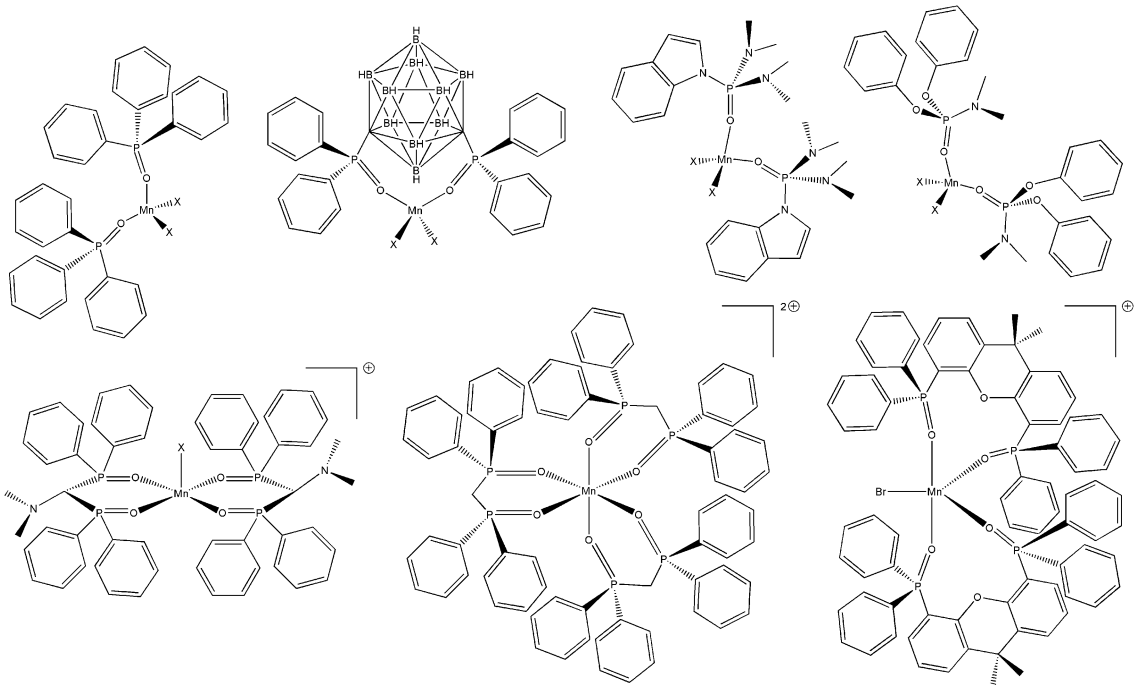

Figure 10. Examples of luminescent Mn^{II} complexes with [O=P]-donors in the coordination sphere.

As commonly occurs for metal centres of the first transition series, coordination numbers higher than six are rare. Among the few examples, the yellow-emitting seven-coordinated complex obtained by Feldmann and co-workers by reacting $MnBr_2$ and 18-crown-6 in ionic liquid exhibited noticeable photoluminescence quantum yield [72]. In this compound, the Mn^{II} centre interacts with two bromide ions and five of the six oxygen atoms of the crown ether.

1.6. Zinc(II) coordination chemistry and luminescence

Another abundant element of interest for the preparation of luminescent materials is zinc. Zinc has atomic number 30 and electronic configuration [Ar]$4s^2 3d^{10}$. The concentration of zinc in Earth's crust is quite high, around 75 ppm. The element is a chalcophile, thus it is commonly found in minerals together with sulphur and other heavy chalcogens. Examples of minerals are sphalerite and wurtzite, two forms of zinc sulfide. After proper doping, ZnS is a semiconducting material of interest for the preparation of luminescent devices such as cathode-ray tubes and X-ray screens. Moreover, ZnS and ZnSe are widely employed for the preparation of luminescent quantum dots, commonly exhibiting strong dependence of the emission maxima upon the size of the nanoparticles [73]. Zinc is also an essential trace element for animals, plants and microorganisms, and it is the second most abundant d-block metal in humans after iron, being involved in many enzymes and generally behaving as acid-base catalyst [14,74].

The main oxidation state is Zn^{II} (d^{10}). Given the relatively small ionic radius, divalent zinc is a quite strong Lewis acid. Complexes derived from Zn^{II} have coordination numbers between four and six and the metal centre tends to form covalent interactions mainly with O-, N- and S-donor ligands, as well as halides and cyanide. As an example, divalent zinc is commonly found in biological systems with imidazole heterocycles derived from histidine residues in the coordination sphere. Tetrahedral, trigonal bipyramidal, square-based pyramidal and octahedral geometries were reported, depending upon the electronic and steric features of the coordinated ligands. The tetrahedral geometry is the most common since it satisfies the 18-electrons rule. Rare examples of Zn^{I} complexes are however present in the literature, usually dinuclear species with Zn-Zn bonds, such as the decamethyldizincocene compound Cp*-Zn-Zn-Cp* (Cp* = pentamethylcyclopentadienide) [75]. Zinc however maintains the 3d shell completely filled in all its oxidation states, therefore it is not considered a transition metal. The Zn-Zn bond in Zn^{I} derivatives is in fact attributed to the overlap of half-filled 4s orbitals.

The Zn^{II} metal centre is diamagnetic, and the completely filled d-shell does not make possible d-d transitions. The absence of stable oxidation states above Zn^{II} disfavours MLCT transitions. Therefore the luminescence of the majority of Zn^{II} complexes reported

is related to fluorescence from ligand-centred or ligand-to-ligand charge transfer excited states, enhanced by coordination to the metal centre [76-88]. The effects of coordination in these cases are an increase of the rigidity of the molecule that disfavours the radiative decay routes, together with an alteration of the energy levels of the ligands caused by the partial delocalization of the electron density on the metal centre. Antibonding σ* molecular orbitals with d-component from Zn^{II} and suitable energy can be however also involved in emitting excited states, with mechanisms considered in between LMCT and LLCT [90-92]. A simplified picture of the excited states for the ideal tetrahedral geometry is provided by the molecular orbitals diagrams reported in Figure 11.

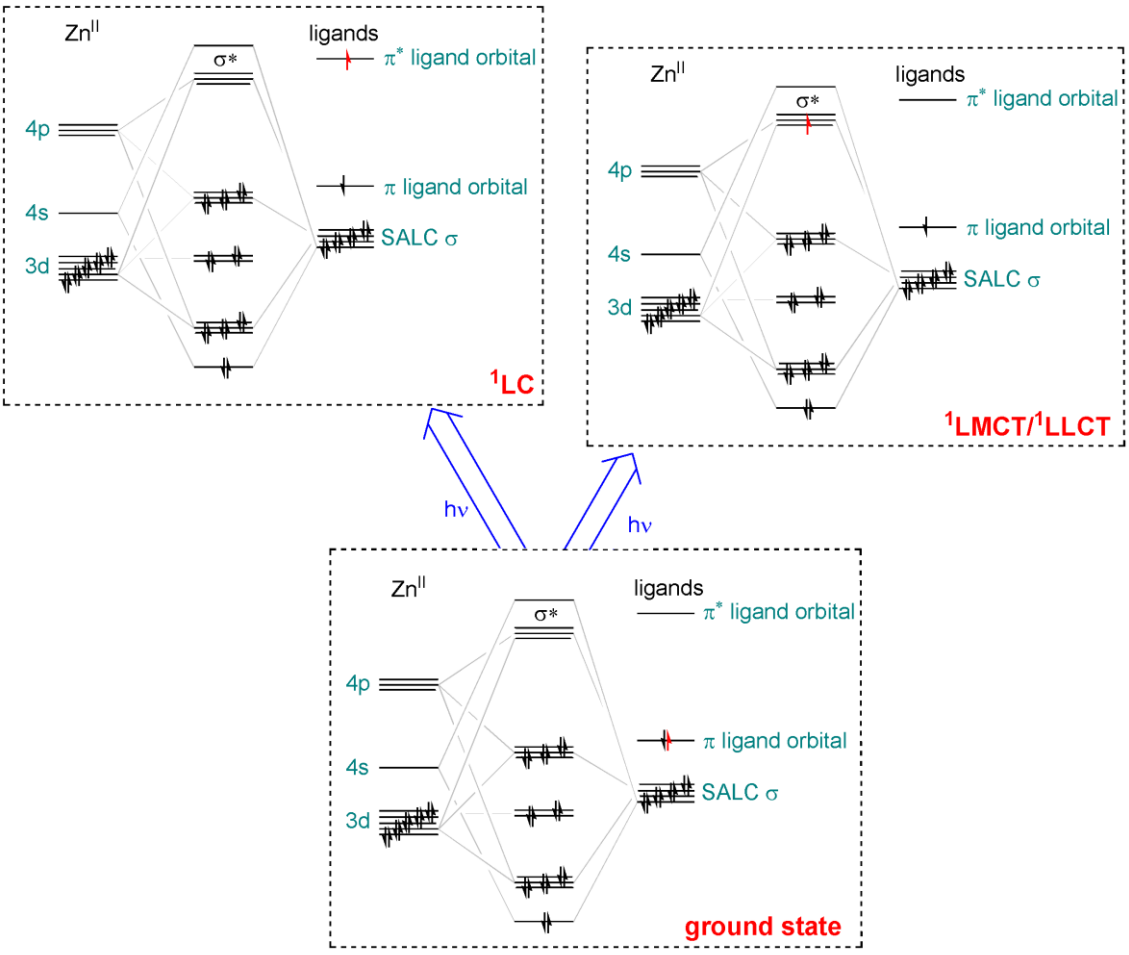

Figure 11. Molecular orbitals diagrams for the tetrahedral geometries representing the ^{1}LC and ^{1}LMCT/^{1}LLCT transitions.

Despite not common, phosphorescence from Zn^{II} complexes is possible when the degree of intersystem crossing is sufficient, and in few cases emissions related to TADF decay were observed [93-95]. In this context, an approach to generate excited states suitable for radiative decay is through the excited state intramolecular proton transfer (ESIPT), where the tautomeric form of the ligand is formed after the excitation. In recent years, zinc(II) complexes with N-donor ligands based on the 1-hydroxy-1*H*-imidazole moiety and characterized by noticeable luminescence due to the population of excited states in tautomeric imidazole N-oxide form were reported [96-101].

The first application of zinc(II) derivatives as emitters for OLEDs dates back to 2000, with complexes having general formula $[Zn(N^O)_2]$ (N^O = 8-hydroxyquinolinate, conjugate base of *N*-methyl salicylimine, 2-(2-benzothiazolyl)phenate) and [Zn(O^N^NO)] (O^N^N^O = conjugate base of *N*,*N*'-disalicylidenehexane-1,6-diamine) [102]. The complexes are depicted in Figure 12. The first examples of blue-phosphorescent complex were reported by Wang and co-workers using diphenyl-6,6'-dimethyl-2,2'-bipyrimidine as chelating ligand (Figure 12). The unusual radiative decay was evidenced by lifetimes in the tents of μs range [103].

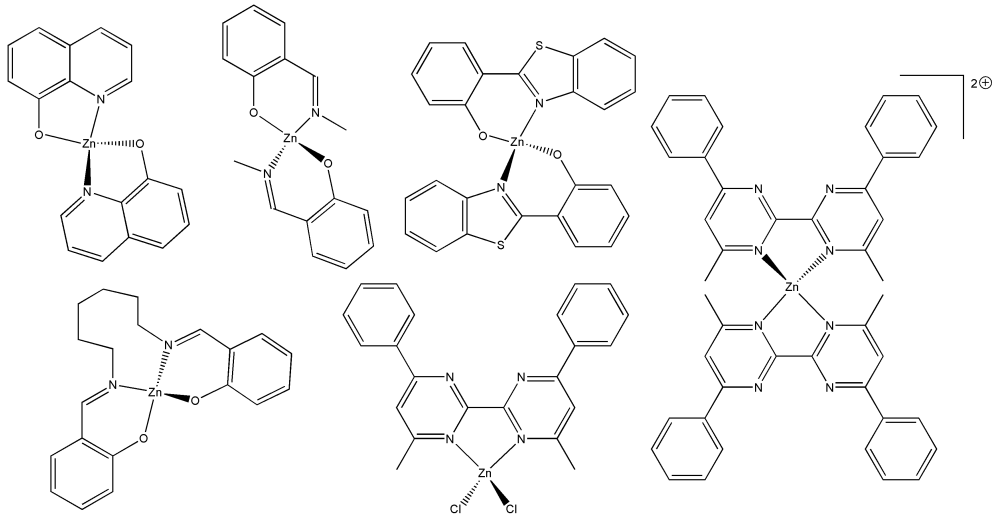

Figure 12. Selected examples of fluorescent and phosphorescent Zn^{II} derivatives.

Most of the luminescent zinc(II) complexes actually reported have imines, five- and six-membered N-donor heterocycles and O-donors derived from phenate moieties in the coordination sphere. Differently from manganese(II), [O=P]-donor ligands were scarcely investigated. Most of the literature outcomes concern the use of triphenylphosphine

oxide in combination with Zn^{II} halides [104-107], but the fluorescence of $[ZnBr_2(O=PPh_3)_2]$ at the solid state was only recently investigated [108]. It is however worth noting that $[ZnCl_2(O=PPh_3)_2]$ exhibited non-linear optical properties [109]. Green phosphorescence from tetrahedral neutral bromo- and iodo-complexes with *N*,*N*,*N*′,*N*′-tetramethyl-*P*-indol-1-ylphosphonic diamide was however observed [108], and the Zn^{II} bromo-complex with the *H*-phosphinate 9,10-dihydro-9-oxa-10-phosphaphenanthrene-10-oxide exhibited dual emission related to the superposition of phosphorescence in the red region and fluorescence centred in the near-UV range [54]. Selected complexes are shown in Figure 13.

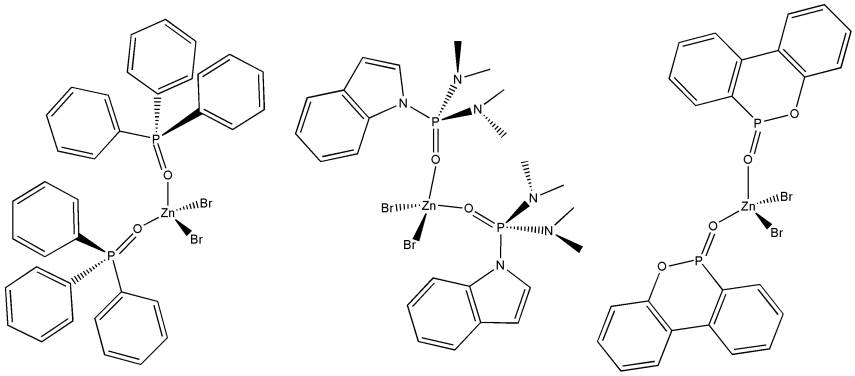

Figure 13. Zinc(II) luminescent complexes with [O=P]-donor ligands.

1.7. Iminophosphoranes as ligands

A class of ligands structurally related to the phosphine oxides is composed by iminophosphoranes (or phosphinimines or phosphazenes), having general formula $NR'=PR_3$. The chemistry of iminophosphophosphoranes started with the pioneering report of Staudinger concerning the oxidation of phosphine with organoazides [110]. From the coordination chemistry point of view, iminophosphoranes are strong σ and π donors because of the presence of a noticeable electron density on the nitrogen atom, highlighted by the ylidic form depicted in Figure 14. The electron-donating properties of the iminophosphorane functions can be tuned via both the N- and the P-bonded substituents. On the other hand, iminophosphoranes do not exhibit π-acidity towards d-block metal centres.

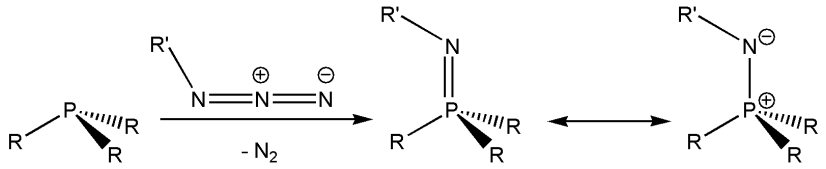

Figure 14. Staudinger reaction and resonance forms of iminophosphoranes.

Iminophosphoranes are considered hard donors and are therefore adapted to interact with electron-deficient metal centres, while they are easily displaced from the coordination sphere of electron-richer metals [111,112]. Nevertheless, mixed ligands in which they are associated with softer coordinative functions can bind to a larger range of metals, and polydentate ligands containing the iminophosphorane moiety were investigated in combination with several d-block metal centres for catalytic applications [113,114].

The studies on the possible use of iminophosphoranes as ligands for the preparation of luminescent complexes appear very limited. A detailed investigation was reported only for gold(III), palladium(II), and platinum(II) complexes with an iminophosphorane ligand bearing an 8-aminoquinoline fragment on the nitrogen atom, that showed phosphorescent emissions attributed to ^{3}LC or ^{3}MLCT transitions [115]. The compounds are depicted in Figure 15.

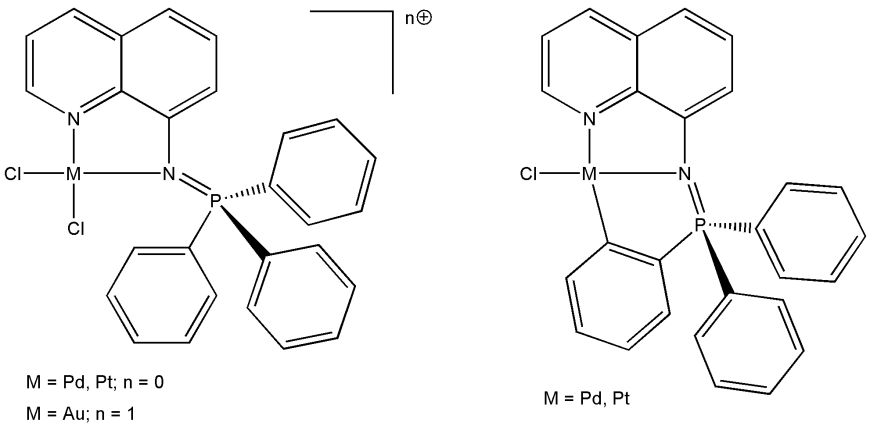

Figure 15. Pd^{II}, Pt^{II} and Au^{III} luminescent iminophosphorane complexes.

For what concerns the metal centres considered in the present thesis, the only examples of manganese(II) complexes actually reported are three-coordinated species obtained from the reaction of bis(phosphinimino)methane ligands with the

bis(trimethylsilylamide) precursor [Mn{N(SiMe$_3$)$_2$}] [116,117]. The reaction is shown in Figure 16. The same synthetic approach was used for the preparation of analogous zinc(II) methyl complexes, starting from dimethylzinc [118]. The reaction was extended to bis(phosphinimino)methane ligands with different substituents on the nitrogen atoms, allowing the preparation of other organometallic zinc(II) complexes [119]. On considering neutral ligands containing only one iminophosphorane moiety, Hayes and co-workers reported some Zn^{II} complexes with ligands functionalized with a dibenzofuran heterocycle bonded to the phosphorus atom [120]. Selected examples are shown in Figure 17. In all the cases, no study concerning the luminescence of the isolated species was carried out.

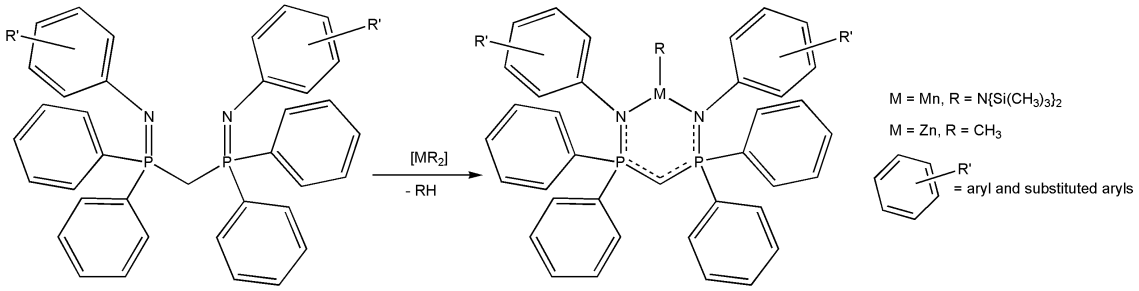

Figure 16. Manganese(II) and zinc(II) complexes with bis(iminophosphorane)-based ligands.

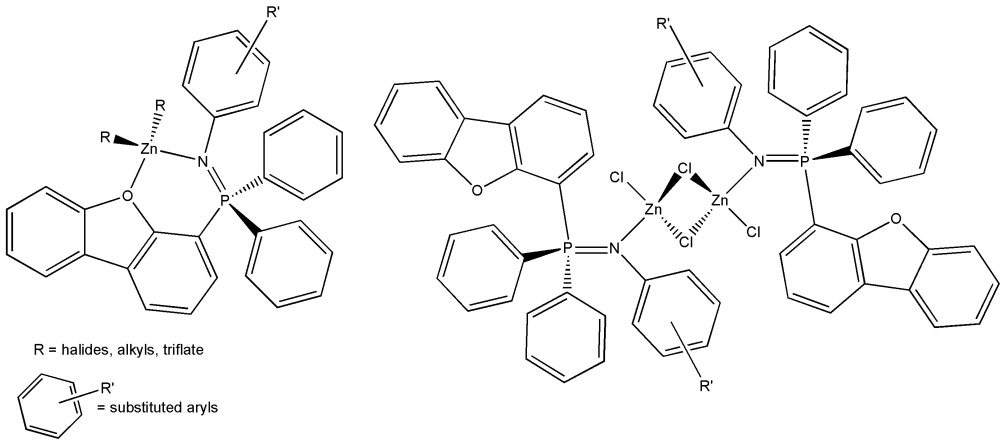

Figure 17. Zn^{II} complexes with iminophosphorane ligands functionalized with a dibenzofurane heterocycle.

2. Aim of the thesis

The first objective of the thesis is the synthesis and characterization of manganese(II) and zinc(II) iminophosphorane halide-complexes, using ligands derived from the functionalization of triphenylphosphine and bis(diphenylphosphino)methane with aromatic and benzylic azides and considering halide derivatives having general formula MX_2 as metal precursors. The roles of the substituents at the nitrogen atoms, of the number of iminophosphorane moieties and of the nature of the coordinated halides in the determination of the geometry of the complexes are of particular interest.

The second objective of the thesis is the determination of the photoluminescence properties of the isolated compounds by means of steady-state and time-resolved luminescence measurements, trying to correlate coordination geometries and luminescence features and to determine reasonable excited states involved in the ligand-metal energy transfers and in the radiative decays, also with the support of computational calculations.

Given the scarce information present in the literature about photoluminescent iminophosphorane coordination compounds, the general aim of the thesis is to verify if iminophosphorane ligands structurally related to well-known phosphine oxides are suitable ligands for the preparation of luminescent complexes of selected earth-abundant d-block elements in their most common oxidation states.

3. Experimental section

3.1. Materials and methods

Commercial solvents (Merck) were purified following procedures described in the literature [121]. Deuterated solvents were Euriso-Top products, used as received. Anhydrous MnX_2 halides (X = Cl, Br, I) were purchased from Alfa Aesar, whereas anhydrous ZnX_2 halides (X = Cl, Br, I) were Merck products. The other inorganic and organic reactants (sodium nitrite, sodium azide, benzyl bromide, 1-(bromomethyl)-4-methylbenzene, triphenylphosphine, bis(diphenylphosphino)methane or DPPM, phenylhydrazine hydrochloride, diisopropyl azodicarboxylate, aniline, *p*-toluidine) were Merck products, used without further purification. The organic azides were prepared under a fume hood following reported methods [122,123]. Safety note: organic azides are potentially explosive compounds. All the manipulations were carried out using limited quantities of reactants, with careful control of the temperature during all the synthetic steps.

The syntheses of the iminophosphorane ligands and of all the complexes were carried out under inert atmosphere, working in a glove box (MBraun Labstar with MB 10 G gas purifier) filled with N_2 and equipped for organic and inorganic syntheses.

Magnetic susceptibilities were measured on solid samples at 298 K using an MK1 magnetic susceptibility balance (Sherwood Scientific ltd, magnetic field strength 3.5 kGauss).

Melting points were registered using a FALC 360 D instrument equipped with a video recording device. Thermogravimetric analyses (TGA) were carried out under N_2 atmosphere with a Perkin Elmer TGA 4000 instrument. The heating rate was set at 10 °C min^{-1} from 35 °C up to 500 °C.

IR spectra were collected in the 4000 – 450 cm^{-1} range using a Perkin-Elmer Spectrum One spectrophotometer. The samples were dispersed in KBr under N_2 atmosphere.

Mono- and bidimensional nuclear magnetic resonance (NMR) spectra were collected employing Bruker Avance 300 and Avance 400 instruments operating respectively at 300.13 MHz and 400.13 MHz of ^1H resonance. ^1H NMR spectra were referred to the

partially non-deuterated fraction of the solvent, itself referred to tetramethylsilane. $^{31}P\{^{1}H\}$ NMR resonances were referred to 85% H_3PO_4 in water.

Absorption spectra in solution were recorded at room temperature with a Yoke 6000Plus double-beam spectrophotometer.

Photoluminescence emission (PL) and excitation (PLE) spectra as well as lifetime decay curves were registered on solid samples at room temperature using a Horiba Jobin Yvon Fluorolog-3 spectrofluorometer. Air-tight quartz sample holders were used and filled in the glove box to avoid interactions of the air-sensible complexes with moisture. A continuous wave xenon arc lamp was used as source and the excitation wavelength was selected using a double Czerny-Turner monochromator. Suitable long-pass filters were placed in front of the acquisition systems. The detector was composed of a single monochromator iHR320 and a photomultiplier tube Hamamatsu R928. Excitation and emission spectra were corrected for the instrumental functions. Time-resolved analyses were performed in Multi Channel Scaling mode (MCS) or time correlated single photon counting mode (TCSPC) employing Horiba SpectraLED and NanoLED pulsed sources. The room-temperature photoluminescence quantum yields (Φ) at the solid state were measured by means of an OceanOptics HR4000CG UV-VIS-NIR detector, fiber-coupled to an integrating sphere connected to OceanOptics UV LED continuous sources ($\lambda_{excitation}$ max = 310 and 365 nm). Values are reported as average of three measurements.

Cyclic voltammetry measurements were performed using an eDAQ ET014-199 instrument in acetone containing 0.1 M $LiClO_4$. All the measurements were carried out under argon at room temperature. The working electrode was 1-mm glassy carbon disk, while the auxiliary electrode was Pt-coated titanium rod. The electrodes were provided by eDAQ. Ferrocene was introduced as internal standard and a Pt wire was used as pseudo-reference electrode.

Computational geometry optimizations, IR simulations and time-dependent DFT (TD-DFT) calculations [124] were carried out using the PBEh-3c method, which is a reparametrized version of the hybrid-GGA PBE0 functional (with 42% HF exchange) that uses a split-valence double-zeta basis set (def2-mSVP) and adds three corrections considering dispersion, basis set superposition and other basis set incompleteness effects [125]. The software used was ORCA version 5.0.3 [126], running on Intel x86-64-based workstations. The output was elaborated using MultiWFN, version 3.8 [127].

3.2. Synthesis of the ligands

3.2.1. Synthesis of $NPh{=}PPh_3$ and $N(CH_2Ph){=}PPh_3$.

The iminophosphorane ligands were prepared based on the same reported procedure, which implied the dissolution of triphenylphosphine in diethyl ether followed by a slow addition of the appropriate azide. Both reactions were carried out in the glovebox under N_2 inert atmosphere, at room temperature, and stirred overnight. The products were filtered right from the solvent and dried *in vacuo*.

N-phenyl-1,1,1-triphenylphosphanimine $NPh{=}PPh_3$.

In a typical preparation to obtain the ligand N-phenyl-1,1,1-triphenylphosphanimine, 1.851 g (7.1 mmol) of triphenylphosphine were dissolved in 30 mL of diethyl ether, then 1.101 g (9.3 mmol) of phenyl azide were slowly added under stirring. The light yellow solid shows photoluminescence in the green region, under the UV lamp. Yield > 70%.

$NPh{=}PPh_3$. M.p. 132 °C (dec.). IR (KBr, cm^{-1}): 3068-3004 (ν_{CH} aromatic), 1590-1437 (ν_{CC} aromatic), 1338 (ν_{NC}), 1106 ($\nu_{PN}+\delta_{CH}$). ^1H NMR ($CDCl_3$, 300 K) δ 7.80 (dd, 6H, J_{HH} = 7.8 Hz, J_{PH} = 11.7 Hz, P-Ph), 7.55 (t, 3H, J_{HH} = 7.8 Hz, P-Ph), 7.48 (m, 6H, P-Ph), 7.06 (t, 2H, J_{HH} = 7.6 Hz, N-Ph), 6.86 (d, 2H, N-Ph), 6.70 (t, 1H, N-Ph). $^{31}P\{^1H\}$ NMR ($CDCl_3$, 300 K) δ 3.1 (s, FWHM = 23 Hz). $^{13}C\{^1H\}$ NMR ($CDCl_3$, 300 K) δ 151.1 (d, J_{PC} = 2.5 Hz, N-Ph, C_{ipso}), 132.7 (d, J_{PC} = 9.5 Hz, P-Ph), 131.7 (d, J_{PC} = 2.8 Hz, P-Ph), 131.1 (d, J_{PC} = 98.9 Hz, P-Ph, C_{ipso}), 128.7 (d, J_{PC} = 1.3 Hz, N-Ph), 128.6 (d, J_{PC} = 12.0 Hz, P-Ph), 123.5 (d, J_{PC} = 17.7 Hz, N-Ph), 117.4 (s, N-Ph). UV-VIS (CH_2Cl_2, r.t., nm): < 400, 342 sh, 298 sh, 256. PL (solid, $\lambda_{excitation}$ = 300 nm, nm): 496 (FWHM = 4800 cm^{-1}). PLE (solid, $\lambda_{emission}$ = 510 nm, nm): < 450. τ (solid, $\lambda_{excitation}$ = 373 nm, $\lambda_{emission}$ = 415 nm, ns): 1.9. Φ (solid, $\lambda_{excitation}$ = 310 nm): < 1%.

N-benzyl-1,1,1-triphenylphosphanimine $N(CH_2Ph){=}PPh_3$.

To synthesize N-benzyl-1,1,1-triphenylphosphanimine, 1.65 g (6.3 mmol) of triphenylphosphine were dissolved in 30 mL of diethyl ether, then 0.787 g (9.3 mmol) of benzyl azide were slowly added under stirring. The light yellow solid shows a pale photoluminescence, in the light blue region, under the UV lamp. Yield > 70%.

$N(CH_2Ph){=}PPh_3$. M.p. 105 °C (dec.). IR (KBr, cm^{-1}): 3071-3022 (ν_{CH} aromatic), 2816-2784 (ν_{CH} alphatic), 1493-1437 (ν_{CC} aromatic), 1115-1105 ($\nu_{PN}+\delta_{CH}$). ^1H NMR ($CDCl_3$, 300 K) δ 7.74 (dd, 6H, J_{HH} = 7.7 Hz, J_{PH} =

10.9 Hz, P-Ph), 7.57-7.40 (m, 11H, CH_2-Ph and P-Ph), 7.29 (t, 2H, J_{HH} = 7.3 Hz, CH_2-Ph), 7.17 (t, 1H, J_{HH} = 7.3 Hz, CH_2-Ph), 4.44 (d, 2H, J_{PH} = 18.3 Hz, CH_2-Ph). $^{31}P\{^1H\}$ NMR ($CDCl_3$, 300 K) δ 12.7 (s, FWHM = 260 Hz). $^{13}C\{^1H\}$ NMR ($CDCl_3$, 300 K) δ 132.7 (d, J_{PC} = 9.2 Hz, P-Ph), 131.5 (d, J_{PC} = 2.2 Hz, P-Ph), 128.5 (d, J_{PC} = 11.7 Hz, P-Ph), 127.8 (s, CH_2-Ph), 127.2 (s, CH_2-Ph), 125.6 (s, CH_2-Ph), 48.7 (d, J_{PC} = 3.2 Hz, CH_2-Ph). C_{ipso} not assigned. UV-VIS (CH_2Cl_2, r.t., nm): < 375, 294 sh, 272, 266, 260. PL (solid, $\lambda_{excitation}$ = 300 nm, nm): 509 (FWHM = 5100 cm^{-1}). PLE (solid, $\lambda_{emission}$ = 520 nm, nm): < 400. τ (solid, $\lambda_{excitation}$ = 373 nm, $\lambda_{emission}$ = 420 nm, ns): 6.9 (average). Φ (solid, $\lambda_{excitation}$ = 310 nm): < 1%.

3.2.2. Synthesis of N(CH_2Tol)=PPh_3.

The procedure to synthesize N-(methylbenzyl)-1,1,1-triphenylphosphanimine N(CH_2Tol)=PPh_3 was slightly different with respect to the solvents used. 1.5 g (5.7 mmol) of triphenylphosphine were dissolved in 20 mL of toluene, then 0.935 g (6.4 mmol) of *p*-methylbenzyl azide were slowly added under stirring. The reaction was stirred overnight. Toluene was removed under reduced pressure, and hexane was used to precipitate the product. The white solid was then filtered and dried *in vacuo*. The product does not show photoluminescence under the UV lamp. Yield > 70%.

N(CH_2Tol)=PPh_3. M.p. 77 °C (dec.). IR (KBr, cm^{-1}): 3074-3007 (ν_{CH} aromatic), 2919, 2798 (ν_{CH} alphatic), 1511-1436 (ν_{CC} aromatic), 1117-1107 (ν_{PN}+δ_{CH}). ^1H NMR ($CDCl_3$, 300 K) δ 7.72 (dd, 6H, J_{HH} = 7.8 Hz, J_{PH} = 11.2 Hz, P-Ph), 7.58-7.38 (m, 9H, P-Ph), 7.36 (d, 2H, J_{HH} = 7.8 Hz, CH_2-Tol), 7.08 (d, 2H, J_{HH} = 7.8 Hz, CH_2-Tol), 4.38 (d, 2H, J_{PH} = 18.3 Hz, CH_2-Tol), 2.33 (s, 3H, Tol). $^{31}P\{^1H\}$ NMR ($CDCl_3$, 300 K) δ 11.0 (s, FWHM = 105 Hz). $^{13}C\{^1H\}$ NMR ($CDCl_3$, 300 K) δ 132.6 (d, J_{PC} = 9.1 Hz, P-Ph), 131.3 (d, J_{PC} = 2.5 Hz, P-Ph), 128.5 (s, CH_2-Tol), 128.4 (d, J_{PC} = 11.7 Hz, P-Ph), 127.1 (s, CH_2-Tol), 48.5 (d, J_{PC} = 3.6 Hz, CH_2-Tol), 21.1 (s, Tol). C_{ipso} not assigned. UV-VIS (CH_2Cl_2, r.t., nm): < 350, 300 sh, 273, 266, 260. PL (solid, $\lambda_{excitation}$ = 350 nm, nm): 503 (FWHM = 5900 cm^{-1}). PLE (solid, $\lambda_{emission}$ = 520 nm, nm): < 400. τ (solid, $\lambda_{excitation}$ = 373 nm, $\lambda_{emission}$ = 430 nm, ns): 4.4 (average). Φ (solid, $\lambda_{excitation}$ = 310 nm): < 1%.

3.2.3. Synthesis of NPh=PPh_2(CH_2)PPh_2=NPh

The ligand 1,1'-methylenebis-(N,1,1-triphenylphosphanimine) NPh=PPh_2(CH_2)PPh_2=NPh was prepared following the same synthetic approach described for the monodentate benzylic iminophosphoranes. The stoichiometry was however different from the previous iminophosphorane, because the ligand is bidentate, and a double amount of azide is required (1 DPPM: 2 azide). [129].

In a typical preparation, 1.19 g (3.1 mmol) of bis(diphenylphosphino)methane (DPPM) were dissolved in 25 ml of toluene, heated at 60 °C, then 0.733 g (6.2 mmol) of phenyl

azide were slowly added under stirring. The reaction was stirred overnight. After cooling down the mixture, almost all the toluene was removed under reduced pressure and a few mL of hexane were added to precipitate the product. The white solid was filtered and then dried *in vacuo*. The product shows photoluminescence in the light-blue region under the UV lamp. Yield > 50%.

NPh=PPh$_2$(CH$_2$)PPh$_2$=NPh. M.p. 128 °C (dec.). IR (KBr, cm^{-1}): 3059-3005 (ν_{CH} aromatic), 1591-1438 (ν_{CC} aromatic), 1331 (ν_{NC}), 1115, 1104 (ν_{PN}+δ_{CH}). ^{1}H NMR ($CDCl_3$, 300 K) δ 7.73 (dd, 8H, J_{HH} = 8.0 Hz, J_{PH} = 11.0 Hz, P-Ph), 7.43 (t, 4H, J_{HH} = 7.6 Hz, P-Ph), 7.31 (dd, 8H, J_{HH} = 7.6 Hz, J_{HH} = 8.0 Hz, P-Ph), 7.02 (t, 4H, J_{HH} = 7.7 Hz, N-Ph), 6.68 (t, 2H, J_{HH} = 7.7 Hz, N-Ph), 6.60 (d, 4H, J_{HH} = 7.7 Hz, N-Ph), 3.72 (t, 2H, J_{PH} = 13.8 Hz, P-CH$_2$-P). ^{31}P{^{1}H} NMR ($CDCl_3$, 300 K) δ -0.5 (s, FWHM = 10 Hz). UV-VIS (CH_2Cl_2, r.t., nm): < 400, 330 sh, 297 sh, 257.

3.2.4. Synthesis of N(CH$_2$Tol)=PPh$_2$(CH$_2$)PPh$_2$=N(CH$_2$Tol)

As for 1,1'-methylenebis-(N,1,1-triphenylphosphanimine), 1,1'-methylenebis-((N-(4-methylbenzyl))-1,1-diphenylphosphanimine) was synthetized in glovebox under N_2 inert atmosphere, following the same synthetic procedure and with 1:2 ratio between DPPM and azide. In a typical preparation, 1.48 g (2.2 mmol) of bis(diphenylphosphino)methane (DPPM) were dissolved in 25 mL of dichloromethane, then 1.195 g (8.1 mmol) of *p*-methylbenzyl azide were slowly added under stirring. The reaction was stirred overnight. Dichloromethane was removed under reduced pressure and hexane ($\approx$ 5ml) was added to precipitate the product. The yellow solid was filtered and then dried *in vacuo*. The product shows photoluminescence in the green region under the UV lamp. Yield > 50%.

N(CH$_2$Tol)=PPh$_2$(CH$_2$)PPh$_2$=N(CH$_2$Tol). M.p. 115 °C (dec.). IR (KBr, cm^{-1}): 3049-3002 (ν_{CH} aromatic), 2917-2772 (ν_{CH} alphatic), 1511-1432 (ν_{CC} aromatic), 1113-1098 (ν_{PN}+δ_{CH}). ^{1}H NMR ($CDCl_3$, 300 K) δ 7.60 (dd, 8H, J_{HH} = 7.8 Hz, J_{PH} = 11.6 Hz, P-Ph), 7.43 (t, 4H, J_{HH} = 7.5 Hz, P-Ph), 7.39-7.20 (m, 8H, P-Ph), 7.11 (d, 4H, J_{HH} = 7.6 Hz, CH$_2$-Tol), 6.99 (d, 4H, J_{HH} = 7.6 Hz, CH$_2$-Tol), 3.90-3.77 (m, 6H, CH$_2$-Tol and P-CH$_2$-P), 2.29 (s, 6H, Tol). ^{31}P{^{1}H} NMR ($CDCl_3$, 300 K) δ 34.2 (s, FWHM = 3 Hz). UV-VIS (CH_2Cl_2, r.t., nm): < 390, 292 sh, 273, 265, 260.

3.3. Synthesis of the complexes

The procedure followed to synthesize metal complexes implied the dissolution of the metal halide in acetonitrile, followed by the addition of the ligand. A centrifuge on the first filtered product, dissolved in 20 mL of dichloromethane, was often used to obtain

a cleaner product. In the case of manganese dichloride, reflux at 80 °C (solvent T_{eb}) was required because of solubility issues. After removing the solvents under reduced pressure, 5 mL of diethyl ether were used to precipitate the final products. All the syntheses were performed in glovebox under N_2 inert atmosphere. Synthesis performed with the monodentate ligands took several hours to occur, while synthesis with the bidentate ligand resulted quite faster.

3.3.1. Synthesis of [ZnBr₂{N(CH₂Ar)=PPh₃}₂] (Ar = Ph, Tol)

[$ZnBr_2${$N(CH_2Ph)=PPh_3$}$_2$].

In a typical preparation, 0.113 g (0.5 mmol) of zinc dibromide were dissolved in 25 mL of acetonitrile, then 0.367 g (1.0 mmol) of *N*-benzyl-1,1,1-triphenylphosphanimine $N(CH_2Ph)=PPh_3$ were added under stirring. After the workup phase, the white solid obtained was dried *in vacuo*. The product shows a weak photoluminescence in the light-blue region under the UV lamp. Yield > 50%.

[$ZnBr_2${$N(CH_2Ph)=PPh_3$}$_2$]. M.p. 143 °C (dec.). IR (KBr, cm^{-1}): 3076-3023 (ν_{CH} aromatic), 2918-2850 (ν_{CH} alphatic), 1589-1435 (ν_{CC} aromatic), 1115-1070 ($\nu_{PN}+\delta_{CH}$). ^{1}H NMR ($CDCl_3$, 300 K) δ 7.90-7.10 (m, 20H, Ph), 4.33 (s, br, 2H, CH_2-Ph). $^{31}P\{^1H\}$ NMR ($CDCl_3$, 300 K) δ 38.6 (s, FWHM = 5 Hz). UV-VIS (CH_2Cl_2, r.t., nm): < 300, 276, 268, 260 sh. PL (solid, $\lambda_{excitation}$ = 300 nm, nm): 463 (FWHM = 7300 cm^{-1}). PLE (solid, $\lambda_{emission}$ = 470 nm, nm): < 430. τ (solid, $\lambda_{excitation}$ = 373 nm, $\lambda_{emission}$ = 460 nm, ns): 5.0. Φ (solid, $\lambda_{excitation}$ = 310 nm): 4%.

[$ZnBr_2${$N(CH_2Tol)=PPh_3$}$_2$].

In a typical preparation, 0.113 g (0.5 mmol) of zinc dibromide were dissolved in 25 mL of acetonitrile, then 0.343 g (0.9 mmol) of N-(methylbenzyl)-1,1,1-triphenylphosphanimine $N(CH_2Tol)=PPh_3$ were added under stirring. After the workup phase, the white solid obtained was dried *in vacuo*. The product shows no photoluminescence under the UV lamp. Yield < 50%.

[$ZnBr_2${$N(CH_2Tol)=PPh_3$}$_2$]. M.p. 157 °C (dec.). IR (KBr, cm^{-1}): 3074-3022 (ν_{CH} aromatic), 2920-2843 (ν_{CH} alphatic), 1589-1411 (ν_{CC} aromatic), 1111-1084 ($\nu_{PN}+\delta_{CH}$). ^{1}H NMR ($CDCl_3$, 300 K) δ 7.80 (dd, 6H, J_{HH} = 7.8 Hz, J_{PH} = 12.9 Hz, P-Ph), 7.72 (t, 3H, J_{HH} = 7.4 Hz, P-Ph), 7.60 (m, 6H, P-Ph), 7.07 (d, 2H, J_{HH} = 7.7 Hz, CH_2-Tol), 6.94 (d, 2H, J_{HH} = 7.7 Hz, CH_2-Tol), 4.33 (d, 2H, J_{HH} = 14.9 Hz, CH_2-Tol), 2.26 (s, 3H, Tol). $^{31}P\{^1H\}$ NMR ($CDCl_3$, 300 K) δ 38.4 (s, FWHM = 4 Hz). $^{13}C\{^1H\}$ NMR ($CDCl_3$, 300 K) δ 134.7 (d, J_{PC} = 3.0 Hz, P-Ph), 133.8 (d, J_{PC} = 11.1 Hz, P-Ph), 129.8 (d, J_{PC} = 13.1 Hz, P-Ph), 129.0 (s, CH_2-Tol), 128.3 (s, CH_2-Tol), 45.8 (d, J_{PC} = 1.6 Hz, CH_2-Tol), 21.1 (s, Tol). C_{ipso} not assigned. UV-VIS (CH_2Cl_2, r.t., nm): < 400, 275, 268, 262. PL (solid, $\lambda_{excitation}$

= 300 nm, nm): 470 (FWHM = 6800 cm^{-1}). PLE (solid, $\lambda_{emission}$ = 570 nm, nm): < 370, max 314. τ (solid, $\lambda_{excitation}$ = 373 nm, $\lambda_{emission}$ = 470 nm, ns): 7.0 (average). Φ (solid, $\lambda_{excitation}$ = 310 nm): 5%.

3.3.2. Synthesis of $[MnX_2\{N(CH_2Ph)=PPh_3\}_2]$ (X = Cl, Br, I)

$[MnCl_2\{N(CH_2Ph)=PPh_3\}_2]$.

In a typical preparation, 0.063 g (0.5 mmol) of manganese dichloride were dissolved in 25 mL of acetonitrile and refluxed at 80 °C. After manganese chloride dissolved into the solvent, the mixture was cooled down, to avoid the degradation of the ligand. Then, 0.367 g (1.0 mmol) of N-benzyl-1,1,1-triphenylphosphanimine $N(CH_2Ph)=PPh_3$ were added under stirring. After the workup phase, the light-pink solid obtained was dried *in vacuo*. The product shows photoluminescence in the orange region under the UV lamp. Yield > 50%.

$[MnCl_2\{N(CH_2Ph)=PPh_3\}_2]$. M.p. 80 °C (dec.). χ_M^{corr} (cgsu): $1.50 \cdot 10^{-2}$. IR (KBr, cm^{-1}): 3078-3023 (ν_{CH} aromatic), 2918-2850 (ν_{CH} alphatic), 1588-1438 (ν_{CC} aromatic), 1114-1071 ($\nu_{PN}+\delta_{CH}$). $^{31}P\{^1H\}$ NMR ($CDCl_3$, 300 K) δ 39.2 (s, FWHM = 66 Hz). UV-VIS (CH_2Cl_2, r.t., nm): < 400, 300 sh, 276, 268, 261. PL (solid, $\lambda_{excitation}$ = 290 nm, nm): 515 sh, 597. PL (solid, $\lambda_{excitation}$ = 346 nm, nm): 597 (FWHM = 2500 cm^{-1}). PL (solid, $\lambda_{excitation}$ = 437 nm, nm): 597 (FWHM = 2500 cm^{-1}). PLE (solid, $\lambda_{emission}$ = 595 nm, nm): 503 (weak), 454 (weak), 437 (weak), < 375. PLE (solid, $\lambda_{emission}$ = 595 nm, nm): 300-390 (weak), < 300. τ (solid, $\lambda_{excitation}$ = 445 nm, $\lambda_{emission}$ = 595 nm, μs): 1329. Φ (solid, $\lambda_{excitation}$ = 310 nm): 3%.

$[MnBr_2\{N(CH_2Ph)=PPh_3\}_2]$.

In a typical preparation, 0.1075 g (0.5 mmol) of manganese dibromide were dissolved in 25 mL of acetonitrile at room temperature. 0.367 g (1.0 mmol) of N-benzyl-1,1,1-triphenylphosphanimine $N(CH_2Ph)=PPh_3$ were then added under stirring. After the workup phase, the light pink solid obtained was dried *in vacuo*. The product shows photoluminescence in the orange region under the UV lamp. Yield < 50%.

$[MnBr_2\{N(CH_2Ph)=PPh_3\}_2]$. M.p. 96 °C (dec.). χ_M^{corr} (cgsu): $1.45 \cdot 10^{-2}$. IR (KBr, cm^{-1}): 3073-3021 (ν_{CH} aromatic), 2918-2849 (ν_{CH} alphatic), 1588-1438 (ν_{CC} aromatic), 1113-1069 ($\nu_{PN}+\delta_{CH}$). $^{31}P\{^1H\}$ NMR ($CDCl_3$, 300 K) δ 39.3 (s, FWHM = 33 Hz). UV-VIS (CH_2Cl_2, r.t., nm): < 400, 276, 268, 260. PL (solid, $\lambda_{excitation}$ = 300 nm, nm): 589 (FWHM = 2400 cm^{-1}). PL (solid, $\lambda_{excitation}$ = 430 nm, nm): 589 (FWHM = 2400 cm^{-1}). PLE (solid, $\lambda_{emission}$ = 590 nm, nm): 503 (weak), 460 (weak), 440 (weak), < 390. τ (solid, $\lambda_{excitation}$ = 290 nm, $\lambda_{emission}$ = 590 nm, μs): 836. Φ (solid, $\lambda_{excitation}$ = 310 nm): 4%.

[MnI_2{$N(CH_2Ph)=PPh_3$}$_2$].

In a typical preparation, 0.154 g (0.5 mmol) of manganese diiodide were dissolved in 25 mL of acetonitrile. 0.367 g (1.0 mmol) of N-benzyl-1,1,1-triphenylphosphanimine $N(CH_2Ph)=PPh_3$ were then added under stirring. The reaction was stirred overnight. After the workup phase, the light-pink solid was dried *in vacuo*. The product shows photoluminescence in the green region under the UV lamp. Yield < 50%.

[MnI_2{$N(CH_2Ph)=PPh_3$}$_2$]. M.p. 95 °C (dec.). χ_M^{corr} (cgsu): $1.75 \cdot 10^{-2}$. IR (KBr, cm^{-1}): 3077-3022 (ν_{CH} aromatic), 2908-2850 (ν_{CH} alphatic), 1588-1433 (ν_{CC} aromatic), 1128-1071 ($\nu_{PN}+\delta_{CH}$). $^{31}P\{^1H\}$ NMR ($CDCl_3$, 300 K) δ 39.2 (s, FWHM = 18 Hz). UV-VIS (CH_2Cl_2, r.t., nm): < 350, 298 sh, 276, 269, 262. PL (solid, $\lambda_{excitation}$ = 320 nm, nm): 465 sh, 538. PLE (solid, $\lambda_{emission}$ = 538 nm, nm): 470 (weak), < 400. τ (solid, $\lambda_{excitation}$ = 290 nm, $\lambda_{emission}$ = 540 nm, μs): 64 (71%), 293 (29%). Φ (solid, $\lambda_{excitation}$ = 310 nm): 1%.

3.3.3. Synthesis of [$ZnX_2(NPh=PPh_3)_2$] (X = Cl, Br, I)

[$ZnCl_2(NPh=PPh_3)_2$].

In a typical preparation, 0.068 g (0.5 mmol) of zinc dichloride were dissolved in 25 of mL acetonitrile, then 0.353 g (1.0 mmol) of N-phenyl-1,1,1-triphenylphosphanimine were added under stirring. After the workup phase, the white solid was dried *in vacuo*. The product shows a weak photoluminescence in the light blue region under the UV lamp. Yield < 50%.

[$ZnCl_2(NPh=PPh_3)_2$]. M.p. 172 °C (dec.). IR (KBr, cm^{-1}): 3145-3021 (ν_{CH} aromatic), 1590-1438 (ν_{CC} aromatic), 1336 (ν_{NC}), 1109 ($\nu_{PN}+\delta_{CH}$). ^1H NMR ($CDCl_3$, 300 K) δ 8.00-7.40 (m, br, 15H, P-Ph), 7.22-6.85 (m, br, 5H, N-Ph). $^{31}P\{^1H\}$ NMR ($CDCl_3$, 300 K) δ 31.2 (s, FWHM = 100 Hz). UV-VIS (CH_2Cl_2, r.t., nm): < 400, 333 sh, 302, 258 sh. PL (solid, $\lambda_{excitation}$ = 320 nm, nm): 509 (FWHM = 5300 cm^{-1}). PLE (solid, $\lambda_{emission}$ = 520 nm, nm): < 470, max 360. τ (solid, $\lambda_{excitation}$ = 373 nm, $\lambda_{emission}$ = 520 nm, ns): 76 (20%), 478 (80%). Φ (solid, $\lambda_{excitation}$ = 310 nm): 2% (approximate, photodecomposition).

[$ZnBr_2(NPh=PPh_3)_2$].

In a typical preparation, 0.113 g (0.5 mmol) of zinc dibromide were dissolved in 25 mL of acetonitrile, then 0.353 g (1.0 mmol) of N-phenyl-1,1,1-triphenylphosphanimine were added under stirring. After the workup phase, the white solid was dried *in vacuo*. The

product shows a weak photoluminescence in the light blue region under the UV lamp. Yield > 50%.

[$ZnBr_2(NPh=PPh_3)_2$]. M.p. 134 °C (dec.). IR (KBr, cm^{-1}): 3094-3023 (ν_{CH} aromatic), 1590-1435 (ν_{CC} aromatic), 1337 (ν_{NC}), 1160 ($\nu_{PN}+\delta_{CH}$). ^1H NMR ($CDCl_3$, 300 K) δ 8.00-7.35 (m, br, 15H, P-Ph), 7.15-6.80 (m, br, 5H, N-Ph). $^{31}P\{^1H\}$ NMR ($CDCl_3$, 300 K) δ 32.0 (s, FWHM = 106 Hz). UV-VIS (CH_2Cl_2, r.t., nm): < 400, 335 sh, 262 sh. PL (solid, $\lambda_{excitation}$ = 350 nm, nm): 510 (FWHM = 5300 cm^{-1}). PLE (solid, $\lambda_{emission}$ = 510 nm, nm): < 470, max 347. τ (solid, $\lambda_{excitation}$ = 373 nm, $\lambda_{emission}$ = 510 nm, ns): 222 (av.). τ (solid, $\lambda_{excitation}$ = 290 nm, $\lambda_{emission}$ = 510 nm, μs): 303 (av.). Φ (solid, $\lambda_{excitation}$ = 310 nm): 3% (approximate, photodecomposition).

[$ZnI_2(NPh=PPh_3)_2$].

In a typical preparation, 0.160 g (0.5 mmol) of zinc dibromide were dissolved in 25 mL acetonitrile, then 0.353 g (1.0 mmol) of N-phenyl-1,1,1-triphenylphosphanimine were added under stirring. After the workup phase, the white solid was dried *in vacuo*. The product shows photoluminescence between the green and the blue region under the UV lamp. Yield < 50%.

[$ZnI_2(NPh=PPh_3)_2$]. M.p. 112 °C (dec.). IR (KBr, cm^{-1}): 3080-3025 (ν_{CH} aromatic), 1590-1438 (ν_{CC} aromatic), 1340 (ν_{NC}), 1112 ($\nu_{PN}+\delta_{CH}$). ^1H NMR ($CDCl_3$, 300 K) δ 8.00-7.35 (m, br, 15H, P-Ph), 7.20-6.80 (m, br, 5H, N-Ph). $^{31}P\{^1H\}$ NMR ($CDCl_3$, 300 K) δ 31.7 (s, FWHM = 29 Hz). UV-VIS (CH_2Cl_2, r.t., nm): < 400, 299 sh, 276, 268. PL (solid, $\lambda_{excitation}$ = 350 nm, nm): 505 (FWHM = 5200 cm^{-1}). PLE (solid, $\lambda_{emission}$ = 510 nm, nm): < 470, max 349. τ (solid, $\lambda_{excitation}$ = 373 nm, $\lambda_{emission}$ = 510 nm, ns): 254 (av.). τ (solid, $\lambda_{excitation}$ = 290 nm, $\lambda_{emission}$ = 510 nm, μs): 555 (av.). Φ (solid, $\lambda_{excitation}$ = 310 nm): 1% (approximate, photodecomposition).

3.3.4. Synthesis of [$MnX_2(NPh=PPh_3)_2$] (X = Cl, Br, I)

[$MnCl_2(NPh=PPh_3)_2$].

In a typical preparation, 0.063 g (0.5 mmol) of manganese dichloride were dissolved in 25 mL of acetonitrile and refluxed at 80°C. After manganese chloride dissolved into the solvent, the mixture was cooled down, to avoid the degradation of the ligand. Then 0.353 g (1.0 mmol) of N-phenyl-1,1,1-triphenylphosphanimine were added under

stirring. After the workup phase, the white solid was dried *in vacuo*. The product shows photoluminescence in the green region under the UV lamp. Yield < 50%.

[$MnCl_2(NPh{=}PPh_3)_2$]. M.p. 88 °C (dec.). χ_M^{corr} (cgsu): $1.65 \cdot 10^{-2}$. IR (KBr, cm^{-1}): 3055 (ν_{CH} aromatic), 1590-1438 (ν_{CC} aromatic), 1345 (ν_{NC}), 1113 ($\nu_{PN}+\delta_{CH}$). $^{31}P\{^1H\}$ NMR ($CDCl_3$, 300 K) δ 38.1 (s, FWHM = 855 Hz). UV-VIS (CH_2Cl_2, r.t., nm): < 400, 338 sh, 299 sh, 275 sh, 267, 261. PL (solid, $\lambda_{excitation}$ = 350 nm, nm): 460 sh, 530 (FWHM = 2900 cm^{-1}). PLE (solid, $\lambda_{emission}$ = 560 nm, nm): 447 (weak), 432 (weak), < 425, max 359. τ (solid, $\lambda_{excitation}$ = 290 nm, $\lambda_{emission}$ = 530 nm, μs): 1658 (72%), 423 (28%). τ (solid, $\lambda_{excitation}$ = 373 nm, $\lambda_{emission}$ = 410 nm, ns): 2.

[$MnBr_2(NPh{=}PPh_3)_2$].

In a typical preparation, 0.1075 g (0.5 mmol) of manganese dibromide were dissolved in 25 mL acetonitrile, then 0.353 g (1.0 mmol) of N-phenyl-1,1,1-triphenylphosphanimine were added under stirring. After the workup phase, the light-pink solid was dried *in vacuo*. The product shows photoluminescence in the green region under the UV lamp. Yield < 50%.

[$MnBr_2(NPh{=}PPh_3)_2$]. M.p. 177 °C (dec.). χ_M^{corr} (cgsu): $1.60 \cdot 10^{-2}$. IR (KBr, cm^{-1}): 3078-3024 (ν_{CH} aromatic), 1590-1438 (ν_{CC} aromatic), 1340 (ν_{NC}), 1110 ($\nu_{PN}+\delta_{CH}$). $^{31}P\{^1H\}$ NMR ($CDCl_3$, 300 K) δ 25.5 (s, FWHM = 1100 Hz). UV-VIS (CH_2Cl_2, r.t., nm): < 350, 277, 269, 263. PL (solid, $\lambda_{excitation}$ = 360 nm, nm): 529 (FWHM = 2600 cm^{-1}). PLE (solid, $\lambda_{emission}$ = 570 nm, nm): 455, 435, 375, 361, 337 sh, < 300. τ (solid, $\lambda_{excitation}$ = 290 nm, $\lambda_{emission}$ = 580 nm, μs): 235. Φ (solid, $\lambda_{excitation}$ = 365 nm): 22%.

[$MnI_2(NPh{=}PPh_3)_2$].

In a typical preparation, 0.154 g (0.5 mmol) of manganese diiodide were dissolved in 25 mL of acetonitrile, then 0.353 g (1.0 mmol) of N-phenyl-1,1,1-triphenylphosphanimine were added under stirring. After the workup phase, the yellowish-green solid was dried *in vacuo*. The product shows intense photoluminescence in the green region under the UV lamp. Yield < 50%.

[$MnI_2(NPh{=}PPh_3)_2$]. M.p. 93 °C (dec.). χ_M^{corr} (cgsu): $1.46 \cdot 10^{-2}$. IR (KBr, cm^{-1}): 3077-3034 (ν_{CH} aromatic), 1599-1438 (ν_{CC} aromatic), 1395 (ν_{NC}), 1113 ($\nu_{PN}+\delta_{CH}$). $^{31}P\{^1H\}$ NMR ($CDCl_3$, 300 K) δ 37.0 (s, FWHM = 88 Hz). UV-VIS (CH_2Cl_2, r.t., nm): < 400, 364, 295 sh, 276, 268. PL (solid, $\lambda_{excitation}$ = 388 nm, nm): 538 (FWHM = 2200 cm^{-1}). PLE (solid, $\lambda_{emission}$ = 570 nm, nm): 470, 445 sh, 390, 372, < 360. τ (solid, $\lambda_{excitation}$ = 290 nm, $\lambda_{emission}$ = 530 nm, μs): 48. Φ (solid, $\lambda_{excitation}$ = 365 nm): 7%.

3.3.5. Synthesis of [$MnBr_2${$N(CH_2Tol){=}PPh_2(CH_2)PPh_2{=}N(CH_2Tol)$}] and [$MnBr_2${$NPh{=}PPh_2(CH_2)PPh_2{=}NPh$}]

[$MnBr_2${$N(CH_2Tol){=}PPh_2(CH_2)PPh_2{=}N(CH_2Tol)$}].

The synthesis was performed in glovebox under N_2 inert atmosphere, following a procedure similar to the ones previously reported for the monodentate complexes, but changing the stoichiometry. 0.161g (0.7 mmol) of manganese dibromide were dissolved in 25 mL of acetonitrile, then 0.680 g (1.0 mmol) of 1,1'-methylenebis-((N-(4-methylbenzyl))-1,1-diphenylphosphanimine) were added under stirring. The product suddenly precipitated and was easily filtered. The solid was dissolved in 25 mL of dichloromethane to be centrifuged, since a first IR characterization showed the presence of acetonitrile. After the centrifuge, almost all dichloromethane was removed under reduced pressure, but no solid precipitated. Therefore, all dichloromethane was removed this time and 5 mL of diethyl ether afforded the precipitation. The white solid was filtered and dried *in vacuo*. The product shows photoluminescence in the reddish-orange region under the UV lamp and no traces of acetonitrile were detected in the IR spectrum. Yield <50%.

[$MnBr_2${$N(CH_2Tol){=}PPh_2(CH_2)PPh_2{=}N(CH_2Tol)$}]. M.p. 150 °C (dec.). χ_M^{corr} (cgsu): $1.45 \cdot 10^{-2}$. IR (KBr, cm^{-1}): 3080-3015 (ν_{CH} aromatic), 2916-2852 (ν_{CH} alphatic), 1589-1438 (ν_{CC} aromatic), 1124-1085 ($\nu_{PN}+\delta_{CH}$). $^{31}P\{^1H\}$ NMR ($CDCl_3$, 300 K) δ 36.0 (s, FWHM = 104 Hz). UV-VIS (CH_2Cl_2, r.t., nm): < 400, 295 sh, 274, 268, 262. PL (solid, $\lambda_{excitation}$ = 350 nm, nm): 524 (minor), 627 (FWHM = 2200 cm^{-1}). PLE (solid, $\lambda_{emission}$ = 590 nm, nm): 489, 457, 443 sh, < 400. τ (solid, $\lambda_{excitation}$ = 290 nm, $\lambda_{emission}$ = 620 nm, μs): 824. τ (solid, $\lambda_{excitation}$ = 290 nm, $\lambda_{emission}$ = 505 nm, μs): 416. Φ (solid, $\lambda_{excitation}$ = 310 nm): 9%.

[$MnBr_2\{NPh{=}PPh_2(CH_2)PPh_2{=}NPh\}$].

As for the previous bidentate metal complex, the procedure followed was the same. A white-pink solid was obtained, showing reddish orange emission under the UV lamp. Yield < 50%.

[$MnBr_2\{NPh{=}PPh_2(CH_2)PPh_2{=}NPh\}$]. M.p. 200 °C (dec.). χ_M^{corr} (cgsu): $1.72 \cdot 10^{-2}$. IR (KBr, cm^{-1}): 3078-3024 (ν_{CH} aromatic), 2926-2851 (ν_{CH} aliphatic), 1592-1438 (ν_{CC} aromatic), 1351 (ν_{NC}), 1112-1039 ($\nu_{PN}+\delta_{CH}$). $^{31}P\{^1H\}$ NMR ($CDCl_3$, 300 K) δ 26.7 (s, FWHM = 62 Hz). UV-VIS (CH_2Cl_2, r.t., nm): < 375, 276 sh, 268. PL (solid, $\lambda_{excitation}$ = 350 nm, nm): 602 (FWHM = 2000 cm^{-1}). PLE (solid, $\lambda_{emission}$ = 590 nm, nm): 489, 449, 435 sh, 398, < 385. τ (solid, $\lambda_{excitation}$ = 445 nm, $\lambda_{emission}$ = 600 nm, μs): 1697. Φ (solid, $\lambda_{excitation}$ = 310 nm): 6%.

4. Results and discussion

4.1. Synthesis and luminescence of monodentate iminophosphoranes and of the related zinc(II) complexes

The experimental activity started with the preparation of iminophosphorane derivatives obtained from the reaction of triphenylphosphine with benzylic or aromatic azides. In particular, benzyl azide N_3CH_2Ph and *p*-methylbenzyl azide N_3CH_2Tol were synthesized in nearby quantitative yield from the corresponding organic bromides through displacement reaction with sodium azide. Phenyl azide N_3Ph was instead obtained in moderate yield from the nitrosation of phenylhydrazine (Scheme 1) [122,123]. Given the potentially dangerous purification steps usually involved in the preparation of the thermally unstable N_3Ph, another synthetic approach recently reported in the literature was considered [130]. Several attempts were carried out but the reaction, based on the activation of triphenylphosphine with diisopropyl azodicarboxylate followed by the attack of aniline or *p*-toluidine, never afforded the desired product. N_3Ph was however obtained in pure form without distillation steps through chromatography on silica column, using pentane as eluent.

The reaction between PPh_3 and the organic azides allowed to isolate the iminophosphorane ligands *N*-benzyl-1,1,1-triphenylphosphanimine $N(CH_2Ph)=PPh_3$, *N*-(methylbenzyl)-1,1,1-triphenylphosphanimine $N(CH_2Tol)=PPh_3$ and *N*-phenyl-1,1,1-triphenylphosphanimine $NPh=PPh_3$ under mild conditions (Scheme 1). The syntheses were carried out under inert atmosphere to avoid the decomposition of the P=N bond by moisture. The characterization data are in line with literature outcomes [112,128]. The presence of P=N bonds was indirectly confirmed by the methylene resonances in the ^1H NMR spectra of $N(CH_2Ph)=PPh_3$ and $N(CH_2Tol)=PPh_3$, corresponding to doublets around 4.4 ppm with $^4J_{PH}$ coupling constant of 18.3 Hz. The coupling of some of the carbon atoms of the N-bonded phenyl ring with the ^{31}P nucleus was instead diagnostic in the case of $NPh=PPh_3$. For instance, the ^{13}C nuclei in *ortho* position resonate at 123.5 ppm with a $^3J_{PC}$ coupling constant of 17.7 Hz. For what concerns other diagnostic signals, the methyl substituent of $N(CH_2Tol)=PPh_3$ corresponds to a sharp singlet at 2.33 ppm in

the ^{1}H NMR spectrum, while the other *p*-tolyl hydrogen atoms are associated with a pseudo-*AB* spin system between 7.38 and 7.06 ppm. In all the cases a single ^{31}P{^{1}H} NMR resonance was detected, between 11 and 12.7 ppm for the benzylic iminophosphoranes and at 3.1 ppm for NPh=PPh$_3$. Selected NMR spectra are shown in Figures 18-20.

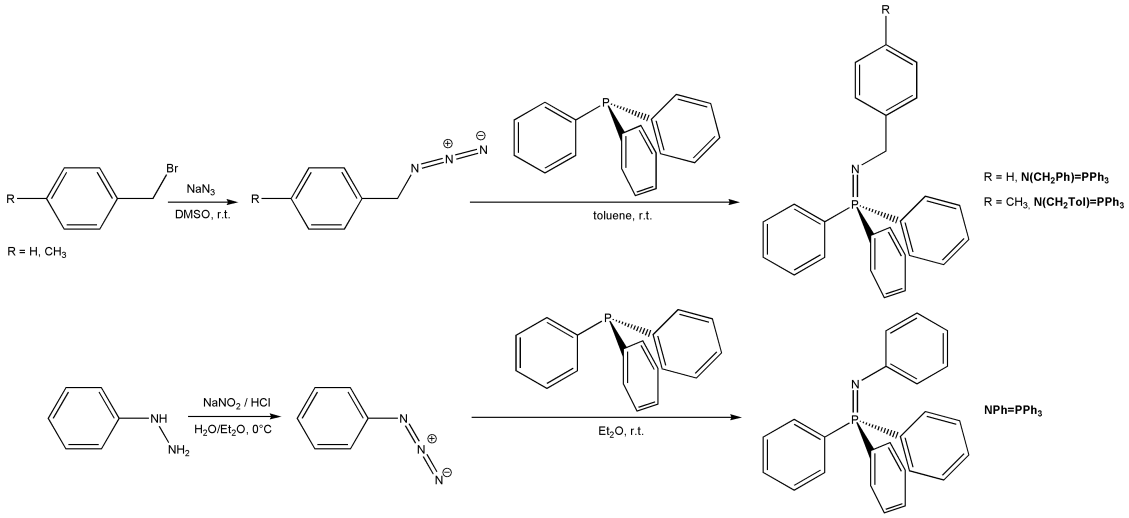

Scheme 1. Synthesis of the iminophosphoranes N(CH$_2$Ph)=PPh$_3$, N(CH$_2$Tol)=PPh$_3$ and NPh=PPh$_3$.

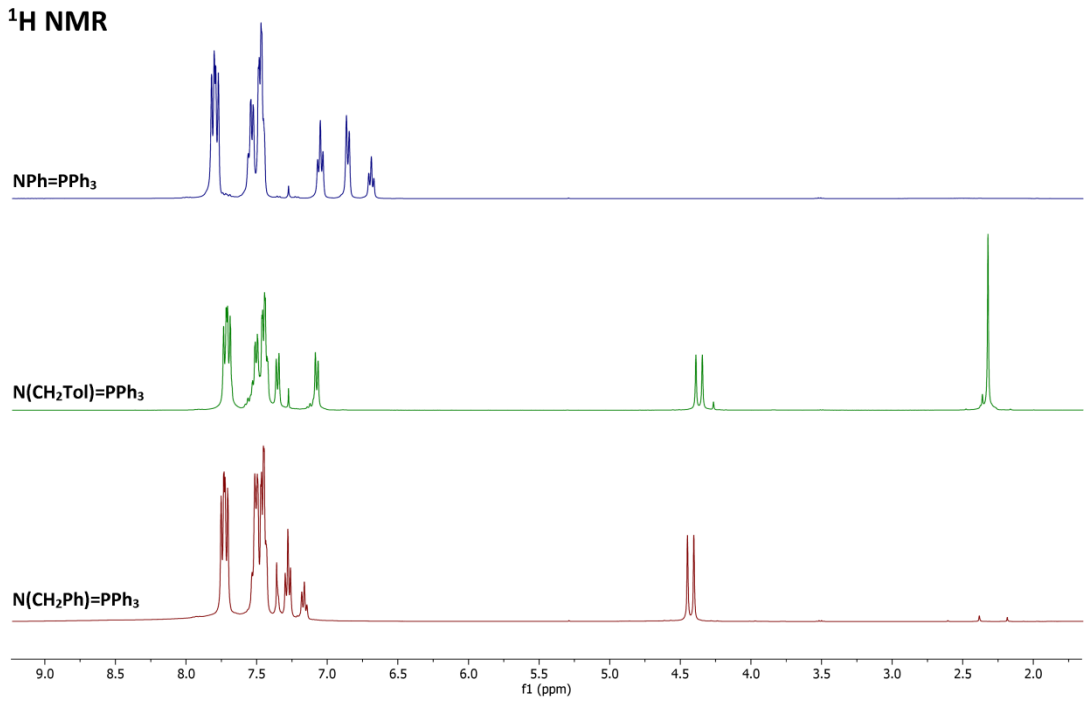

Figure 18. ^{1}H NMR spectra of N(CH$_2$Ph)=PPh$_3$, N(CH$_2$Tol)=PPh$_3$ and NPh=PPh$_3$ (CDCl$_3$, 300 K).

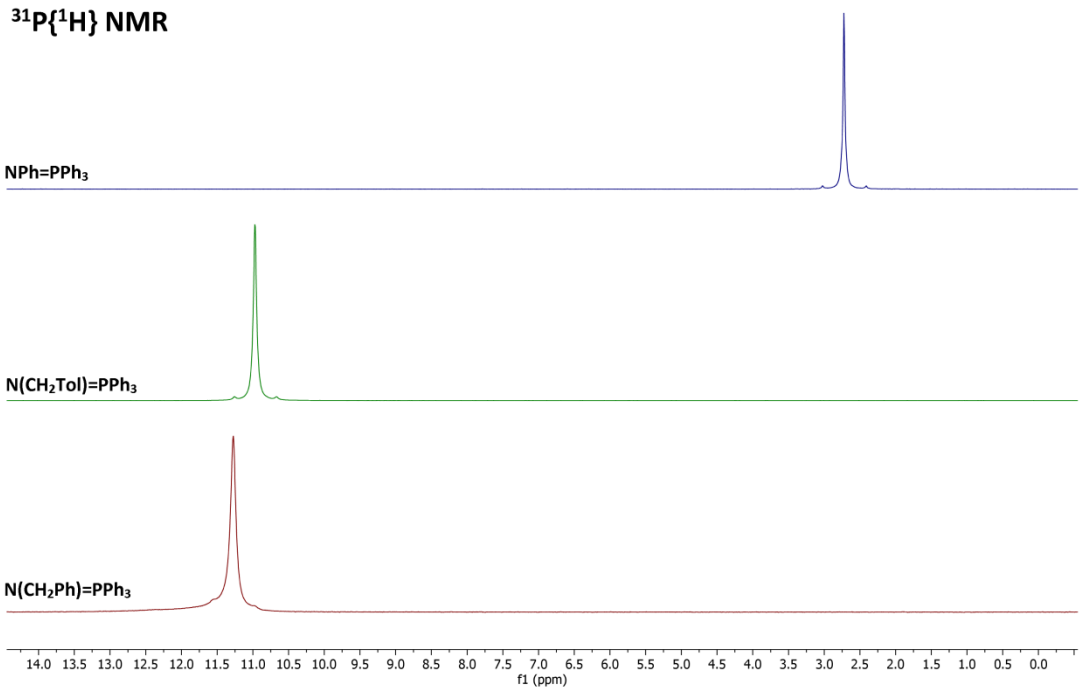

Figure 19. $^{31}P\{^{1}H\}$ NMR spectra of $N(CH_2Ph)=PPh_3$, $N(CH_2Tol)=PPh_3$ and $NPh=PPh_3$ ($CDCl_3$, 300 K).

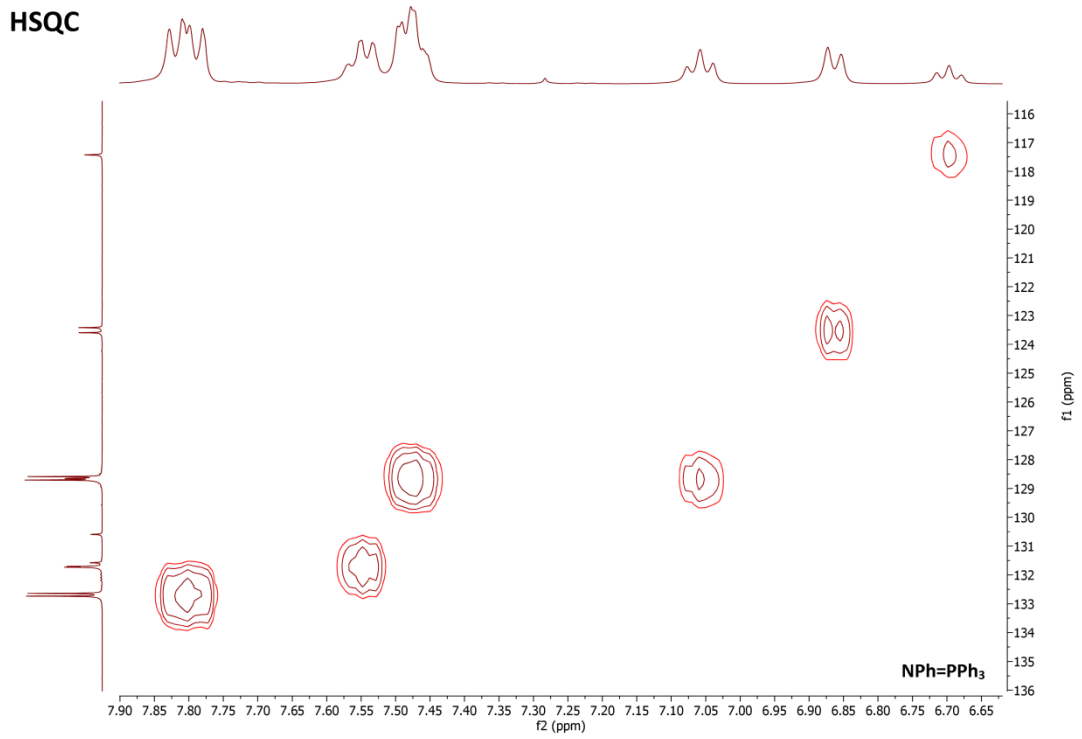

Figure 20. ^{13}C-^{1}H HSQC spectrum of $NPh=PPh_3$ ($CDCl_3$, 300 K).

Particular attention was devoted to the assignment of the $\nu_{P=N}$ IR stretching in the synthesized iminophosphorane derivatives. Considering the rough analogy with the P=O

bond [131], the stretching is expected to fall in the 1000 – 1200 cm^{-1} region, superimposed to several other vibrations. The simulated IR spectrum of $NPh{=}PPh_3$ obtained from the DFT-optimized structure of the species suggests that the wavenumber of the ν_{PN} vibration is around 1100 cm^{-1}, combined with δ_{CH} vibrational modes. The IR spectra of the iminophosphoranes, the DFT-optimized structure of $NPh{=}PPh_3$ and its vibrationally elongated geometry with displacement vectors for the $\nu_{P=N}{+}\delta_{CH}$ mode (predicted value 1112 cm^{-1}) are shown in Figure 21.

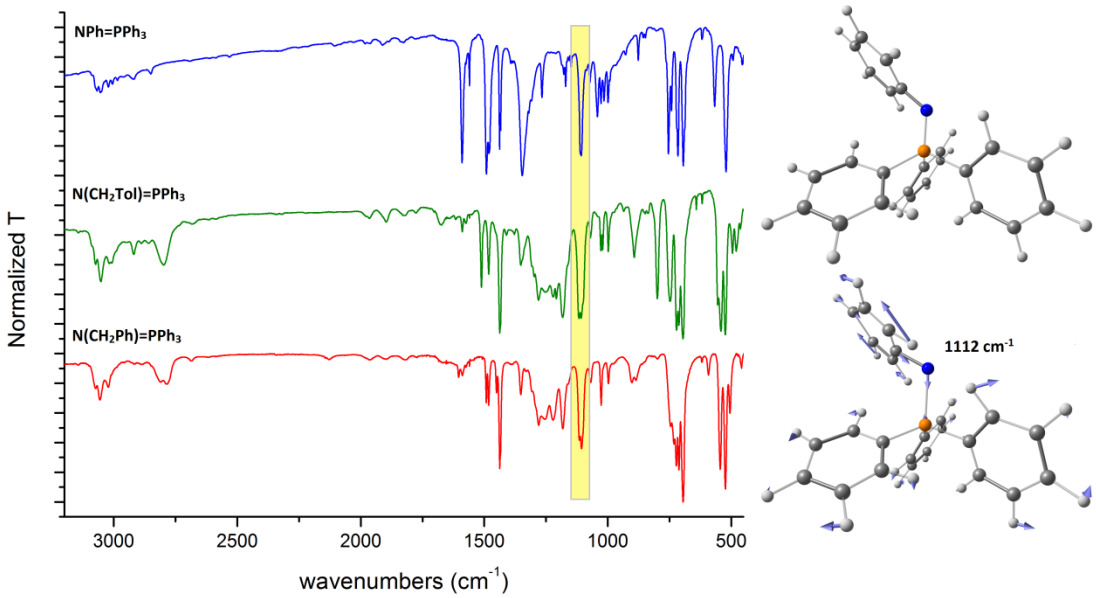

Figure 21. IR spectra (KBr) of $N(CH_2Ph){=}PPh_3$, $N(CH_2Tol){=}PPh_3$ and $NPh{=}PPh_3$. DFT-optimized structure of $NPh{=}PPh_3$ and displacement vectors for the $\nu_{P=N}{+}\delta_{CH}$ vibrational mode. Colour map: P, orange; N, blue; C, grey; H, white.

The absorption and emission features of the isolated iminophosphoranes were also investigated. Owing to the growing interest towards organophosphorus compounds containing the {P=O} moiety as luminescent markers and as materials for optoelectronic applications [132-135], the absorption and emission features of the isolated iminophosphoranes were also investigated [132-135]. Dichloromethane solutions of the iminophosphoranes absorb radiations in the UV range, and the absorption interval is slightly more extended in the case of $NPh{=}PPh_3$, perhaps because of the partial conjugation of the P=N bond and the N-bonded phenyl ring, hypothesis supported by the plot of the HOMO of $NPh{=}PPh_3$ (Figure 22). The UV-VIS spectra of $N(CH_2Ph){=}PPh_3$

and NPh=PPh_3 are compared in Figure 22. On the other hand, the appreciable luminescence exhibited by the compounds at the solid state resulted scarcely dependent upon the nature of the N-bonded substituents (see Figure 22). The emission maxima are comprised between 496 and 509 nm, with FWHM values around 5000 cm^{-1}. The observed colours of the emissions fall in the green-bluish green sector of the CIE 1931 chromaticity diagram, close to the white light region (Figure 22; the CIE 1931 chromaticity coordinates are provided in the caption) [136].

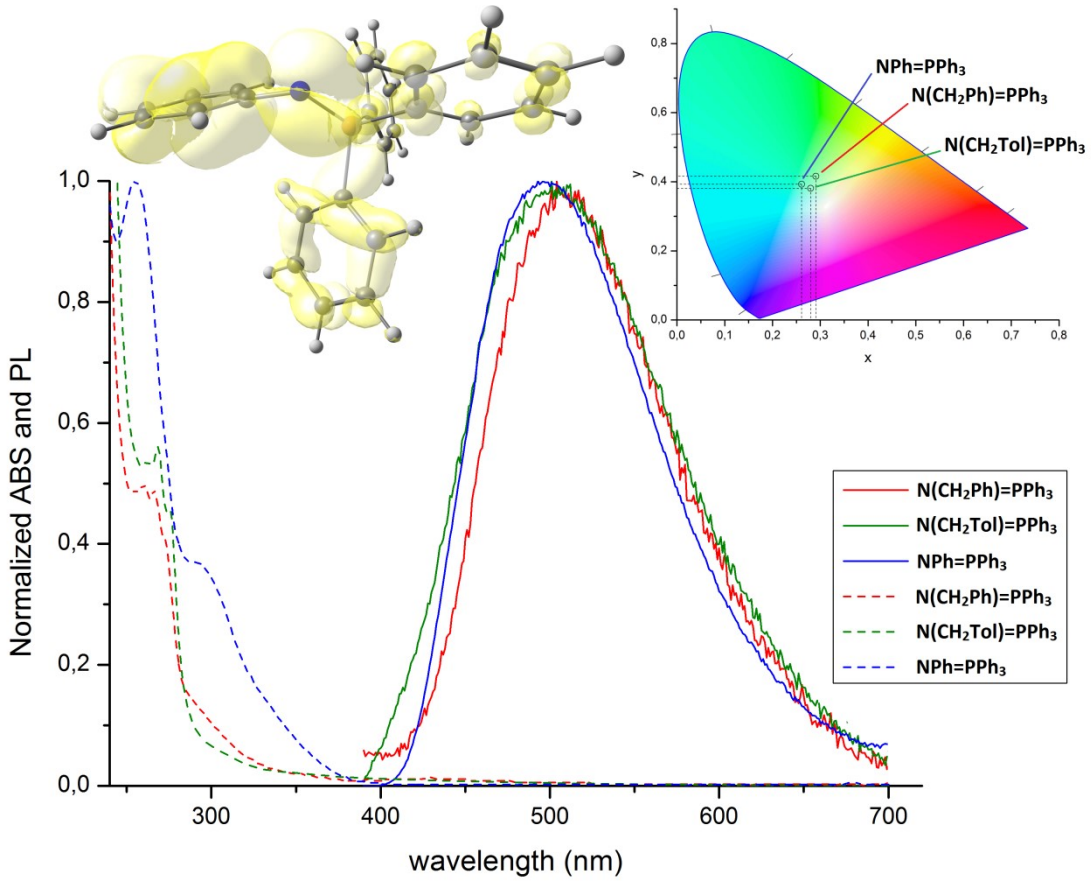

Figure 22. Normalized UV-VIS spectra (CH_2Cl_2 solution, r.t., dashed lines) and normalized PL spectra (solid state, r.t., $\lambda_{excitation}$ = 325 − 360 nm, solid lines) of N(CH_2Ph)=PPh_3, N(CH_2Tol)=PPh_3 and NPh=PPh_3. DFT-optimized structure of NPh=PPh_3 and with plot of the HOMO (yellow tones, surface isovalue = 0.01 a.u.). Colour map: P, orange; N, blue; C, grey; H, white. CIE 1931 chromaticity diagram, chromaticity coordinates: N(CH_2Ph)=PPh_3, x = 0.291, y = 0.416; N(CH_2Tol)=PPh_3, x = 0.280, y = 0.381; NPh=PPh_3, x = 0.261, y = 0.393.

The excitation range at the solid state is more extended with respect to the solution, reaching the violet region of the visible spectrum, probably because of the influence of intramolecular interactions. The UV-VIS and PLE spectra of NPh=NPh_3 are compared as

example in Figure 23. The lifetimes of the emissions fall in a few nanoseconds range, strongly indicating the fluorescent nature of the observed transitions. An example of luminescence decay curve is provided in Figure 23. The photoluminescence quantum yield (Φ) values measured for solid samples are all below 1%, indicating the presence of fast non-radiative decay routes. The emissions of the iminophosphoranes at room temperature once dissolved in dichloromethane were unfortunately too weak to allow the determination of the Φ values in solution.

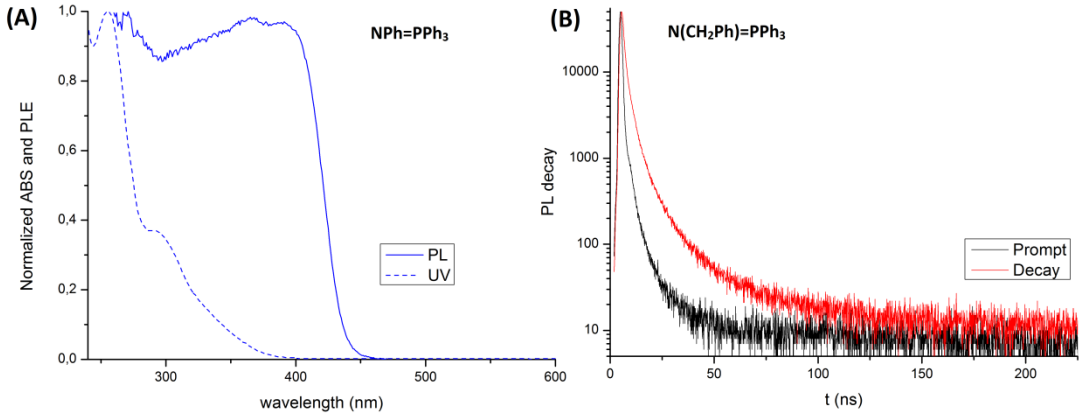

Figure 23. (A) Normalized PL (solid state, r.t., $\lambda_{emission}$ = 510 nm) and UV-VIS (CH_2Cl_2 solution, r.t.) spectra of $NPh{=}PPh_3$. (B) Luminescence decay curve of $N(CH_2Ph){=}PPh_3$ (solid state, r.t., $\lambda_{excitation}$ = 373 nm, $\lambda_{emission}$ = 420 nm).

TD-DFT calculations allowed to optimize the first singlet excited states of $N(CH_2Ph){=}PPh_3$ and $NPh{=}PPh_3$. The predicted values for the lowest energy $S_1 \rightarrow S_0$ transitions are comprised between 436 and 482 nm, in acceptable agreement with the experimental outcomes. According to the hole-electron distributions depicted in Figure 24 [137], the transitions mostly occur between orbitals localized on the {NR} fragment and on the P-bonded phenyl rings. The fluorescent emission has thus intraligand charge transfer nature.

Attempts to further investigate the electronic features of $NPh{=}PPh_3$ were carried out carrying by means of cyclic voltammetry (Figure 25). The species is characterized under the experimental conditions applied by three irreversible oxidation processes between 0.3 and 0.9 V *vs* Fc^+/Fc, with two clearly distinguishable peaks at 0.41 and 0.69 V *vs* Fc^+/Fc. The cathodic region shows an irreversible reduction peak around -2.07 V *vs* Fc^+/Fc,

immediately followed by a dominant process attributable to the electropolymerization of the species [138].

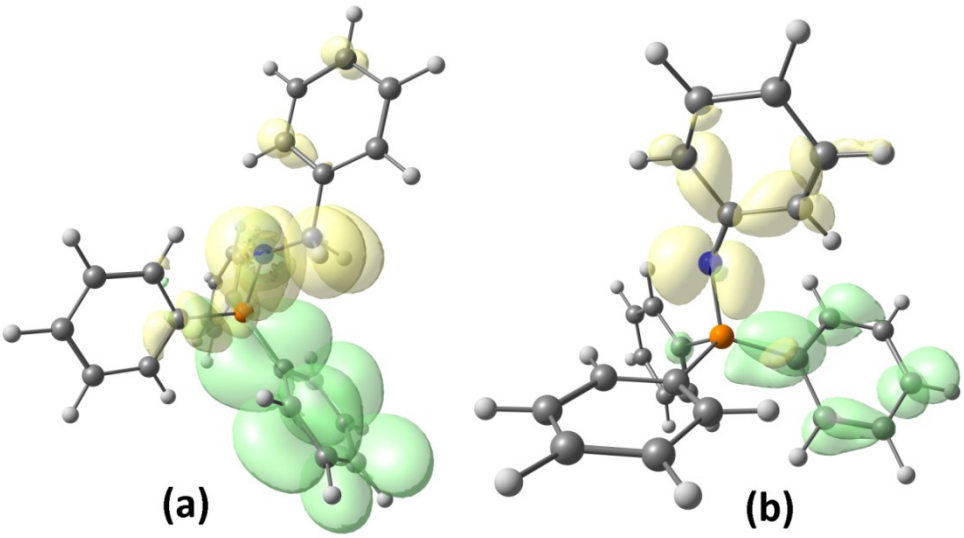

Figure 24. First singlet excited state geometries of $N(CH_2Ph)=PPh_3$ (a) and $NPh=PPh_3$ (b) with hole (yellow) and electron (green) isosurfaces for the $S_1 \leftarrow S_0$ transitions. The emissions are the reverse processes.

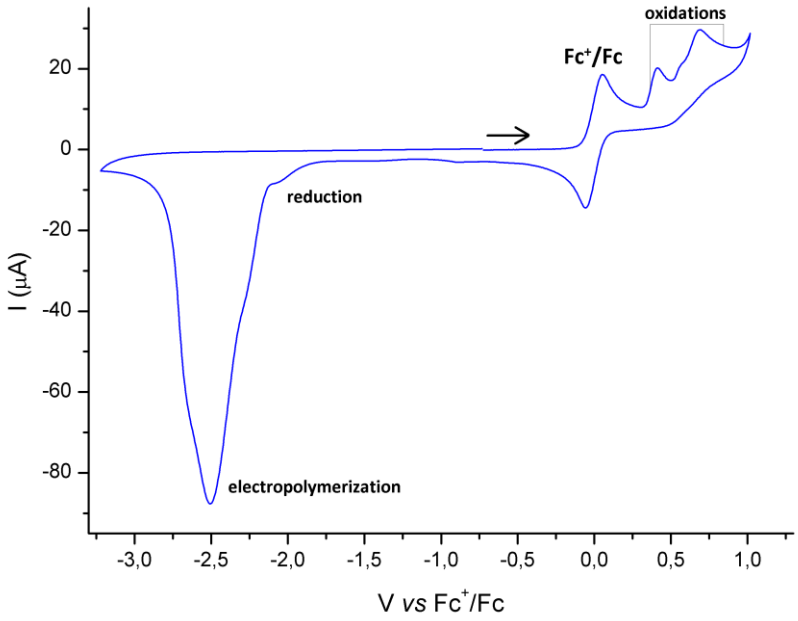

Figure 25. Cyclic voltammogram of $NPh=PPh_3$. Acetone/$LiClO_4$, r.t., Ar atmosphere, glassy carbon electrode, ferrocene (Fc) as internal reference, scan rate 250 mV/s.

The studies on the coordination ability of the iminoposphoranes were carried out considering anhydrous zinc(II) bromide as metal precursor. Preliminary reactions were

carried out using freshly distilled ethanol as solvent under inert atmosphere, but the NMR data of the isolated products clearly indicated the decomposition of the ligands, with formation of N-H bonds or addition of hydroxyl fragments. As an example, the ^{1}H NMR spectrum of the solid isolated from $ZnBr_2$ and two equivalents of $N(CH_2Ph)=PPh_3$ after evaporation of the solvent under reduced pressure showed a broad resonance around 8.6 ppm (FWHM = 50 Hz), without HSQC correlation with carbon atoms. It is likely to suppose that the Lewis acid behaviour of zinc(II) enhances the reactivity of the P=N bond towards water traces and protic solvents. A comparable outcome was observed considering anhydrous manganese(II) halides as precursors (*vide infra*). Coordination compounds having proposed general formula $[ZnBr_2(NR=PPh_3)_2]$ (R = CH_2Ph, CH_2Tol, Ph) were instead prepared under mild conditions using anhydrous acetonitrile as solvent and a 2:1 ligand:precursor ratio. In the case of $NPh=PPh_3$, the reactions were successfully extended to $ZnCl_2$ and ZnI_2 to verify possible influences of the coordinated halides. The general synthesis of the Zn^{II} complexes is sketched in Scheme 2.

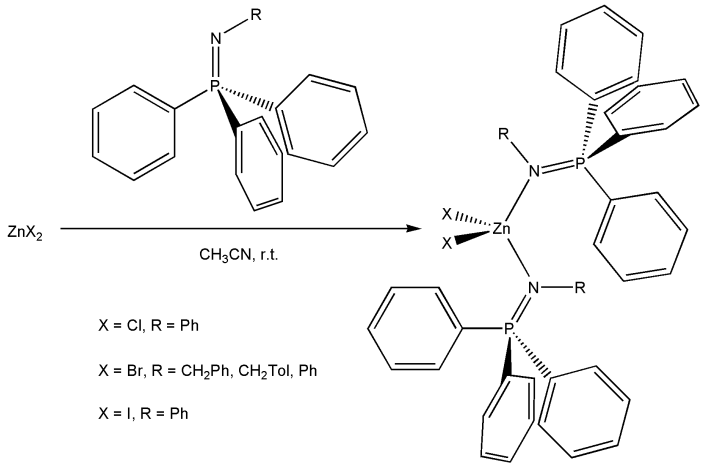

Scheme 2. Synthesis of $[ZnX_2(NR=PPh_3)_2]$ complexes.

The NMR spectra of the complexes showed the resonances expected for the iminophosphorane ligands, altered by coordination. Noticeable high-frequency shifts, around 30 ppm, were in particular observed for all the $^{31}P\{^{1}H\}$ NMR resonances, probably related to the σ-donation of electron density from the {N=P} moiety to the metal centre. Another effect is the broadening of the signals for the bulkier $NPh=PPh_3$ derivatives, indicating fluxional behaviour in solution enhanced by the steric hindrance

around Zn^{II}. The fluxionality is less evident for the $N(CH_2Ph)=PPh_3$ and $N(CH_2Tol)=PPh_3$ complexes, but the methylene resonances around 4.5 ppm in the ^1H NMR spectra are slightly broadened with respect to the free iminophosphoranes. The ^1H and $^{31}P\{^1H\}$ NMR spectra of $[ZnBr_2\{N(CH_2Tol)=PPh_3\}_2]$ and $[ZnBr_2(NPh=PPh_3)_2]$ are shown as examples in Figure 26.

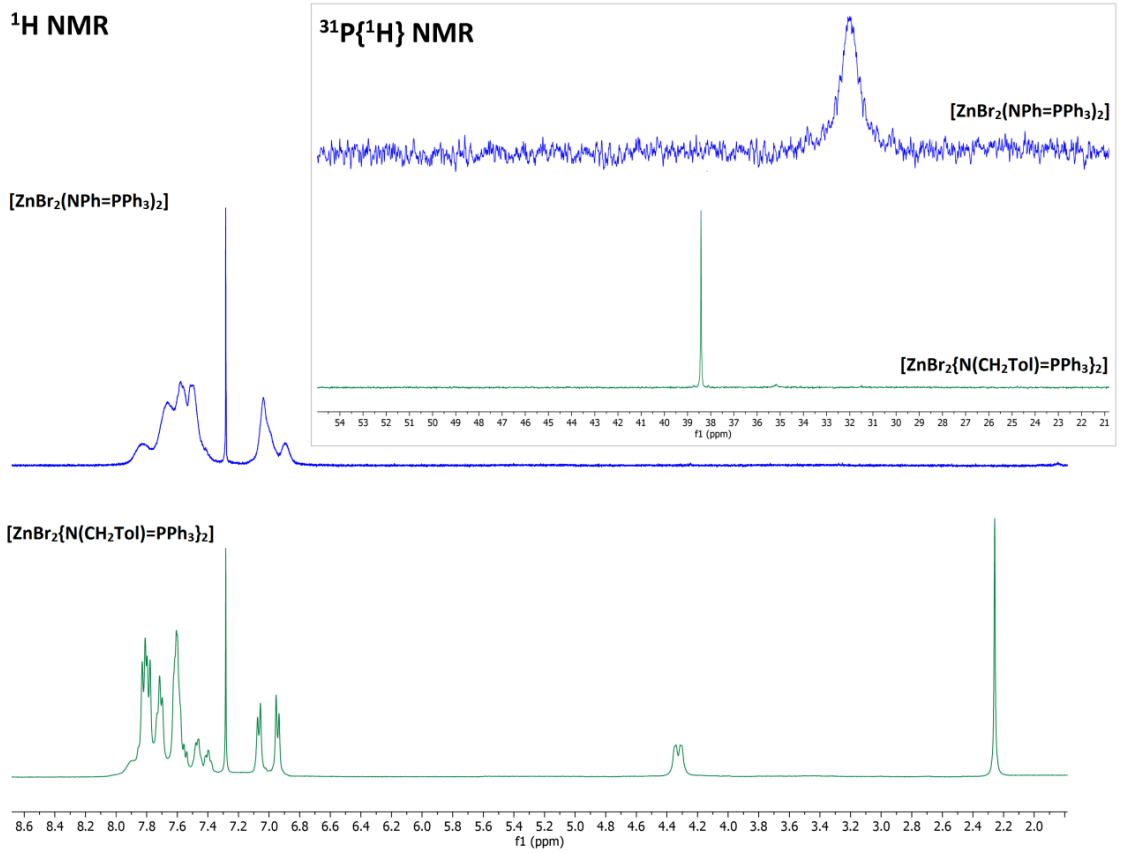

Figure 26. ^1H NMR and $^{31}P\{^1H\}$ NMR spectra of $[ZnBr_2\{N(CH_2Tol)=PPh_3\}_2]$ and $[ZnBr_2(NPh=PPh_3)_2]$ ($CDCl_3$, 300 K).

No signal related to coordinated acetonitrile was observed, and this result was confirmed by the lack of $\nu_{C\equiv N}$ stretchings in the IR spectra, as observable in Figure 27. The vibrations of the complexes in the 4000 − 450 cm^{-1} range are in line with those of the free ligands. Despite the coordination to ZnX_2 fragments, the $\nu_{P=N}$ stretchings did not result particularly altered compared to the free iminophosphoranes, but it is worth noting that scarce variations were observed also for the $\nu_{P=O}$ stretchings of related [O=P]-donor ligands upon coordination to Zn^{II} halides [54,108].

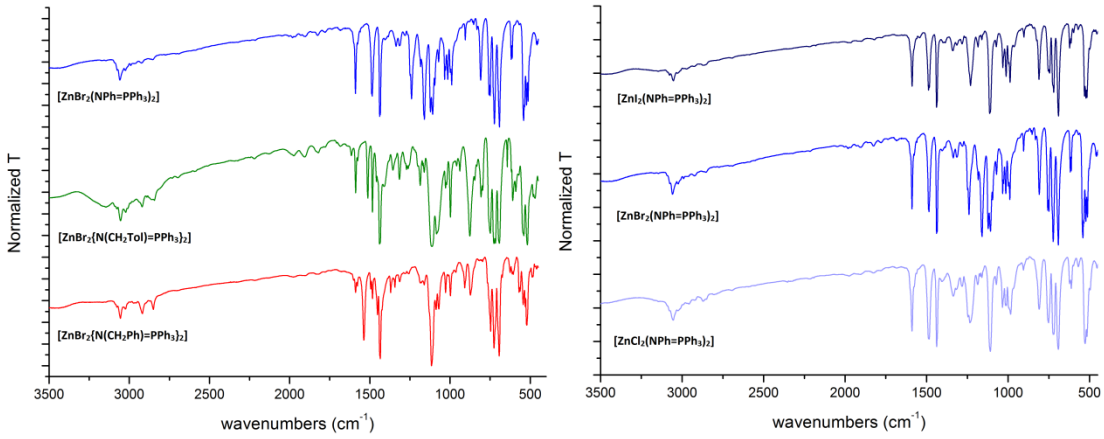

Figure 27. IR spectra (KBr) of $[ZnBr_2(NR{=}PPh_3)_2]$ (R = CH_2Ph, CH_2Tol, Ph) and of $[ZnX_2(NPh{=}PPh_3)_2]$ (X = Cl, Br, I).

In analogy with the typical coordinating behaviour of ligands such as triphenylphosphine oxide towards Zn^{II} halides [104,139], tetrahedral geometries are proposed for the $[ZnX_2(NR{=}PPh_3)_2]$ complexes here described. The DFT-optimized geometries of $[ZnBr_2\{N(CH_2Ph){=}PPh_3\}_2]$ and $[ZnBr_2(NPh{=}PPh_3)_2]$ are shown in Figure 28, with selected computed bond lengths and angles provided in the caption.

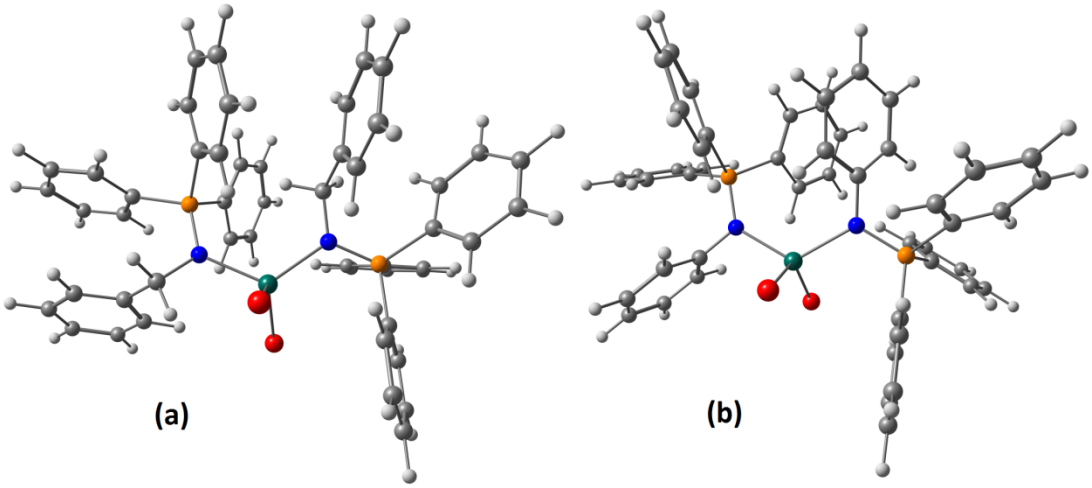

Figure 28. DFT-optimized geometries of $[ZnBr_2\{N(CH_2Ph){=}PPh_3\}_2]$ (a) and $[ZnBr_2(NPh{=}PPh_3)_2]$ (b). Colour map: Zn, turquoise; Br, red; P, orange; N, blue; C, grey; H, white. Selected computed bond lengths (Å) and angles (°) for $[ZnBr_2\{N(CH_2Ph){=}PPh_3\}_2]$: Zn-N, 2.094 (av.); Zn-Br, 2.427 (av.); P=N, 1.608 (av.); Br-Zn-Br, 123.3; N-Zn-N, 120.4. Selected computed bond lengths (Å) and angles (°) for $[ZnBr_2(NPh{=}PPh_3)_2]$: Zn-N, 2.079 (av.); Zn-Br, 2.414 (av.); P=N, 1.611 (av.); Br-Zn-Br, 130.5; N-Zn-N, 121.9.

The N-Zn-N and Br-Zn-Br are meaningfully higher than the 109.5° corresponding to the ideal tetrahedral geometry. The τ_4 parameter (τ_4 = {360°-α-β}/141°, where α and β are the biggest angles in the first coordination sphere; ideal values are 1 for tetrahedron and 0 for square plane) [140], equal to 0.82 for $[ZnBr_2\{N(CH_2Ph)=PPh_3\}_2]$ and 0.76 for $[ZnBr_2(NPh=PPh_3)_2]$, indicates that the seesaw geometry better describes the two Zn^{II} complexes. The P=N bond lengths are elongated with respect to the free ligands only by about 0.04 Å, according to the scarce variations of the related stretchings observed in the IR spectra.

Despite the absorption features in solution do not diverge from those of the free ligands (see for instance Figure 29), the emissions of the complexes are different and markedly influenced by the nature of the N-bonded substituents. The compounds $[ZnBr_2\{N(CH_2Ph)=PPh_3\}_2]$ and $[ZnBr_2\{N(CH_2Tol)=PPh_3\}_2]$ have superimposable emissions, blue-shifted by about 30 nm with respect to the corresponding free iminophosphoranes (Figure 29).

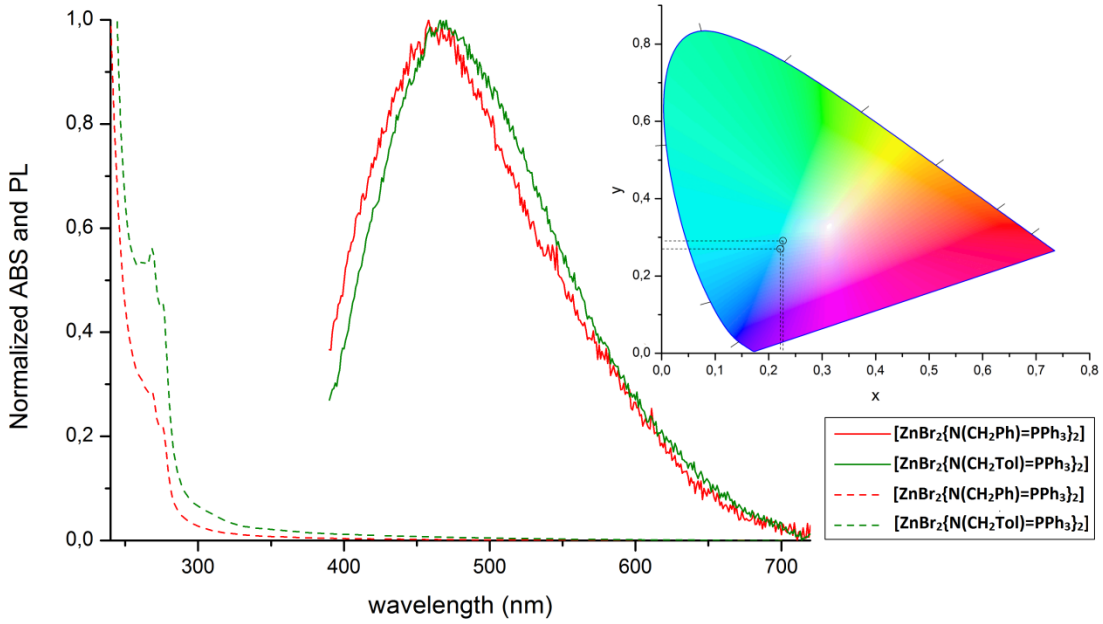

Figure 29. Normalized UV-VIS (CH_2Cl_2 solution, r.t., dashed lines) and PL (solid state, r.t., $\lambda_{excitation}$ = 300 nm, solid lines) spectra of $[ZnBr_2\{N(CH_2Ph)=PPh_3\}_2]$ and $[ZnBr_2\{N(CH_2Tol)=PPh_3\}_2]$ and CIE 1931 chromaticity diagram. Chromaticity coordinates: $[ZnBr_2\{N(CH_2Ph)=PPh_3\}_2]$, x = 0.222, y = 0.270; $[ZnBr_2\{N(CH_2Tol)=PPh_3\}_2]$, x = 0.227, y = 0.291.

The measured lifetimes are in the few nanoseconds range, according to a fluorescent emission in the greenish-blue range. Considering an average luminescence quantum yield (Φ) around 5% and an average lifetime (τ) of 6 ns, the radiative (k_r) and non-radiative (k_{nr}) kinetic constants estimated according to $\Phi = k_r/(k_r+k_{nr}) = \tau k_r$ [141] are respectively around $8 \cdot 10^6$ s^{-1} and $2 \cdot 10^8$ s^{-1}.

The emissions of the $[ZnX_2(NPh{=}PPh_3)_2]$ complexes (X = Cl, Br, I) at the solid state are roughly superimposable, centred around 510 nm and with FWHM values between 5200 and 5300 cm^{-1} (Figure 30). The emission maxima are slightly red-shifted compared to the free ligand (maximum at 496 nm). As a consequence, the emissions fall in the green region of the CIE 1931 chromaticity diagram. The PLE spectra reported in Figure 30 are also scarcely influenced by the coordinated halides, showing similar profiles with maxima centred between 347 and 360 nm. The PLE bands roughly correspond to the weak lowest energy transitions detected in the corresponding absorption spectra in solution, as observable in Figure 30.

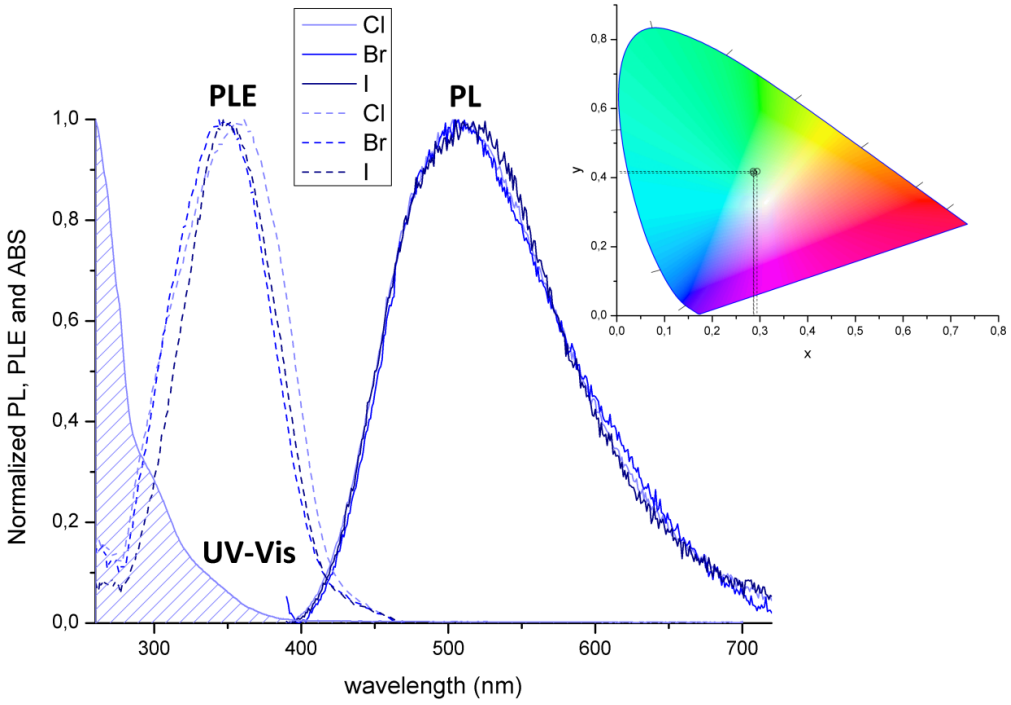

Figure 30. Normalized UV-VIS spectrum of $[ZnCl_2(NPh{=}PPh_3)_2]$ (CH_2Cl_2, r.t.) and normalized PLE (solid state, r.t., $\lambda_{emission}$ = 510 – 520 nm) and PL (solid state, r.t., $\lambda_{excitation}$ = 320 – 350 nm) of $[ZnX_2(NPh{=}PPh_3)_2]$ (X = Cl, Br, I). CIE 1931 chromaticity diagram. Chromaticity coordinates: X = Cl, x = 0.287, y = 0.413; X = Br, x = 0.294, y = 0.418; X = I, x = 0.286, y = 0.418.

The main difference of the $[ZnX_2(NPh{=}PPh_3)_2]$ complexes compared to the related species with N-bonded benzylic fragments concerns the lifetimes of the emissions. Time-correlated single photon counting (TCSPC) measurements indicated decays in the hundreds of ns range for the three complexes, best fitted with a biexponential decay (Figure 31). The luminescence decay is thus about two orders of magnitude slower with respect to the free iminophosphorane, and also much slower than that of the $[ZnBr_2\{N(CH_2Ar){=}PPh_3\}_2]$ (Ar = Ph, Tol) complexes. Moreover, multi-channel scaling (MSC) measurements (Figure 31) revealed decays in the hundreds of μs range for $[ZnBr_2(NPh{=}PPh_3)_2]$ and $[ZnI_2(NPh{=}PPh_3)_2]$, most likely related to the population of excited triplet states.

The luminescence decay curves clearly indicate that the emissions of the $[ZnX_2(NPh{=}PPh_3)_2]$ cannot be described as simple fluorescent decays. The long lifetimes and the presence of tails in the hundreds of μs range support the idea of exchange between singlet and triplet excited states, with intersystem crossing processes affected by the nature of the coordinated halide. Despite being not common, the possible involvement of triplet states was already documented in the recent literature for other Zn^{II} derivatives [93,94,96,103,108]. The choice of the halide also affects the rate of $T_1 \rightarrow S_0$ radiative decay. The previously described well-separated hole and electron distributions for the free iminophosphorane suggest scarce contribution of the exchange energy in the relative stabilization of the triplet state, favouring the reverse intersystem crossing (RISC) process. Such a hypothesis was confirmed by the calculation of the excited singlet-triplet energy gap for the free ligand, carried out both at the excited singlet and triplet state geometries. The values obtained are around 900 cm^{-1}, and it is worth noting that the possibility of RISC is usually invoked for energy gaps below 1000 cm^{-1} [3]. The processes expected to be involved in the radiative decay are sketched in the inset of Figure 31. Unfortunately the non-radiative decay processes resulted however dominant, with photoluminescence quantum yield values comprised between 1% and 3%. Moreover, the measurements were affected by the photodecomposition of the complexes after prolonged irradiation with UV light, particularly evident for the iodo-derivative. The Φ values here reported are thus to be considered only as indicative.

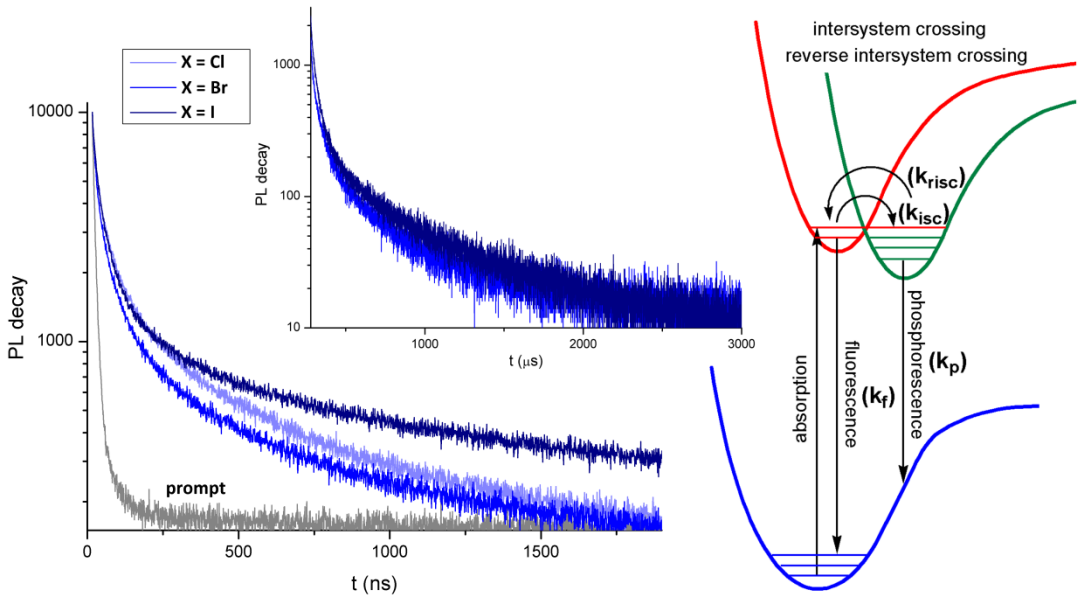

Figure 31. Semi-log plots of the luminescence decay curves (solid state, r.t.) of $[ZnX_2(NPh{=}PPh_3)_2]$ (X = Cl, Br, I). $\lambda_{excitation}$ = 373 nm (TCSPC), 290 nm (MSC). $\lambda_{emission}$ = 510 − 520 nm. Sketch of the expected steps involved in the radiative decay process: fluorescence (k_r), phosphorescence (k_{nr}), intersystem crossing (k_{isc}) and reverse intersystem crossing (k_{risc}).

Cyclic voltammetry measurements were carried out on $[ZnBr_2(NPh{=}PPh_3)_2]$ to verify possible influences of the coordination on the electronic structure of the iminophosphorane. The superposition with free $NPh{=}PPh_3$ under the same experimental conditions is observable in Figure 32.

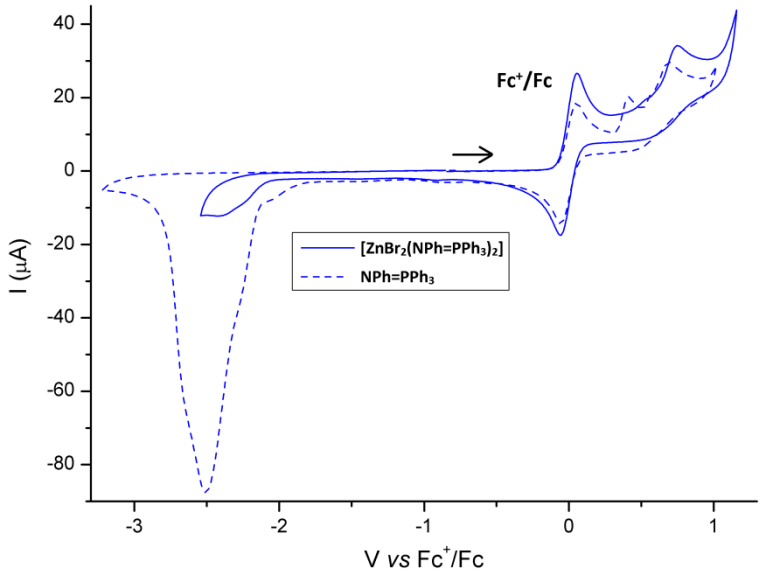

Figure 32. Cyclic voltammograms of $[ZnBr_2(NPh{=}PPh_3)_2]$ and $NPh{=}PPh_3$. Acetone/$LiClO_4$, r.t., Ar atmosphere, glassy carbon electrode, ferrocene (Fc) as internal reference, scan rate 250 mV/s.

The oxidation processes remain irreversible, but are shifted at higher potential, probably because the interaction with the metal centre makes the iminophosphoranes less electron rich. The first cathodic process observed for $[ZnBr_2(NPh{=}PPh_3)_2]$ appears also attributable to the coordinated N-donors. It is worth noting that the coordination to Zn^{II} blocks the iminophosphorane electropolymerization, a result indicating that the complex is quite stable in solution, despite the fluxional behaviour observed by means of NMR spectroscopy.

4.2. Synthesis and luminescence of manganese(II) complexes with monodentate iminophosphoranes

The reactions of monodentate iminophosphoranes with suitable metal centres were extended to Mn^{II} halides under the experimental conditions previously described for the Zn^{II} complexes. Given the strictly comparable behaviour exhibited by $N(CH_2Ph){=}PPh_3$ and $N(CH_2Tol){=}PPh_3$ towards $ZnBr_2$, the study was limited to $N(CH_2Ph){=}PPh_3$ as benzylic iminophosphorane. Based on the experimental outcomes, the general formula proposed for all the isolated species is $[MnX_2(NR{=}PPh_3)_2]$ (X = Cl, Br, I; R = CH_2Ph, Ph). Considering the related molecular masses, the molar magnetic susceptibility values χ_M^{corr} calculated for solid samples according the equations $\chi_M(cgsu) = L(cm)\cdot m(g)^{-1}\cdot(R\text{-}R_0)\cdot 10^{-9}\cdot M(g/mol)$ (L = height of the sample; m = mass of the sample; $R\text{-}R_0$ = instrument response; M = molecular weight) [142] and $\chi_M^{corr} = \chi_M - \chi_M^{dia}$ (χ_M^{dia} = diamagnetic contribution, calculated on the basis of tabulated Pascal constants according to reference [143]) are associated to magnetic moments close to 5.9 BM, *i.e.* the expected value for a high-spin d^5 metal centre. The IR spectra, shown in Figure 33, resemble those of the corresponding free iminophosphoranes and show negligible dependence upon the choice of the coordinated halides. In analogy with what was previously discussed for the Zn^{II} complexes, the ν_{PN} stretchings are assigned in the region around 1100 cm^{-1}. The $^{31}P\{^1H\}$ NMR spectra are in all the cases composed of a single resonance in the 25 − 40 ppm range, broadened because of the paramagnetic relaxation. The effect is particularly evident for the $[MnX_2(NPh{=}PPh_3)_2]$ complexes (see for instance Figure 34), possibly

suggesting that different relaxation mechanisms are present, related to association-dissociation equilibria influenced by the steric bulk of the N-bonded substituents [144].

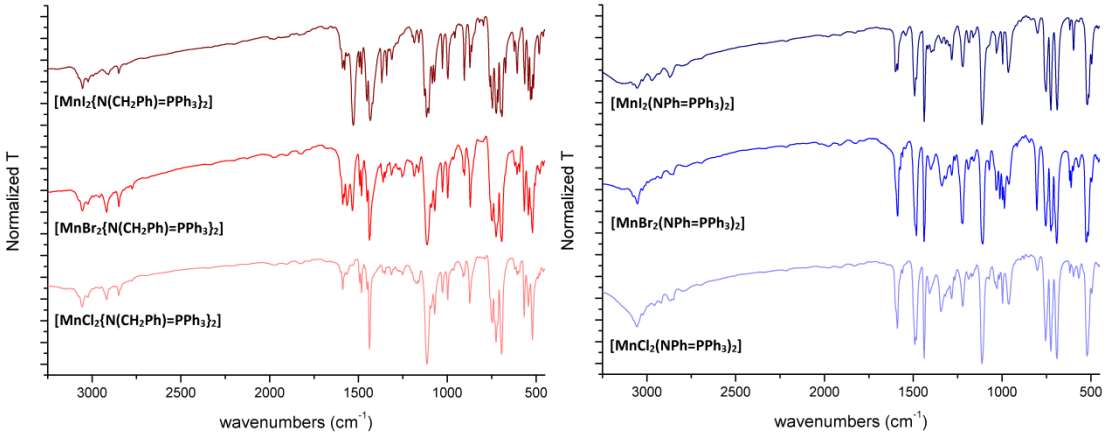

Figure 33. IR spectra (KBr) of the $[MnX_2(NR{=}PPh_3)_2]$ (X = Cl, Br, I; R = CH_2Ph, Ph) complexes.

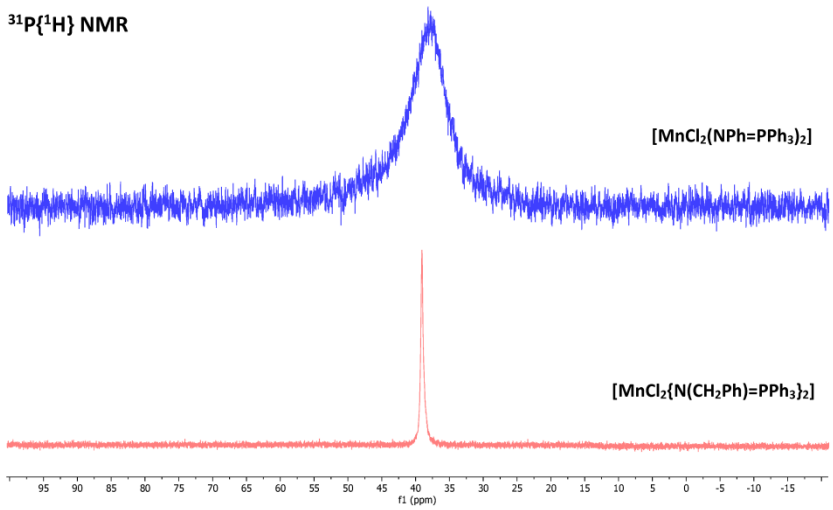

Figure 34. $^{31}P\{^1H\}$ NMR spectra of $[MnCl_2\{N(CH_2Ph){=}PPh_3\}_2]$ and $[MnCl_2(NPh{=}PPh_3)_2]$. $CDCl_3$, 300 K.

As for the Zn^{II} complexes, the absorption spectra of the Mn^{II} derivatives are limited to the UV portion of the spectrum, as observable in Figure 35. The luminescence of the Mn^{II} complexes, present only at the solid state, resulted deeply influenced by the choice of the N-bonded substituents and of the coordinated halides (see Figure 36). The complexes $[MnCl_2\{N(CH_2Ph){=}PPh_3\}_2]$ and $[MnBr_2\{N(CH_2Ph){=}PPh_3\}_2]$ showed bright orange-yellowish orange emissions upon excitation with UV light. The PL bands, centred between 589 and 597 nm, have FWHM values around 2500 cm^{-1}, more in line with a metal-centred transition rather than a ligand-centred or a charge transfer radiative

decay. The emission spectra resemble what is reported in the literature for Mn^{II} luminescent complexes with coordination numbers greater than four, five in particular [44,60,71,145].

The direct involvement of the metal centre was confirmed by the PLE spectra, dominated by ligand-centred processes for wavelengths below 390 nm, but where the direct excitation of the metal centre is also observable. In particular, Figure 36 shows the amplification of the PLE spectra in the 400 − 530 nm, where the $^4G \leftarrow {}^6A$ transition can be recognized, separated into three bands because of the crystal field influence. No variation of the PL spectra was observed trying to selectively irradiate the ligands and the metal centre, thus indicating that only a single emitting species is present and that the $N(CH_2Ph)=PPh_3$ ligand acts as an antenna towards Mn^{II}.

Different luminescent behaviour was observed for the related iodo-complex $[MnI_2\{N(CH_2Ph)=PPh_3\}_2]$. The appreciable yellowish green emission corresponds to the superposition of two bands in the PL spectrum, one centred at 538 nm typical of Mn^{II} in a tetrahedral environment, with a shoulder around 465 nm resembling the emission previously described for $[ZnBr_2\{N(CH_2Ph)=PPh_3\}_2]$. The PLE spectrum shows ligand-centred processes comparable to those of the chloro- and bromo-complexes, while the participation of Mn^{II} transitions can be hardly detected also changing the emission wavelength. The steady-state luminescence measurements suggest that the geometry of $[MnI_2\{N(CH_2Ph)=PPh_3\}_2]$ is most likely tetrahedral, and that the radiative decay from the excited states of the coordinated benzylic iminophosphoranes competes with the metal-centred process.

The three $[MnX_2(NPh=PPh_3)_2]$ (X = Cl, Br, I) complexes showed appreciable yellowish green emission, and the related PL bands are centred between 529 and 538 nm, with FWHM values in the 2200 − 2900 cm^{-1} range. The PL bands appear attributable to the $^4T_1(4G) \rightarrow {}^6A_1({}^6S)$ transition of Mn^{II} in a tetrahedral field. The assignment was confirmed by the PLE spectra, where the $^4G \leftarrow {}^6A$ transitions are present between 400 and 530 nm, superimposed to ligand-centred processes. In the case of $[MnCl_2(NPh=PPh_3)_2]$ a shoulder around 460 nm is superimposed in the PL spectrum, most likely due to a ligand-centred radiative process. The same band, much less evident, is present also for $[MnBr_2(NPh=PPh_3)_2]$, while it is absent for the related iodo-complex.

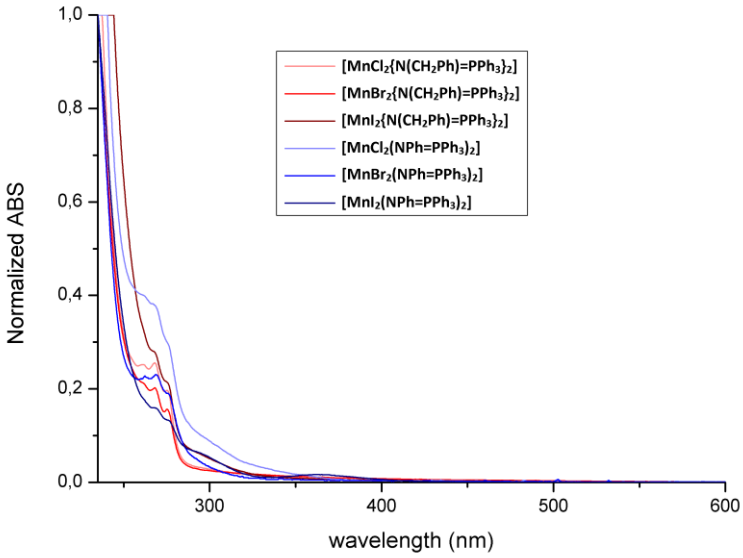

Figure 35. Normalized UV-VIS spectra (CH_2Cl_2 solution, r.t.) of the $[MnX_2(NR{=}PPh_3)_2]$ (X = Cl, Br, I; R = CH_2Ph, Ph) complexes.

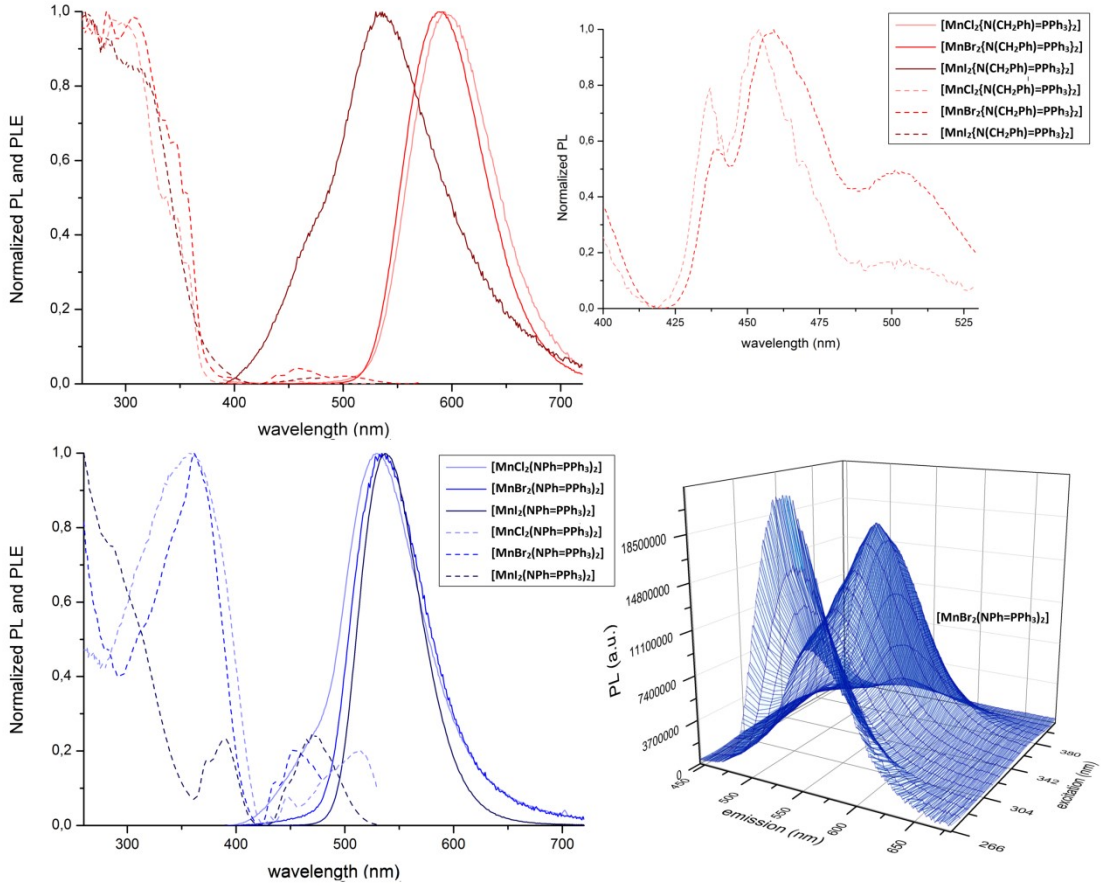

Figure 36. Normalized PLE (solid state, r.t., $\lambda_{emission}$ = 538 − 595 nm, dashed lines) and PL (solid state, r.t., $\lambda_{excitation}$ = 290 − 380 nm, solid lines) spectra of the $[MnX_2(NR{=}PPh_3)_2]$ (X = Cl, Br, I; R = CH_2Ph, Ph) complexes. 3D luminescence spectrum of $[MnBr_2(NPh{=}PPh_3)_2]$ (solid state, r.t.).

Despite the superposition of different bands observed in some cases, the PL spectra are scarcely dependent upon the excitation wavelength, as observable for instance in the 3D luminescence spectrum of $[MnBr_2(NPh{=}PPh_3)_2]$ reported in Figure 36. The metal-centred emissions were confirmed by the luminescence decay curves, shown in Figure 37. The lifetime values range from tens to thousands of μs with a clear dependance upon the choice of the halide, as commonly observed for luminescent manganese(II) halide complexes [63]. The τ values are meaningfully reduced on increasing the halide atomic number thanks to the acceleration of the radiative decay, ascribed to an increased degree of spin-orbit coupling [146]. It is however worth noting that biexponential decay was observed for $[MnI_2\{N(CH_2Ph){=}PPh_3\}_2]$ and $[MnCl_2(NPh{=}PPh_3)_2]$, according to the superposition of two emission bands in the corresponding PL spectra. The trend is not perfectly monoexponential also for $[MnBr_2(NPh{=}PPh_3)_2]$, but the decays are too similar to be separated and an average value is considered. The estimated lifetimes remain however in the μs range, allowing to suppose that the Mn^{II} radiative decay superimposes with phosphorescent decay from the ligands.

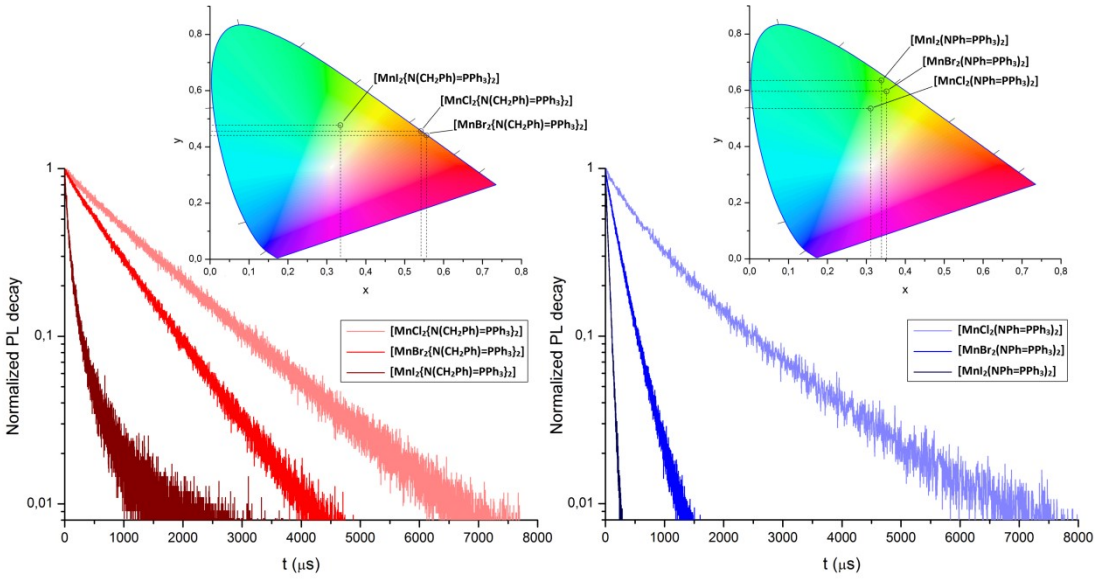

Figure 37. Semi-log plots of the luminescence decay curves (MSC, solid state, r.t.) of the $[MnX_2(NR{=}PPh_3)_2]$ (R = CH_2Ph, Ph; X = Cl, Br, I) complexes. $\lambda_{excitation}$ = 290 nm, $\lambda_{emission}$ = 530 − 595 nm. CIE 1931 chromaticity diagrams. Chromaticity coordinates: X = Cl, R = CH_2Ph, x = 0.556, y = 0.441; X = Br, R = CH_2Ph, x = 0.542, y = 0.456; X = I, R = CH_2Ph, x = 0.335, y = 0.477; X = Cl, R = Ph, x = 0.311, y = 0.535; X = Br, R = Ph, x = 0.352, y = 0.596; X = I, R = Ph, x = 0.339, y = 0.635.

The changes of halide and of N-bonded substituent on the iminophosphorane ligands determine noticeable variations of the colour of the emissions, as observable from the CIE 1931 diagrams reported in Figure 37. The yellowish orange and orange emissions of $[MnCl_2\{N(CH_2Ph)=PPh_3\}_2]$ and $[MnBr_2\{N(CH_2Ph)=PPh_3\}_2]$ are characterized by almost unitary colour purity, a feature of potential technological interest. The photoluminescence quantum yield values remain unfortunately generally low, as previously discussed for the Zn^{II} derivatives. The highest value, 22%, was measured for $[MnBr_2(NPh=PPh_3)_2]$. Such a result is closely comparable to the Φ value reported for the triphenylphosphine oxide bromo-complex $[MnBr_2(O=PPh_3)_2]$, 23% [63] Given a measured average τ value of 235 μs, the corresponding radiative and non-radiative constants are $k_r = 9.4 \cdot 10^2\ s^{-1}$ and $k_{nr} = 3.3 \cdot 10^3\ s^{-1}$. For comparison, the constants determined for the Mn^{II} bromo-complex with benzylic iminophosphorane (Φ = 4%, τ = 836 μs) are $k_r = 4.8 \cdot 10^1\ s^{-1}$ and $k_r = 1.1 \cdot 10^3\ s^{-1}$. The rates of the non-radiative decay processes are thus comparable between the two complexes, while the radiative decay is meaningfully slower for $[MnBr_2\{N(CH_2Ph)=PPh_3\}_2]$ with respect to $[MnBr_2(NPh=PPh_3)_2]$. Such a result could be related to different first coordination spheres around the metal centre in the two complexes.

As stated before, the luminescence data suggest that not all the $[MnX_2(NR=PPh_3)_2]$ complexes have tetrahedral geometry and that higher coordination numbers are expected for $[MnX_2\{N(CH_2Ph)=PPh_3\}_2]$ (X = Cl, Br). It is worth remembering the tendency exhibited by the chloride and bromide ions to behave as bridging ligands towards Mn^{II} centres [33,34]. Attempts to further elucidate the structure of the complexes were carried out by means of DFT calculations on the bromo-complexes. In the case of $[MnBr_2\{N(CH_2Ph)=PPh_3\}_2]$ preliminary calculations indicated as unlikely the formation of six-coordinated species. A stationary point constituted by two five-coordinated manganese centres joined by two bridging bromo-ligands was instead obtained (Figure 38). The coordination sphere of each metal centre is completed by terminal bromo-ligands and two benzylic iminophosporanes. The structure here proposed is only hypothetical, since the characterization data are compatible with other arrangements of ligands and metal centres, leading for example to the formation of coordination polymers. The single crystal X-ray structure determination is in this case mandatory to unambiguously define the structure of the compound and of its chloro-analogue. On the

other hand, the green emission of $[MnBr_2(NPh{=}PPh_3)_2]$ appears compatible only with the tetrahedral geometry, and the DFT-optimized structure of the complex is shown in Figure 38. The computed τ_4 value is 0.82, in line with the geometries previously described for the Zn^{II} bromo-complexes.

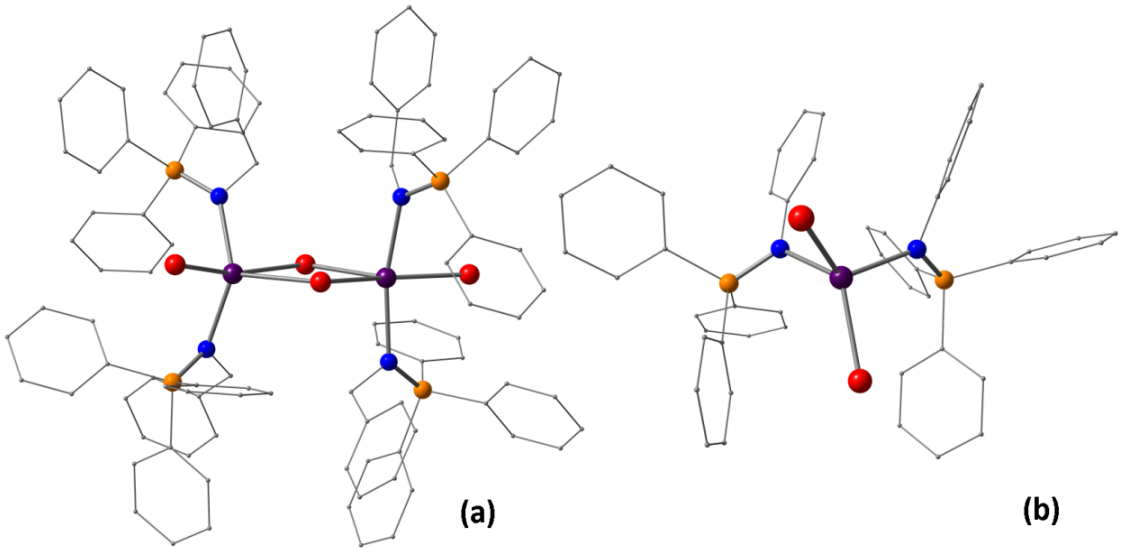

Figure 38. DFT-optimized geometries of $[MnBr_2\{N(CH_2Ph){=}PPh_3\}_2]_2$ (a) and $[MnBr_2(NPh{=}PPh_3)_2]$ (b). Colour map: Mn, violet; Br, red; P, orange; N, blue; C, grey. Hydrogen atoms are omitted for clarity. Selected computed bond lengths (Å) and angles (°) for $[MnBr_2\{N(CH_2Ph){=}PPh_3\}_2]_2$: Mn---Mn 4.218; Mn-N, 2.258 (av.); Mn-Br(μ), 2.779 (av.); Mn-Br, 2.570 (av.); P=N, 1.610 (av.); Br(μ)-Mn-Br(μ), 81.3 (av.); N-Mn-N, 151.3. Selected computed bond lengths (Å) and angles (°) for $[MnBr_2(NPh{=}PPh_3)_2]$: Mn-N, 2.246 (av.); Mn-Br, 2.493 (av.); P=N, 1.615 (av.); Br-Mn-Br, 111.6; N-Mn-N, 100.7.

The coordination number four is usually observed in the case of Mn^{II} halide complexes when the partial negative charge of the donor atoms makes the coordination of other ligands unfavourable. Such an effect is supported by the steric bulk of the substituents on the ligands and competes with the tendency of the metal centre to reach the coordinative saturation. The P=N bond in iminophosphoranes is expected to be less polar than the P=O one because of the different electronegativity of the atoms, thus the formation of Mn^{II} tetrahedral complexes should be less probable compared to what occurs with comparable phosphine oxide ligands. Such a feature should be however almost in part compensated by the bulk of the N-bonded substituents. The different behaviour of $N(CH_2Ph){=}PPh_3$ and $NPh{=}PPh_3$ towards $MnCl_2$ and $MnBr_2$ can be therefore

rationalized by considering that the benzylic substituent generates lower hindrance in the coordination sphere compared to the phenyl one, and the increase of coordination number is thus favoured. The lower tendency of iodide to behave as bridging ligands in manganese(II) derivatives and its greater radius explain why in the case of $[MnI_2\{N(CH_2Ph)=PPh_3\}_2]$ the characterization data agree with the formation of a tetrahedral species. On the other hand, the higher steric bulk determined by the N-bonded phenyl ring in $NPh=PPh_3$ makes the coordinating features of this ligand comparable with those of the related phosphine oxide.

The antenna effect towards Mn^{II} appears effective also in the case of the aromatic iminophosphorane $NPh=PPh_3$, and the luminescence decay curves suggest the involvement of ligand-centred triplet states. Such a hypothesis was corroborated by DFT calculations on $[MnBr_2(NPh=PPh_3)_2]$, sextet and octet states. The spin density plots in Figure 39 show that the unpaired electrons are localized on the Mn^{II} centre for the sextet configuration, while a P-bonded phenyl ring is also involved in the unpaired electron density of the octet configuration. The computed energy difference between the two configurations is around 21700 cm^{-1}, corresponding to a wavelength of about 460 nm. Such a result is in excellent agreement with the previously described PL spectra, supporting the superposition of Mn^{II} emission and ligand phosphorescence. The energy of the $^4T_1(^4G)$ level of Mn^{II} can be estimated at around 20400 cm^{-1} from the onset of the $[MnI_2(NPh=PPh_3)_2]$ band (Figure 36). The limited energy gap between ligand- and metal-centred excited states should favour the ligand→metal energy transfer (ET), but also opens the possibility of the reverse process (BET). A possible explanation for the observed PL spectra can be based on the rate of radiative decay from the $^4T_1(^4G)$ excited state. With X = Cl and, to a lesser extent, X = Br, the emission from the metal centre is relatively slow because of the limited spin-orbit coupling, thus back energy transfer (BET) followed by ligand-centred phosphorescence is a competitive process. In the case of $[MnI_2(NPh=PPh_3)_2]$ the metal-centred luminescence is instead sufficiently fast to overcome other possible radiative decays. The proposed model is summarized in the portion of Jablonski diagram reported in Figure 39.

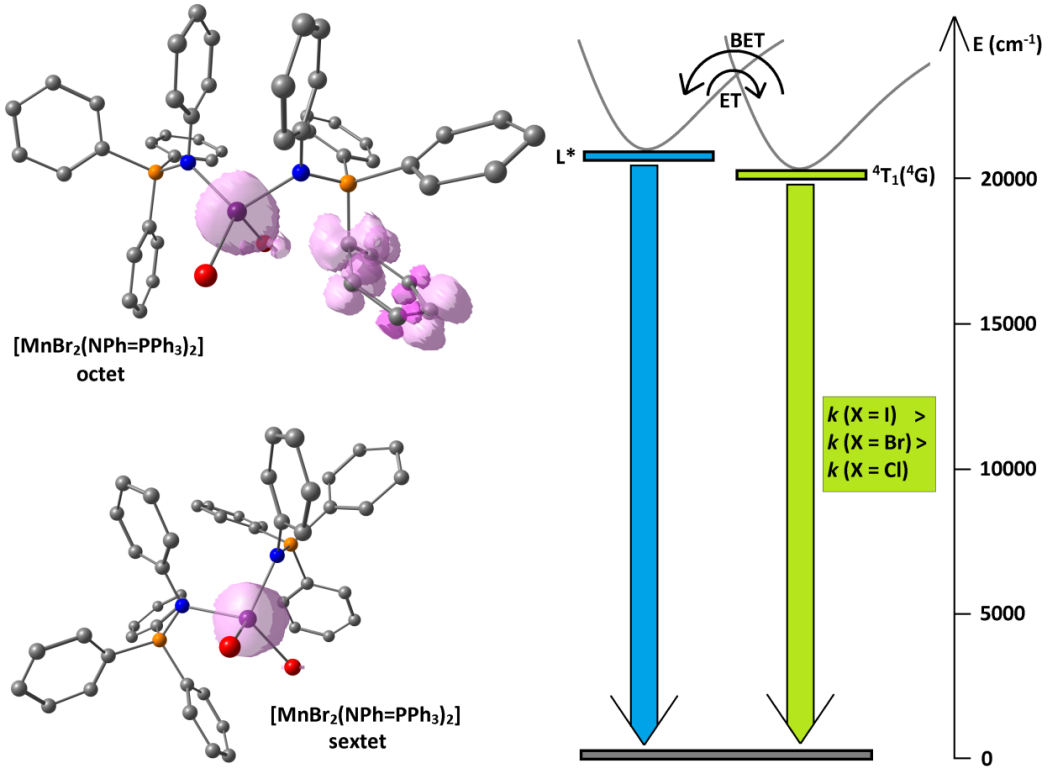

Figure 39. DFT-optimized structures of $[MnBr_2(NPh{=}PPh_3)_2]$, sextet and octet configurations, with spin density surfaces (pink tones). Colour map: Mn, violet; Br, red; P, orange; N, blue; C, grey. Hydrogen atoms are omitted for clarity. Portion of Jablonski diagram illustrating the competition between ligand-centred (L*) and metal-centred emissions.

As anticipated in the discussion concerning the Zn^{II} complexes, the iminophosphorane ligands decompose using ethanol as solvent. In the case of Mn^{II}, preliminary reactions between $NPh{=}PPh_3$ and $MnBr_2$ in EtOH allowed to isolate the known triphenylphosphine oxide complex $[MnBr_2(O{=}PPh_3)_2]$ [55], as depicted in Figure 40. The comparison of the photoluminescence data between the iminophosphorane and the phosphine oxide complexes (Figure 40) shows a limited red-shift of the PL band in the case of $NPh{=}PPh_3$ as ligand. On the other hand, the lifetime of the emission is about the half for $[MnBr_2(NPh{=}PPh_3)_2]$ compared to $[MnBr_2(O{=}PPh_3)_2]$. Given the similar photoluminescence quantum yields values of the two species, it must be concluded that the radiative decay process is faster for the iminophosphorane derivative.

Melting point measurements revealed that all the complexes here described decompose for temperatures below 180 °C. TGA measurements on selected compounds however revealed that the decomposition processes are not concomitantly accompanied by mass loss. For instance, the TGA curves of the complexes $[MX_2(NPh{=}PPh_3)_2]$ (M = Mn, Zn; X =

Br, I) reported in Figure 41 (N_2 atmosphere) show that the mass of the samples starts to meaningfully change for temperatures above 250 °C. In the case of the Zn^{II} complexes, the residual mass at 500 °C is compatible with the formation of metallic zinc.

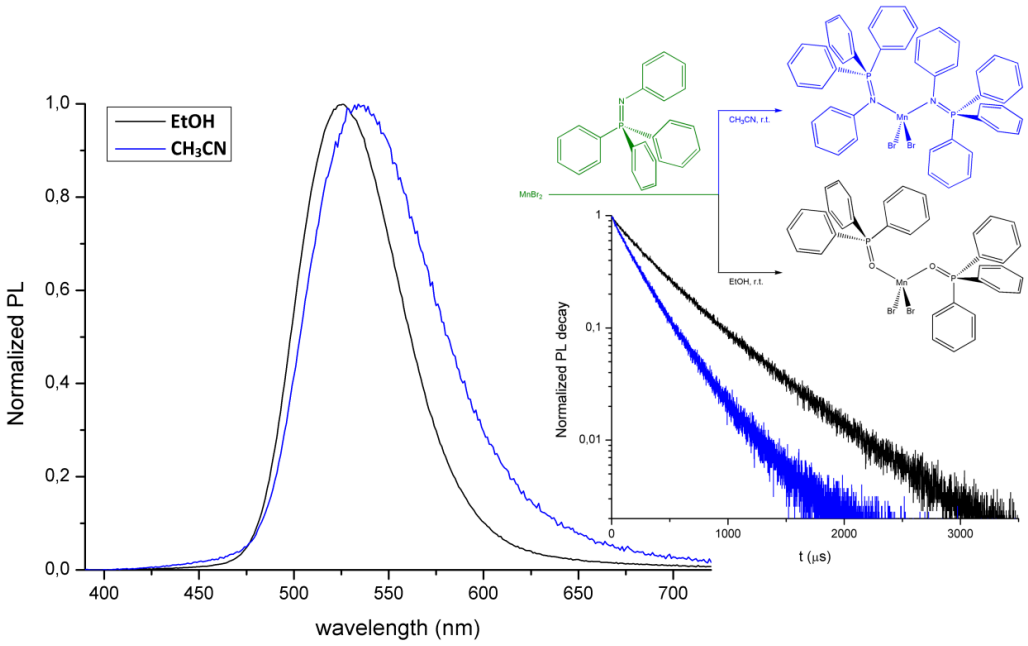

Figure 40. Synthesis of $[MnBr_2(NPh{=}PPh_3)_2]$ and $[MnBr_2(O{=}PPh_3)_2]$. Normalized PL spectra of $[MnBr_2(NPh{=}PPh_3)_2]$ and $[MnBr_2(O{=}PPh_3)_2]$ (solid samples, r.t., $\lambda_{excitation}$ = 300 nm). Luminescence decay curves (MCS) of $[MnBr_2(NPh{=}PPh_3)_2]$ and $[MnBr_2(O{=}PPh_3)_2]$ (solid samples, r.t., $\lambda_{excitation}$ = 290 nm, $\lambda_{emission}$ = 530 − 580 nm).

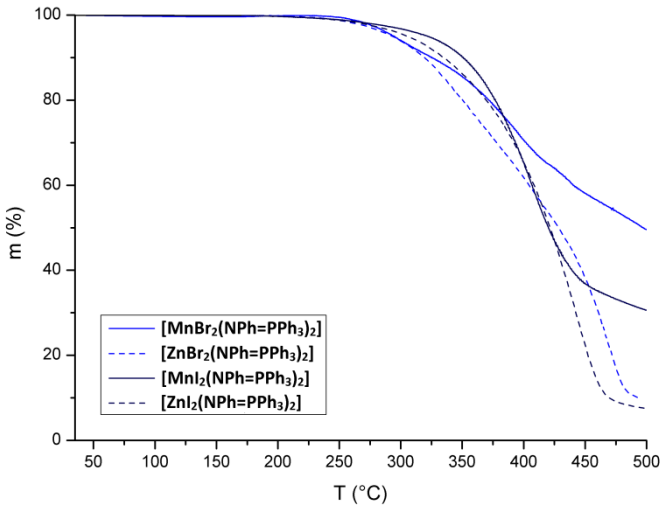

Figure 41. TGA curves of the $[MX_2(NPh{=}PPh_3)_2]$ (M = Mn, Zn; X = Br, I) complexes.

4.3. Preliminary investigation on manganese(II) complexes with bidentate iminophosphoranes

The results obtained with monodentate iminophosphorane ligands prompted to start a preliminary investigation on the possible application of bidentate iminophosphorane ligands for the preparation of luminescent coordination compounds. The compounds 1,1'-methylenebis-((*N*-(4-methylbenzyl))-1,1-diphenylphosphanimine) and and 1,1'-methylenebis-(*N*,1,1-triphenylphosphanimine), respectively indicated as $N(CH_2Tol)=PPh_2(CH_2)PPh_2=N(CH_2Tol)$ and $NPh=PPh_2(CH_2)PPh_2=NPh$, were synthesized by reacting bis(diphenylphosphino)methane with two equivalents of the proper azide, as shown in Scheme 3.

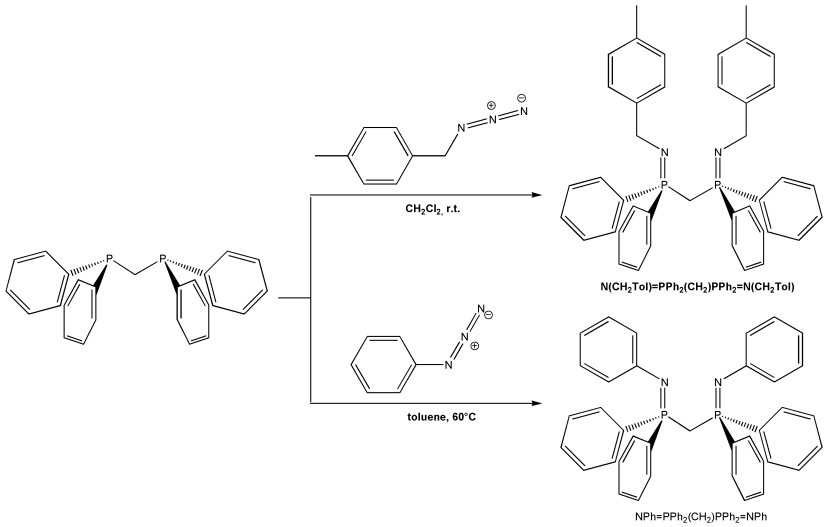

Scheme 3. Synthesis of $N(CH_2Tol)=PPh_2(CH_2)PPh_2=N(CH_2Tol)$ and $NPh=PPh_2(CH_2)PPh_2=NPh$.

The characterization data confirm the formation of the desired products. The aromatic region of the ^1H NMR spectra shows the expected resonances related to the P-bonded phenyl rings and to the N-bonded substituents. The bridging $P\text{-}CH_2\text{-}P$ group resonates around 3.8 ppm, and it is superimposed to the benzylic methylene fragments in the case of $N(CH_2Tol)=PPh_2(CH_2)PPh_2=N(CH_2Tol)$. The 4-methylbenzyl substituents are also associated with a sharp singlet at 2.33 ppm. The $^{31}P\{^1H\}$ NMR spectra are composed in both cases by a single sharp resonance, with chemical shift values strongly influenced by the nature of the substituents on the nitrogen atoms (Figure 42). The IR spectra do not meaningfully differ from those of the related monodentate species (Figure 43), and

the ν_{PN} stretchings are assigned around 1100 cm^{-1}. The UV-VIS spectra (Figure 43) are in line with those of $N(CH_2Tol)=PPh_3$ and $NPh=PPh_3$, and the slightly wider absorption range in the UV region in the presence of N-bonded aromatic substituents is confirmed.

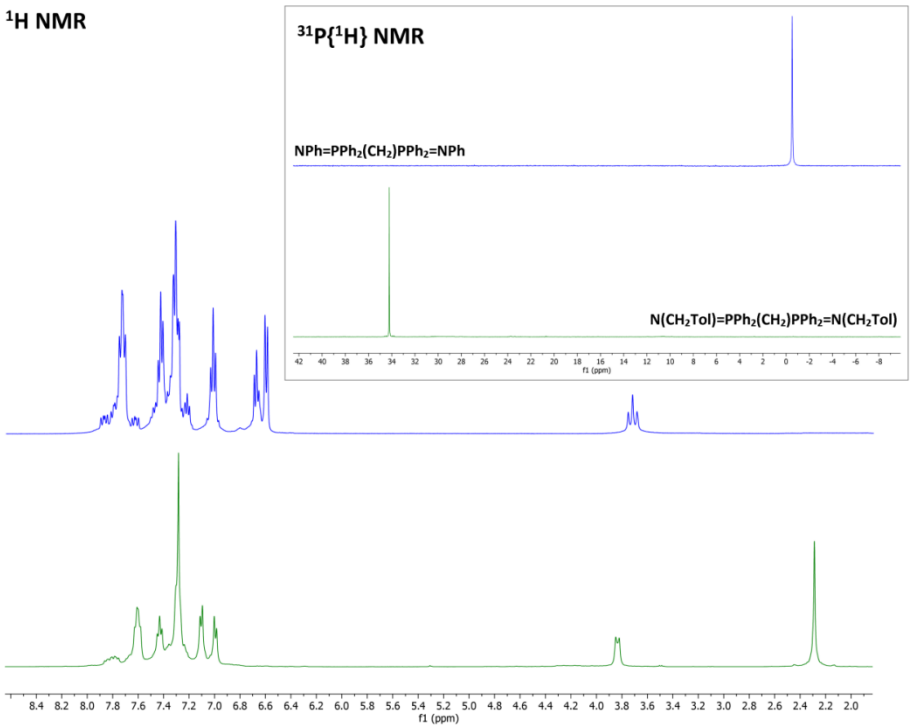

Figure 43. ^{1}H NMR and ^{31P}{^{1}H} NMR spectra of $N(CH_2Tol)=PPh_2(CH_2)PPh_2=N(CH_2Tol)$ and $NPh=PPh_2(CH_2)PPh_2=NPh$ ($CDCl_3$, 300 K).

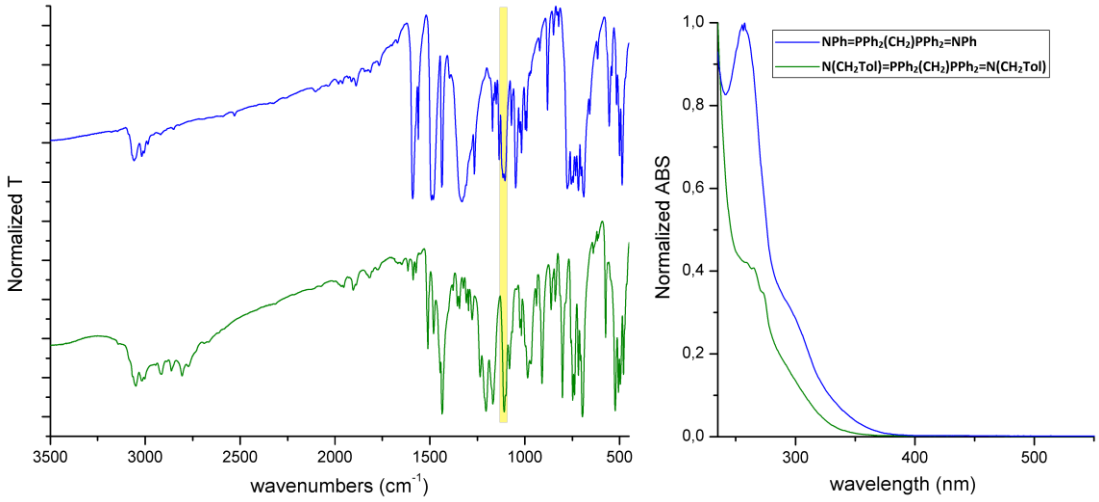

Figure 44. Normalized IR (KBr) and UV-VIS (CH_2Cl_2 solution, r.t.) spectra of $N(CH_2Tol)=PPh_2(CH_2)PPh_2=N(CH_2Tol)$ and $NPh=PPh_2(CH_2)PPh_2=NPh$.

The reaction of the bidentate ligands with anhydrous $MnBr_2$ in acetonitrile in 1:1 ratio allowed the isolation of complexes having formulae $[MnBr_2\{N(CH_2Tol)=PPh_2(CH_2)PPh_2=N(CH_2Tol)\}]$ and $[MnBr_2\{NPh=PPh_2(CH_2)PPh_2=NPh\}]$. The formulae were confirmed by the magnetic susceptibility data, with experimental magnetic moments close to the expected 5.9 BM. The presence of the coordinated ligands was also indicated by the IR spectra of the two complexes (Figure 45). No signal attributable to coordinated acetonitrile was observed. A single resonance is present in the $^{31}P\{^1H\}$ NMR spectra. The UV-VIS spectrum of $[MnBr_2\{N(CH_2Tol)=PPh_2(CH_2)PPh_2=N(CH_2Tol)\}]$ is similar to that of the free ligand, while the coordination to $MnBr_2$ slightly modifies the absorptions of $NPh=PPh_2(CH_2)PPh_2=NPh$, shifted at shorter wavelengths (Figure 45). The compounds have quite good thermal stability, with decomposition starting above 150 °C in the case of $[MnBr_2\{N(CH_2Tol)=PPh_2(CH_2)PPh_2=N(CH_2Tol)\}]$ and around 200 °C for $[MnBr_2\{NPh=PPh_2(CH_2)PPh_2=NPh\}]$.

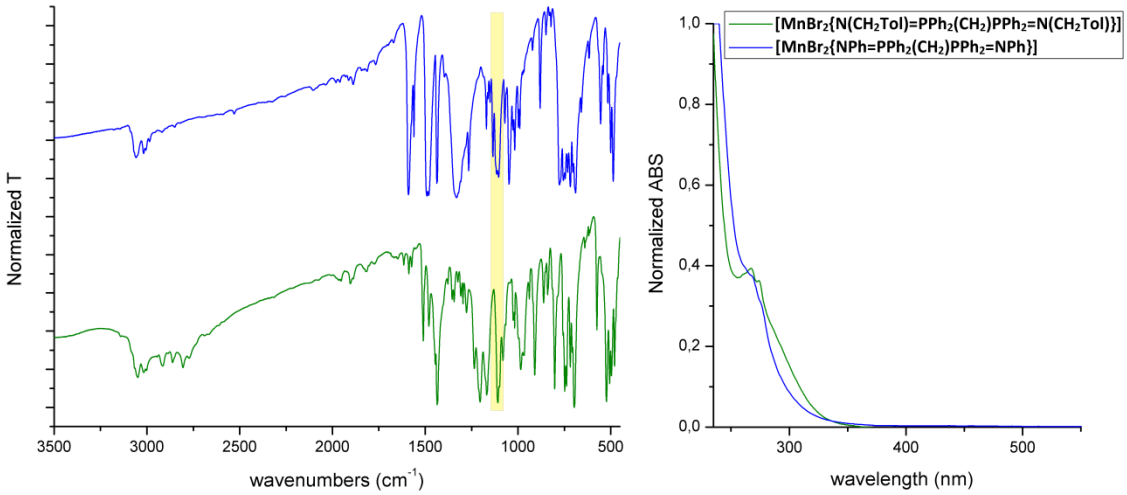

Figure 45. Normalized IR (KBr) and UV-VIS (CH_2Cl_2 solution, r.t.) spectra of $[MnBr_2\{N(CH_2Tol)=PPh_2(CH_2)PPh_2=N(CH_2Tol)\}]$ and $[MnBr_2\{NPh=PPh_2(CH_2)PPh_2=NPh\}]$.

The PL and PLE spectra recorded for solid samples revealed noticeable differences with respect to the related complexes with monodentate iminophosphoranes in the coordination sphere (Figure 46). The emission of $[MnBr_2\{N(CH_2Tol)=PPh_2(CH_2)PPh_2=N(CH_2Tol)\}]$ is composed of two bands, a weaker one at 524 nm and the dominant one at 627 nm. Both emissions are attributable to metal-

centred transitions, with Mn^{II} in two different coordination environments. Such an outcome indicates that [$MnBr_2${$N(CH_2Tol)=PPh_2(CH_2)PPh_2=N(CH_2Tol)$}] separated from the solution in almost two different forms, a result confirmed by further attempts to synthesize the compound. A possible explanation is that [$MnBr_2${$N(CH_2Tol)=PPh_2(CH_2)PPh_2=N(CH_2Tol)$}] could exist both in tetrahedral form, causing the green emission, and in a polynuclear form with a coordination number higher than four, associated to the emission in the red range. The presence of a single resonance in the ^{31}P NMR supports the idea that these species are in equilibrium in solution. The PLE spectra recorded for different emission wavelengths are almost superimposable, thus the selective excitation of one of the two compounds was not possible. The observed luminescence is attributable to ligand excitations for wavelengths below 400 nm, while the direct excitation of Mn^{II} is detectable between 440 and 490 nm. The two species present in [$MnBr_2${$N(CH_2Tol)=PPh_2(CH_2)PPh_2=N(CH_2Tol)$}] samples are however characterized by different luminescence lifetimes, about 416 μs for the green-emitting species and 824 μs for the red-emitting one (Figure 47). It is worth noting that only a metal-centred emission at 589 nm and τ of 836 μs was observed for the related compound [$MnBr_2${$N(CH_2Ph)=PPh_3$}$_2$]. It can be concluded that the use of a bidentate iminophosphorane influences the coordination geometry surrounding the Mn^{II} centre. The possible steric effect of the methyl substituents on the N-bonded 4-methylbenzyl fragments, introduced for ease of characterization of the ligand, must be however investigated in future studies.

The differences between [$MnBr_2${$NPh=PPh_2(CH_2)PPh_2=NPh$}] and [$MnBr_2(NPh=PPh_3)_2$] are yet more marked. The previously discussed green emission of [$MnBr_2(NPh=PPh_3)_2$] supported the formation of a tetrahedral complex, while the PL spectrum of [$MnBr_2${$NPh=PPh_2(CH_2)PPh_2=NPh$}] is composed by a single band centred at 602 nm, with FWHM around 2000 cm^{-1}. The formation of a tetrahedral mononuclear complex is therefore ruled out, and [$MnBr_2${$NPh=PPh_2(CH_2)PPh_2=NPh$}] is most likely a polynuclear species. The X-ray structure diffraction is mandatory for the unambiguous definition of the molecular structure. The metal-centred nature of the emission was confirmed by the PLE spectra, clearly showing the superposition of Mn^{II} and iminophosphorane excitations (Figure 46). As observable from the 3D luminescence spectrum reported in

Figure 46, the emission does not depend upon the excitation wavelength, a result in agreement with the antenna-effect from the bidentate iminophosphorane to the $MnBr_2$ fragment. The luminescence lifetime is noticeably longer than that of $[MnBr_2(NPh{=}PPh_3)_2]$ (average value 235 μs), the measured value being 1697 μs. For the sake of comparison, τ values higher than 1 ms are typical of several Eu^{III} derivatives of technological interest [147]. Another element of interest is provided by the chromaticity diagram (Figure 47). The CIE 1931 chromaticity coordinates related to the emission of $[MnBr_2\{NPh{=}PPh_2(CH_2)PPh_2{=}NPh\}]$ are x = 0.594 and y = 0.405 and correspond to an orange emission with unitary colour purity. Unfortunately, the expected increase of rigidity caused using bidentate ligands did not improve the luminescence quantum yields, with measured values for the two complexes between 6% and 9%. The reduced steric hindrance associated with the lower number of P-bonded phenyl rings perhaps plays a detrimental role in the photoluminescence of the Mn^{II} complexes.

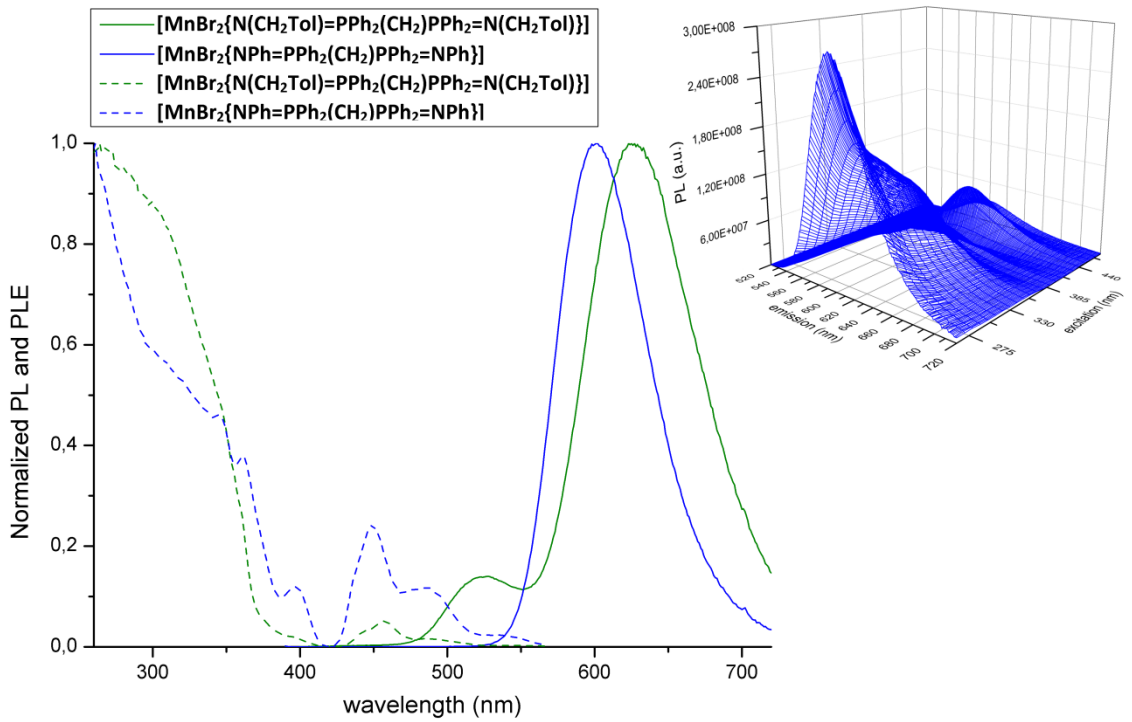

Figure 46. Normalized PLE (solid state, r.t., $\lambda_{emission}$ = 590 nm, dashed lines) and PL (solid state, r.t., $\lambda_{excitation}$ = 350 nm, solid lines) spectra of the of $[MnBr_2\{N(CH_2Tol){=}PPh_2(CH_2)PPh_2{=}N(CH_2Tol)\}]$ and $[MnBr_2\{NPh{=}PPh_2(CH_2)PPh_2{=}NPh\}]$. 3D luminescence spectrum of $[MnBr_2\{NPh{=}PPh_2(CH_2)PPh_2{=}NPh\}]$ (solid state, r.t.).

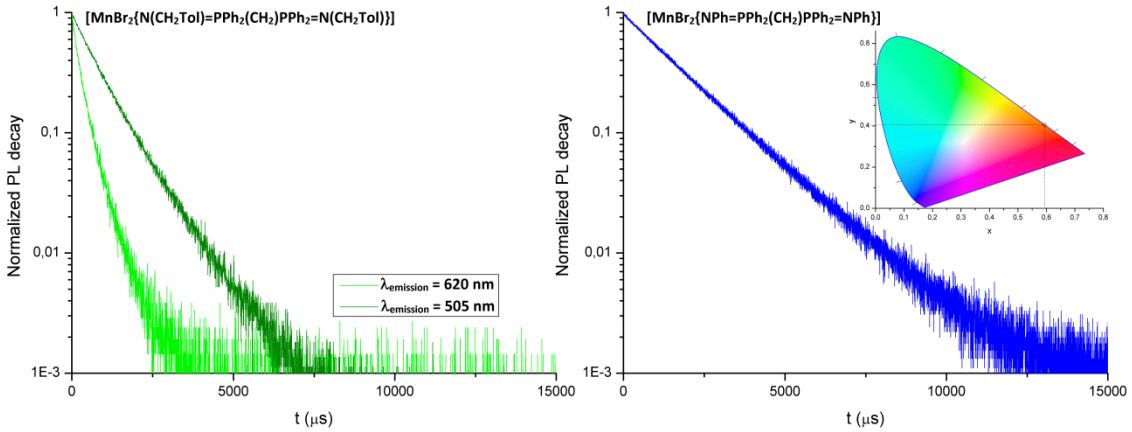

Figure 47. Semi-log plots of the luminescence decay curves (MSC, solid state, r.t.) of $[MnBr_2\{N(CH_2Tol)=PPh_2(CH_2)PPh_2=N(CH_2Tol)\}]$ ($\lambda_{excitation}$ = 290 nm, $\lambda_{emission}$ = 505 and 620 nm) and of $[MnBr_2\{NPh=PPh_2(CH_2)PPh_2=NPh\}]$ ($\lambda_{excitation}$ = 445 nm, $\lambda_{emission}$ = 600 nm). CIE 1931 chromaticity diagram of $[MnBr_2\{NPh=PPh_2(CH_2)PPh_2=NPh\}]$. Chromaticity coordinates: x = 0.594, y = 0.405.

5. Conclusions and future outlook

The preliminary results obtained with this thesis work revealed that iminophosphorane ligands are suitable candidates for the preparation of Zn^{II} and Mn^{II} coordination compounds, showing only some analogies with the related phosphine oxides. The experimental data here provided indicate that triplet states of the ligands can be involved in the photoluminescent mechanisms after the coordination to metal halide fragments, as revealed by long luminescence lifetimes of the ligand-centred emissions of the Zn^{II} derivatives with N-aromatic iminophosphoranes. The same excited states can have a role in the sensitization of Mn^{II} luminescence, sometimes with competition between ligand-centred and metal-centred emissions. The nature of the N-bonded substituents and the presence of bridges between two iminophosphorane moieties influence the geometry of the Mn^{II} complexes, varying from tetrahedral to higher coordination numbers. The structures of the compounds are also dependent upon the choice of the coordinated halides. The emission wavelengths and the lifetimes are deeply related to the coordination sphere surrounding the Mn^{II} centres.

Selected complexes showed promising features in terms of Stokes shift, colour purity and luminescence lifetime. A general limit of the synthesized compounds is the quite low photoluminescence quantum yield. Moreover, in some cases the characterization data did not allow the unambiguous definition of the molecular structures, thus further attempts to isolate single crystals suitable for X-ray diffraction are necessary. Given the changes observed by replacing the N-donor substituents, further compounds must be investigated to better rationalize the coordinating behaviour of iminophosphoranes towards Mn^{II} and Zn^{II}, with the aim of preparing complexes with improved photoluminescent features. Moreover, the electronic features of the ligands are also related to the choice of the P-donor substituents, and in this thesis only triphenyphosphine and bis(diphenylphosphino)methane were considered as reactants. Given the wide chemical flexibility of the Staudinger reaction, it is likely to suppose that complexes with tailored electronic and steric features could be prepared in the next future.

References

[1] V. Balzani, P. Ceroni, A. Juris, Photochemistry and Photophysics, Wiley-VCH, Weinheim, 2014.

[2] A. J. Browne, A. Krajewska, A. S. Gibbs, J. Mater. Chem. C 9 (2021) 11640.

[3] H. Yersin, Highly Efficient OLEDs: Materials Based on Thermally Activated Delayed Fluorescence, Wiley-VCH, Weinheim, 2018.

[4] C. E. Housecroft, A. G. Sharpe, Inorganic Chemistry, 4th edition, Pearson, Harlow, 2012.

[5] M. Montaldi, A. Credi, L. Prodi, M. T. Gandolfi, Handbook of Photochemistry, 3rd edition, Chapter 2, CRC Press, Boca Raton, 2006.

[6] C. Bizzarri, E. Spuling, D. M. Knoll, D. Volz, S. Bräse, Coord. Chem. Rev. 373 (2018) 49.

[7] O. S. Wenger, J. Am. Chem. Soc. 140 (2018) 13522.

[8] C. Förster, K. Heize, Chem. Soc. Rev. 49 (2020) 1057.

[9] C. Wegeberg, O. S. Wenger, JACS Au 1 (2021) 1860.

[10] X. Li, Y. Xie, Z. Li, Chem. Asian J. 16 (2021) 2817.

[11] N. Sinha, J.-R. Jiménez, B. Pfund, A. Prescimone, C. Piguet, O. S. Wenger, Angew. Chem. Int. Ed. 60 (2021) 23722.

[12] J. Beaudelot, S. Oger, Peruško, T.-A. Phan, T. Teunens, C. Moucheron, G. Evano, Chem. Rev. 122, 2022, 16365.

[13] N. N. Greenwood, A. Earnshaw, Chemistry of the Elements, 2nd edition, Elsevier, Amsterdam, 1997.

[14] W. Kaim, B. Schwederski, A. Klein, Bioinorganic Chemistry: Inorganic Elements in the Chemistry of Life, Wiley, Chichester, 2013.

[15] M. Graft, R. Resfeld, G. Panczer, Modern Luminescence Spectroscopy of Minerals and Materials, 2nd edition, Springer, Heidelberg, 2015.

[16] M. K. Chan, W. H. Armstrong, Inorg. Chem. 28 (1989) 3777.

[17] A. E. S. Sleightholme, A. A Shinkle, Q. Liu, Y. Li, C. W. Monroe, L. T. Thompson, J. Power Sources 196 (2011) 5742.

[18] Y. Zhou, W. Zhao, C. Lu, Z. Liao, Prog. Nat. Sci. 28 (2018) 301.

[19] Y. Li, T. Wang, L. Wang, D. Deng, J. Lei, J. Qiang, S. Liao, Y. Huang, J. Alloys Compd. 937 (2023) 168413.

[20] A. J. Brown, P. S. Francis, J. L. Adcock, K. F. Lim, N. W. Barnett, Anal. Chim. Acta 624 (2008) 175.

[21] K. Heinze, Nat. Chem. 13 (2021) 926.

[22] P. Herr, C. Kerzig, C. B. Larsen, D. Häussinger, O. S. Wenger, Nat. Chem. 13 (2021) 956.

[23] C. Wegeberg, O. S. Wenger, Dalton Trans. 51 (2022) 1297.

[24] G. Wilkinson (Ed.), Comprehensive Coordination Chemistry, Vol. 4, Pergamon Press, Oxford, 1987.

[25] B. N. Figgis, M. A. Hitchman, Ligand Field Theory and its applications, Wiley-VCH, New York, 2000.

[26] F. A. Cotton, D. M. L. Goodgame, M. Goodgame, J. Am. Chem. Soc. 84 (1962) 167.

[27] S. Balsamy, P. Natarajan, R. Vedalakshmi, S. Muralidharan, Inorg. Chem. 53 (2014) 6054.

[28] C. Jiang, N. Zhong, C. Luo, H. Lin, Y. Zhang, H. Peng, C.-G. Duan, Chem. Commun. 53 (2017) 5954.

[29] L.-J. Xu, C.-Z. Sun, H. Xiao, Y. Wu, Z.-N. Chen, Adv. Mater. 29 (2017) 1605739.

[30] J. Zhao, T. Zhang, X.-Y. Dong, M.-E. Sun, C. Zhang, X. Li, Y.S. Zhao, S.-Q. Zang, J. Am. Chem. Soc. 141 (2019) 15755.

[31] L. Mao, P. Guo, S. Wang, A.K. Cheetham, R. Seshadri, J. Am. Chem. Soc. 142 (2020) 13582.

[32] L.-J. Xu, X. Lin, Q. He, M. Worku, B. Ma, Nat. Commun. 11 (2020) 4329.

[33] Y. Zhang, W.-Q. Liao, D.-W. Fu, H.-Y. Ye, C.-M. Liu, Z.-N. Chen, R.-G. Xiong, Adv. Mater. 27 (2015) 3942.

[34] Y. Zhang, W.-Q. Liao, D.-W. Fu, H.-Y. Ye, Z.-N. Chen, R.-G. Xiong, J. Am. Chem. Soc. 137 (2015) 4928.

[35] H.-Y. Ye, Q. Zhou, X. Niu, W.-Q. Liao, D.-W. Fu, Y.i. Zhang, Y.-M. You, J. Wang, Z.-N. Chen, R.-G. Xiong, J. Am. Chem. Soc. 137 (2015) 13148.

[36] Y.-M. You, W.-Q. Liao, D. Zhao, H.-Y. Ye, Y. Zhang, Q. Zhou, X. Niu, J. Wang, P.-F. Li, D.-W. Fu, Z. Wang, S. Gao, K. Yang, J.-M. Liu, J. Li, Y. Yan, R.-G. Xiong, Science 357 (2017) 306.

[37] X. Liu, C. Ge, Z. Yang, Y. Song, A. Wang, Y. Kang, B. Li, Q. Dong, Adv. Opt. Mater. 9 (2021) 2100862.

[38] A. S. Berezin, Dyes Pigments 196 (2021) 109782.

[39] S. Zhang, Y. Zhao, Y. Zhou, M. Li, W. Wang, H. Ming, X. Jing, S. Ye, J. Phys. Chem. Lett. 12 (2021) 8692.

[40] A. Jana, V. Gopalan Sree, Q. Ba, S. Chan Cho, S. Uck Lee, S. Cho, Y. Jo, A. Meena, H. Kim, H. Im, J. Mater. Chem. C 9 (2021) 11314.

[41] S. Wang, X. Han, T. Kou, Y. Zhou, Y. Liang, Z. Wu, J. Huang, T. Chang, C. Peng, Q. Wei, B. Zou, J. Mater. Chem. C 9 (2021) 4895.

[42] P. Fu, Y. Sun, Z. Xia, Z. Xiao, J. Phys. Chem. Lett. 12 (2021) 7394.

[43] J. He, H. Zhao, X. Hu, Z. Fangg, J. Wang, R. Zhang, G. Zheng, B. Zhou, F. Long, J. Phys. Chem. C 125 (2021) 22898.

[44] Y. Mei, H. Yu, Z. Wei, G. Mei, H. Cai, Polyhedron 127 (2017) 458.

[45] Y. Qin, P. She, X. Huang, W. Huang, Q. Zhao, Coord. Chem. Rev. 416 (2020) 213331.

[46] P. Tao, S.-J. Liu, W.-Y. Wong, Adv. Opt. Mater. 8 (2020) 2000985.

[47] M. Bortoluzzi, J. Castro, F. Enrichi, A. Vomiero, M. Busato, W. Huang, Inorg. Chem. Commun. 92 (2018) 145.

[48] M. Bortoluzzi, J. Castro, J. Coord. Chem. 72 (2019) 309.

[49] M. Bortoluzzi, J. Castro, A. Gobbo, V. Ferraro, L. Pietrobon, S. Antoniutti, New J. Chem. 44 (2020) 571.

[50] M. Bortoluzzi, J. Castro, A. Gobbo, V. Ferraro, L. Pietrobon, Dalton Trans. 49 (2020) 7525.

[51] M. Bortoluzzi, J. Castro, A. Di Vera, A. Palù, V. Ferraro, New J. Chem. 45 (2021) 12871.

[52] M. Bortoluzzi, V. Ferraro, J. Castro, Dalton Trans. 50 (2021) 3132.

[53] M. Bortoluzzi, J. Castro, V. Ferraro, Inorg. Chim. Acta 536 (2022) 120896.

[54] V. Ferraro, J. Castro, L. Agostinis, M. Bortoluzzi, Inorg. Chim. Acta 545 (2023) 121285.

[55] D. M. L. Goodgame, F. A. Cotton, J. Chem. Soc. (1961) 3735.

[56] B. P. Chandra, B. R. Kaza, J. Lumin. 27 (1982) 101.

[57] F. A. Cotton, L. M. Daniels, P. Huang, Inorg. Chem. 40 (2001) 3576.

[58] Y.-Y. Tang, Z.-X. Wang, P.-F. Li, Y.-M. You, A. Stroppa, R.-G. Xiong, Inorg. Chem. Front. 4 (2017) 154.

[59] X. Huang, Y. Qin, P. She, H. Meng, S. Liu, Q. Zhao, Dalton Trans. 50 (2021) 8831.

[60] A. V. Artem'ev, M. P. Davydova, A. S. Berezin, V. K. Brel, V. P. Morgalyuk, I. Yu. Bagryanskaya, D. G. Samsonenko, Dalton Trans. 48 (2019) 16448.

[61] M. Bortoluzzi, J. Castro, E. Trave, D. Dallan, S. Favaretto, Inorg. Chem. Commun. 90 (2018) 105.

[62] A. S. Berezin, M. P. Davydova, I. Y. Bagryanskaya, O. I. Artyushin, V.K. Brel, A. V. Artem'ev, Inorg. Chem. Commun. 107 (2019) 107473.

[63] J. Chen, Q. Zhang, F.-K. Zheng, Z.-F. Liu, S.-H. Wang, A.-Q. Wu, G.-C. Guo, Dalton Trans. 44 (2015) 3289.

[64] Y. Wu, X. Zhang, L.-J. Xu, M. Yang, Z.-N. Chen, Inorg. Chem. 57 (2018) 9175.

[65] A. S. Berezin, D. G. Samsonenko, V. K. Brel, A. V. Artem'ev, Dalton Trans. 47 (2018) 7306.

[66] Y. Wu, X. Zhang, Y.-Q. Zhang, M. Yang, Z.-N. Chen, Chem. Commun. 54 (2018) 13961.

[67] M. P. Davydova, I. A. Bauer, V. K. Brel, M. I. Rakhmanova, I. Yu. Bagryanskaya, A. V. Artem'ev, Eur. J. Inorg. Chem. (2020) 695.

[68] A. V. Artem'ev, M. P. Davydova, A. S. Berezin, T. S. Sukhikh, D. G. Samsonenko, Inorg. Chem. Front. 8 (2021) 2261.

[69] A. V. Artem'ev, M. P. Davydova, M. I. Rakhmanova, I. Yu. Bagryanskaya, D. P. Pishchur, Inorg. Chem. Front. 8 (2021) 3767.

[70] Y. Y. Qin, P. Tao, L. Gao, P. F. She, S. J. Liu, X. L. Li, F. Y. Li, H. Wang, Q. Zhao, Y. Q. Miao, W. Huang, Adv. Opt. Mater. 7 (2019) 1801160.

[71] H. Meng, W. Zhu, F. Li, X. Huang, Y. Qin, S. Liu, Y. Yang, W. Huang, Q. Zhao, Laser Photonics Rev. 15 (2021) 2100309.

[72] D. Hausmann, A. Kuzmanoski, Claus Feldmann, Dalton Trans. 45 (2016) 6541.

[73] V. Lahariya, S. J. Dhoble, Displays 74 (2022) 102186.

[74] G. Wilkinson (Ed.), Comprehensive Coordination Chemistry, Vol. 5, Pergamon Press, Oxford, 1987.

[75] I. Resa, E. Carmona, E. Gutierrez-Puebla, A. Monge, Science 305 (2004) 1136.

[76] F. Dumur, Synth. Met. 195 (2014) 195.

[77] G. A. Ardizzoia, S. Brenna, S. Durini, B. Therrien, M. Veronelli, Eur. J. Inorg. Chem. (2014) 4310.

[78] G. Volpi, E. Priola, C. Garino, A. Daolio, R. Rabezzana, P. Benzi, A. Giordana, E. Diana, R. Gobetto, Inorg. Chim. Acta 509 (2020) 119662.

[79] G. A. Ardizzoia, G. Colombo, B. Therrien, S. Brenna, Eur. J. Inorg. Chem. (2019) 1825.

[80] S. Di Bella, Dalton Trans. 50 (2021) 6050.

[81] G. A. Ardizzoia, S. Brenna, S. Durini, B. Therrien, Polyhedron 90 (2015) 214.

[82] H.-W. Zheng, M. Wu, D.-D. Yang, Q.-F. Liang, J.-B. Li, X.-J. Zheng, Inorg. Chem. 60 (2021) 11609.

[83] A. N. Gusev, M. A. Kiskin, E. V. Braga, M. A. Kryukova, G. V. Baryshnikov, N. N. Karaush-Karmazin, V. A. Minaeva, B. F. Minaev, K. Ivaniuk, P. Stakhira, H. Ågren, W. Linert, ACS Appl. Electron. Mater. 3 (2021) 3436.

[84] R. Lakshmanan, N. C. Shivaprakash, S. Sindhu, J. Lumin. 196 (2018) 136.

[85] A. S. Burlov, V. G. Vlasenko, Y. V. Koshchienko, M. S. Milutka, E. I. Mal'tsev, A. V. Dmitriev, D. A. Lypenko, N. V. Nekrasova, A. A. Kolodina, N. I. Makarova, A. V. Metelitsa, V. A. Lazarenko, Y. V. Zubavichus, V. N. Khrustalev, D. A. Garnovskii, Appl. Organomet. Chem. 35 (2021) e6107.

[86] A. Ogunsipe, D. Maree, T. Nyokong, J. Mol. Struct. 650 (2003) 131.

[87] D. Tungulin, J. Leier, A. B. Carter, A. K. Powell, R. Q. Albuquerque, A. N. Unterreiner, C. Bizzarri, Chem. Eur. J. 25 (2019) 3816.

[88] R. Tabone, D. Feser, E. D. Lemma, U. Schepers, C. Bizzarri, Front. Chem. 9 (2021) 754420

[89] A. Gusev, V. Shul'gin, E. Braga, E. Zamnius, M. Kryukova, W. Linert, Dyes Pigments 183 (2020) 108626.

[90] J. Cepeda, E. San Sebastian, D. Padro, A. Rodríguez-Diéguez, J. A. Garcıá, J. M. Ugalde, J. M. Seco, Chem. Commun. 52 (2016) 8671.

[91] J.-Q. Wang, Y. Mu, S.-De Han, J. Pan, J.-H. Li, G.-M. Wang, Inorg. Chem. 58 (2019) 9476.

[92] A. Barbieri, G. Accorsi, N. Armaroli, Chem. Commun. (2008) 2185.

[93] Y. Sakai, Y. Sagara, H. Nomura, N. Nakamura, Y. Suzuki, H. Miyazaki, C. Adachi, Chem. Commun. 51 (2015) 3181.

[94] J. Xiong, K. Li, T. Teng, X. Chang, Y. Wei, C. Wu, C. Yang, Chem. Eur. J. 26 (2020) 6887.

[95] J.-H. Wei, W.-T. Ou, J.-B. Luo, D.-B. Kuang, Angew. Chem. Int. Ed. (2022) e202207985.

[96] A. S. Berezin, K. A. Vinogradova, V. P. Krivopalov, E. B. Nikolaenkova, V. F. Plyusnin, A. S. Kupryakov, N. V. Pervukhina, D. Y. Naumov, M. B. Bushuev, Chem. Eur. J. 24 (2018) 12790.

[97] N. A. Shekhovtsov, E. B. Nikolaenkova, A. A. Ryadun, S. N. Vorobyeva, V. P. Krivopalov, M. B. Bushuev, New J. Chem. 47 (2023) 6361.

[98] N. A. Shekhovtsov, E. B. Nikolaenkova, A. A. Ryadun, D. G. Samsonenko, A. Ya. Tikhonov, M. B. Bushuev, Molecules 28 (2023) 1793.

[99] N. A. Shekhovtsov,M. B. Bushuev, J. Photochem. Photobiol. A 433 (2022) 114195.

[100] N. A. Shekhovtsov, A. A. Ryadun, V. F. Plyusnin, E. B. Nikolaenkova, A. Ya. Tikhonov, M. B. Bushuev, New J. Chem. 46 (2022) 22804.

[101] N. A. Shekhovtsov, K. A. Vinogradova, S. N. Vorobyova, A. S. Berezin, V. F. Plyusnin, D. Yu. Naumov, N. V. Pervukhina, E. B. Nikolaenkova, A. Ya. Tikhonovc, M. B. Bushuev, Dalton Trans. 51 (2022) 9818.

[102] T. Sano, Y. Nishio, Y. Hamada, H. Takahashi, T. Usuki, K. Shibata, J. Mater. Chem. 10 (2000) 157.

[103] Q.-D. Liu, R. Wang, S. Wang, Dalton Trans. (2004) 2073.

[104] C. A. Kosky, J. P. Gayda, J. F. Gibson, S. F. Jones, D. J. Williams, Inorg. Chem. 21 (1982) 3173.

[105] J. P. Rose, R. A. Lalancette, J. A. Potenza, H. J. Schugar, Acta Crystallogr. Sect. B 36 (1980) 2409.

[106] X. Liu, G. Wang, Y. Dang, S. Zhang, H. Tian, Y. Ren, X. Tao, CrystEngComm 18 (2016) 1818.

[107] D. C. Batesky, M. J. Goldfogel, D. J. Weix, J. Org. Chem. 82 (2017) 9931.

[108] V. Ferraro, F. Baggio, J. Castro, M. Bortoluzzi, Eur. J. Inorg. Chem. (2022) e202200119.

[109] L. Li, Z.-P. Wang, G.-R. Tian, X.-Y. Song, S.-X. Sun, J. Cryst. Growth 310 (2008) 1202.

[110] H. Staudinger, J. Meyer, Helv. Chim. Acta 2 (1919) 635.

[111] F. Mitsuyo, I. Kenji, I. Yoshio, Bull. Chem. Soc. Jap. 48 (1975) 2044.

[112] B. Venderbosch, J.-P. H. Oudsen, J. I. van der Vlugt, T. J. Korstanje, M. Tromp, Organometallics 39 (2020) 3480.

[113] J. García-Álvarez, S. E. García-Garrido, V. Cadierno, J. Organomet. Chem. 751 (2014) 792.

[114] T. Tannoux, A. Auffrant, Coord. Chem. Rev. 474 (2023) 214845.

[115] M. Frik, J. Jiménez, V. Vasilevski, M. Carreira, A. de Almeida, E. Gascón, F. Benoit, M. Sanaú, A. Casini, M. Contel, Inorg. Chem. Front. 1 (2014) 231.

[116] M. S. Hill, P. B. Hitchcock, J. Organomet. Chem. 689 (2004) 3163.

[117] D. J. Evans, M. S. Hill, P. B. Hitchcock, Dalton Trans. (2003) 570.

[118] M. S. Hill, P. B. Hitchcock, J. Chem. Soc. Dalton Trans. (2002) 4694.

[119] M. Bayram, S. Gondzik, D. Bläser, C. Wölper, S. Schulz, Z. Anorg. Allg. Chem. 642 (2016) 847.

[120] C. A. Wheaton, B. J. Ireland, P. G. Hayes, Z. Anorg. Allg. Chem.637 (2011) 2111.

[121] W. L. F. Armarego, C. L. L. Chai, Purification of Laboratory Chemicals, 5th edition, Butterworth-Heinemann, London, 2003.

[122] R. O. Lindsay, C. F. H. Allen, Org. Synth. 22 (1942) 96.

[123] R. Ul Islam, A. Taher, M. Choudhary, M. J. Witcomb, K. Mallick, Dalton Trans. 44 (2015) 1341.

[124] C. J. Cramer, Essentials of Computational Chemistry, Wiley, Chichester, 2004.

[125] S. Grimme, J. G. Brandenburg, C. Bannwarth, A. Hansen, J. Chem. Phys. 143 (2015) 054107.

[126] F. Neese, Wiley Interdiscip. Rev.: Comput. Mol. Sci. 12 (2022) e1606.

[127] T. Lu, F. Chen, J. Comput. Chem. 33 (2012) 580.

[128] R. S. Foster, H. Jakobi, J. P. A. Harrity, Org. Lett. 14 (2012) 4858.

[129] P. Imhoff, R. Van Asselt, C. J. Elsevier, K. Vrieze, K. Goubitz, K. F. Van Malssen, C. H. Stam, Phosphorus Sulfur Silicon Relat Elem. 47 (1990) 401.

[130] M. Adib, E. Sheikhi, A. Deljoush, Tedrahedron 6 (2011) 4137.

[131] K. Nakamoto, Infrared and Raman Spectra of Inorganic and Coordination Compounds, 6th edition, Wiley, Hoboken (2009).

[132] T. Baumgartner, R. Réau, Chem. Rev. 106 (2006) 4681.

[133] C. Wang, M. Taki, Y. Sato, A. Fukazawa, T. Higashiyama, S. Yamaguchi, J. Am. Chem. Soc. 139 (2017) 10374.

[134] C. H. Chien, C. K. Chen, F.M. Hsu, C. F. Shu, P. T. Chou, C. H. Lai, Adv. Funct. Mater. 19 (2009) 560.

[135] Z. Zhao, G. Yu, Q. Chang, X. Liu, Y. Liu, L. Wang, Z. Liu, Z. Bian, W. Liu, C. Huang, J. Mater. Chem. C 5 (2017) 7344.

[136] E. F. Schubert, Light-emitting diodes, 2nd ed., Cambridge University Press, Cambridge, 2006, pp. 292-303.

[137] Z. Liu, T. Lu, Q. Chen, Carbon 165 (2020) 461.

[138] N. Elgrishi, K. J. Rountree, B. D. McCarthy, E. S. Rountree, T. T. Eisenhart, J. L. Dempsey, J. Chem. Ed. 95 (2018) 197.

[139] Y. Nie, H. Pritzkow, H. Wadepohl, W. Siebert, J. Organomet. Chem. 690 (2005) 4531.

[140] L Yang, D. R. Powell, R. P. Houser, Dalton Trans. (2007) 955.

[141] H. Yersin, A. F. Rausch, R. Czerwieniec, T. Hofbeck, T. Fischer, Coord. Chem. Rev. 255 (2011) 2622.

[142] D. F Evans, J. Phys. E 7 (1974) 247.

[143] G. A. Bain, J. F. Barry, J. Chem. Ed. 85 (2008) 532.

[144] I. Bertini, C. Luchinat, Coord. Chem. Rev. 150 (1996) 77.

[145] Z.-X. Wang, P.-F. Li, W-Q. Liao, Y. Tang, H.-Y Ye, Y. Zhang, Chem. Asian J. 11 (2016) 981.

[146] M. Wrighton, D. Ginley, Chem. Phys. 4, 1974, 295.

[147] J.-C. G. Bünzli, A.-S. Chauvin, H. K. Kim, E. Deiters, S. V. Eliseeva, Coord. Chem. Rev. 254 (2010) 2623.